MODELING THE COUPLING OF ACTION POTENTIAL AND ELECTRODES

A Thesis Submitted in Partial Fulfillment
of the Requirements for the Degree of
Doctor of Engineering (Dr. -Ing)

by
Revathi Appali, born on May 16, 1985 in Hanamkonda, India

urn:nbn:de:gbv:28-diss2014-0010-1

Reviewers

1. Prof. Dr. Ursula van Rienen
   Institute of General Electrical Engineering, University of Rostock
   Department of Computer Science and Electrical Engineering
   Albert-Einstein Str. 2, D-18059, Rostock
   Email: ursula.van-rienen@uni-rostock.de

2. Prof. Dr. Thomas Heimburg
   Membrane Biophysics Group, Niels Bohr Institute
   University of Copenhagen
   Blegdamsvej 17, DK - 2100 Copenhagen ϕ - Denmark
   Email: theimbu@nbi.dk

3. Prof. Dr. Lars Schwabe
   Adaptive and Regenerative Software Systems, University of Rostock
   Department of Computer Science and Electrical Engineering
   Albert-Einstein Str. 22, D-18059, Rostock
   Email: lars.schwabe@uni-rostock.de

Date of submission: March 5, 2013
Date of evaluation: June 28, 2013

Zusammenfassung

Das Gehirn ist ein sehr komplexes System. Seine einzelnen Zellen, die Neuronen, sind miteinander in komplexen Formen verbunden und zeigen eine stark nichtlineare Dynamik. Sie erzeugen, propagieren und empfangen komplexe Informationen. Die Aufgabe, die Funktion der Neuronen und damit die Funktionsweise des Gehirns zu verstehen, wurde in den letzten Jahrzehnten der Nexus der Forschung in der Medizin und den mathematischen Neurowissenschaften.

Die vorliegende Monographie ist eine Studie zur Pulsausbreitung in Nerven. Die wichtigste Aufgabe dieser Arbeit ist die Modellierung und Simulation der Aktionspotenzialausbreitung in einem Neuron und seiner Interaktion mit Elektroden im Rahmen von Neurochip-Anwendungen. Diese Studie hilft in der Verbesserung neuronaler Implantate und findet unmittelbare Anwendung in den Simulationen zu derartigen Implantatsstudien.

Im ersten Teil arbeiten wir mit einemmodifizierten FitzHugh-Nagumo-Modell. Der Zweck dieser Studie liegt darin, das elektrische Feld des Aktionspotenzials und dessen Kopplung an Elektroden zu simulieren. Das Modell wird dann zu einem Netzwerk der Axone erweitert und die gesamte Neurochip-Simulation durchgeführt.

Der zweite Teil beschreibt ein alternatives Modell, das 2005 als ein *Solitonen-Modell* vorgeschlagen wurde. Ziel der vorliegenden Studie ist die Bestätigung des neuen Modells durch Computersimulationen und des besseren Verstndnisses der Rolle der Zellmembran der Neuronen in der Pulsausbreitung. Hierzu werden theoretische elektrostatische Modelle von reinen und gemischt-anionischen Membranen vorgeschlagen.

Abstract

The brain is a very complex system. Its individual cells, neurons, are interconnected in maze pattern and are attributed to highly nonlinear dynamics. They generate, propagate and receive the complex information. The problem of understanding the neurons' function and thereby the brain has been the nexus of research during the last decades, in the fields of medicine and mathematical neurosciences.

The present monograph is a study of pulse propagation in nerves. The main project of this work is modeling and simulation of the action potential propagation in a neuron and its interaction with the electrodes in the context of neurochip application. This study helps in improvisation of neural implants and finds an immediate application in the *in-silico* study of such implants.

In the first part, we work with an adapted model of FitzHugh-Nagumo derived from the Hodgkin-Huxley model. The purpose of this study is to simulate 3D-field of action potential propagating in an axon and its coupling with the electrodes. The model is then applied to a network of axons and the entire neurochip simulation is carried out.

The second part was the result of turning the spotlight-on onto the drawbacks of classical theory of nerve pulse propagation (Hodgkin-Huxley model) and to bring forth, an alternative model that was proposed in 2005-*the soliton model*. The purpose of this study is to substantiate the new model with computer simulations and to comprehend the role of membrane state in the pulse propagation. For which, theoretical electrostatic models of pure and mixed-anionic membranes are proposed.

Acknowledgements

This is a summary of work done over three year period as a member of the DFG research training group 1505/1, welisa, in the Institute of General Electrical Engineering at the University of Rostock, Rostock.

I express my immense gratitude to Professor Ursula van Rienen, who supervised my dissertation. She has always been very supportive and kind. She has really been my *Doktormutter*, as they say in German. She was always receptive and gave tremendous freedom in pursuing this topic. Thanks to Professor Jan Gimsa for being the second supervisor of my thesis. A special thanks to my colleagues at the institute.

Professor Thomas Heimburg has been an inspiration to me and introduced me to the Soliton model of nerve pulse propagation. His interest in nerves and science in general is quite infectious. I wish to thank him for his help during this work. I hope to continue to learn and inspire from him in the future.

I was given the opportunity to spend a couple of months at Niels Bohr Institute, Copenhagen, which enabled me to learn from many quality people, including Prof. Thomas Heimburg, Prof. Andrew Jackon and Prof. Benny Lautrup. They were kind enough to include me in the work of soliton study.

Professor Ales Iglic has been very helpful with his knowledge of Electrical Double Layer and Poisson-Boltzmann equation. He has contributed to this work in proposing the electrostatic model of pure lipid membranes. I wish to thank for his guidance and support.

My dearest friends, Kathy and Recep, shared the ups and downs of student life for over six years. I wish to thank them for always being there. A special thanks to my friends Renhao and Mimi.

No word of thanks would suffice to acknowledge the constant support and encouragement of my family. My uncle, Dr. Ch. Nagarjun Rao, my first inspiration, who took me to his laboratories and brought science into reality. My parents Sharma and Kamala, always supported me in all aspects of my life and encouraged me to pursue my interests. Their blessings and wishes are always with me. I thank my sister Swathi and brother-in-law Phani for all the love and support they extended to me. Thanks for your endless love being miles away.

My deepest gratitude is reserved for my beloved, friend, colleague, guide and

best-half Kiran. Without him, none of this would have been possible. I thank you for supporting me during this phase of life and looking forward to a wonderful time together. Finally, to Rasy, my beautiful daughter, who came into our lives during this graduate study and brought us great bundle of joy. My love to her who supported me during the important phase of writing this dissertation.

Thanks to the almighty for the blessings bestowed upon me.

To my love, Kiran & my sunshine, Rasya

List of Symbols

θ	Speed of pulse
a	Axon radius
C_m	Membrane capacitance
F	Faraday's constant
I_m	Total current through membrane
R	Gas constant
R_i	Specific resistance of intracellular medium
R_m	Specific resistance of membrane
T	Temperature
t	Time
z_j	Valence of ions

Electrostatic

ϵ_0	Permittivity of vacuum
ϵ_r	Relative permittivity
κ	Debye constant
λ_D	Debye length
ψ_D	Dipole potential
ψ_m	Transmembrane potential
ψ_s	Surface potential
ρ	Volume charge density
σ	Surface charge density
$\mathbf{B}$	Magnetic flux
$\mathbf{D}$	Electric displacement
$\mathbf{E}$	Electric field
e	Electron charge
$\mathbf{H}$	Magnetic field
k	Boltzmann constant
N_A	Avagadro number
n_i	Concentration
n_{0w}	Number density of water
p	Water dipole moment
q	Charge
z_i	Charge of ion
V	Volume

Computational Neuroscience

$\alpha_i(V_m)$	Voltage dependent rate constant
$\beta_i(V_m)$	Voltage dependent rate constant
Γ	Conservative flux
${c_j}^i$	Concentraion of ions inside the membrane
${c_j}^o$	Concentration of ions outside of membrane
d_a	Damping coefficient
e_a	Mass coefficient
E_j	Nernst potential
f	Source term

g_j	Ion conductivity
m_∞	m-nullcline
n_∞	n-nullcline
$V(x,t)$	Voltage variable
V_i	Intracellular potential
V_m	Membrane potential
V_o	Extracellular potential
$w(x,t)$	Recovery variable

Biophysical

β	Propagation velocity
κ_T^A	Isothermal lateral compressibility
κ_T^V	Isothermal volume compressibility
$\mathcal{E}$	Energy density
ρ	Density
ρ^A	Lateral area density
c_0	Sound velocity
C_p	Heat capacity at constant pressure
dE	Change in internal energy
dI	Ion flow
dQ	Change in heat
dW	Work
H	Enthalpy
p	Pressure
S	Entropy
T_m	Melting temperature

Contents

List of Tables

List of Figures

Recommended Reading

As this work is interdisciplinary, the following books are recommended to the reader.

- R. Glaser. *Biophysics: An Introduction*. Springer, 2012.
- E. Fermi. *Thermodynamics*, Dover Books on Physics Series. Dover Publ., 1956.
- L. Debnath. *Nonlinear Partial Differential Equations for Scientists and Engineers*. Birkhäuser, 2005.
- H. Butt, K. Graf, and M. Kappl. *Physics and Chemistry of Interfaces*. Physics textbook. John Wiley & Sons, 2003.

Before brains there was no color or sound in the universe, nor was there any flavor or aroma and probably little sense and no feeling or emotion

—Roger. W. Sperry

1 Introduction

During the last decades, medical implants are broadly accepted to treat advanced neurological disorders. Cochlear implant, which helps deaf people hear and Deep Brain Stimulation (DBS), which relieves the symptoms of Parkinson's diseases has emerged as a potentially life-changing modalities for patients. These both implants of the nervous system work by stimulating nerve cells via an implanted electrode. The efficacy of these implants depends on our understanding of nerve signaling and its interactions with the implant-electrode. Over the past four decades, extensive research (both laboratory and clinical) is being carried out to solve the technical challenges and functional enhancement of these implants. Neurochips are one such laboratory aids to translate the biological neural network signals. However, complications involved in the human and animal research lead to an increased interest in *in silico* studies.

The nerve-electrode interactions can be electro-chemical and electro-mechanical in nature. Therefore, the mathematical modeling of such interactions involves inputs from biology, medicine, physics, chemistry and electrical engineering. Although numerous theoretical models are prevailing in this interdisciplinary research area, explaining the external field due to nerve pulse propagation, an insight into the nerve pulse propagation itself can be rewarding in reaching the goals intended for. Therefore this thesis focuses on both the simulation of coupling of nerve signals with electrodes (neurochip-application) and the nerve pulse propagation from a macroscopic point of view.

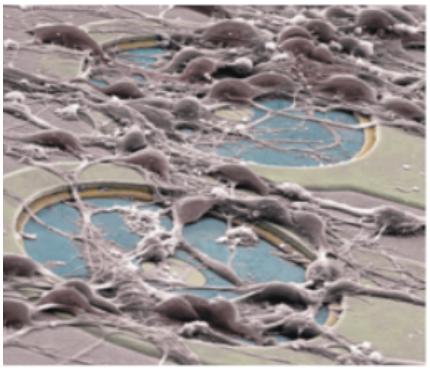

Figure 1.1: Pd-Micro Electrode Array (MEA) of neurochip with cultivated neurons (Courtesy of Biophysics group, University of Rostock, Germany.)

The project is part of the DFG Research Training Group 1505/1 *welisa* in which the DBS and "cochlea implant electrodes" are investigated from a medical, biological, physical and mathematical point of view. Experiments such as recording the activity of neurons cultivated on a neurochip, *in-vitro* stimulation of basalganglian neurons on a neurosensor-chip by the biologists help in determining the modeling parameters of single neuron and neuronal network models. Along with the experiments in medicine and models of DBS, the optimal parameters for DBS shall be optimized and applied.

1.1 Aims of Dissertation

One of the objectives of the research was the numerical modeling and simulation of a three dimensional neuron and neuronal network and its coupling with micro-electrodes within neurochip environment. Initially, the classical mathematical model of neuron is discussed along with its simplifications and models originated from it. Secondly, a three-dimensional model of neuron is proposed based on the classical model, which captures the features like pulse propagation, branching, and collision. The neurochip environment is then realized with a network of neurons using the branching property and the action potentials (AP) are recorded on the electrodes. In the next step, the signals recorded on the electrodes are then sampled into a circuit simulator of a neurochip and compared with the literature values. It is found that our results are qualitatively comparable with the literature. The advantages and drawbacks of the model are discussed.

Further, the classical model is theoretically compared with an emerging alternative model, the soliton model, which is based on the thermodynamics of the nerve membrane. This model is taken up for stability study and shown that it contradicts the conventional knowledge of collision of pulses and is in agreement with the law

of conservation of energy. Furthermore, it is interesting to investigate the electrostatic properties of membrane and the effect of electric field on the membrane state and density. Consequently, a model for the pure zwitterionic and mixed-anionic lipid membranes is proposed with the Poisson-Boltzmann framework with spatial variation of permittivity and orientational ordering of water. The effect of external field on the orientation of lipids is studied and it is found that the membrane state changes with varying electric fields.

In summary, the aim of this work was to develop a neuron model intended for basic study of neurons on a neurochip for DBS and Cochlea implant simulations. Also, the model was expected to be reasonably real, i.e. including the environmental/thermodynamic variables which was then the motivation to take a close look onto the membrane and electrostatics of it. As a result, the soliton model was taken up for developing a model with predictive power.

1.2 Overview

The outline of the thesis is as follows: Chapter 1 serves as an introduction to the work and aims of dissertation. The first part (I) opens with Chapter 2 and reviews the basic neuronal electrophysiology and the Hodgkin-Huxley model. Chapter 3 presents the modified FitzHugh-Nagumo model for pulse propagation and pulse properties are demonstrated through simulations. The basics of numerical calculations using Finite Element Method (FEM) are described there-in. The coupling of 3D- field of axon with the electrodes and the simulations of network of axons in a neurochip is explained in the Chapter 4. We also consider the integrated electronics in the neurochip and discuss the simulation results' relevance with the literature values. The second part (II) sets in with Chapter 5 which reviews the membrane properties: cornerstone of the soliton model and the model itself. Chapter 6 justifies the soliton model with a stability study and a comparison with the classical Hodgkin-Huxley model is carried out. This chapter contains excerpts from [Appali et al.(2010)], [Appali(2012)] and [Lautrup et al.(2011)]. Chapter 7 is dedicated to electrostatic properties of membrane and explains our theoretical models for pure and mixed-anionic lipid membranes. This work is unpublished and carried out with the co-operation of A. Iglic, E. Gongadze, S. Perutkova of University of Ljublijana, Slovenia. Chapter 8 winds up the work by drawing conclusions and indicates possible future work.

Part I

Classical Modeling

The dimmed outlines of phenomenal things all merge into one another unless we put on the focusing-glass of theory, and screw it up sometimes to one pitch of definition and sometimes to another, so as to see down into different depths through the great milestone of the world.

—James Clerk Maxwell

2 Basic Neuronal Electrophysiology

We review basic neuronal electrophysiology and introduce the phenomenological single-compartment neuron model: the Hodgkin-Huxley model. We also discuss the simplified models that have been introduced in the time line. *Note: This chapter contains excerpts from a book chapter authored by me in Advances in Planar Lipid Bilayers and Liposomes (APLBL) [Appali(2012)] and [Appali et al.(2010)].*

2.1 Introduction

Neurons are the basic components of complex nervous systems. These cells are distinctive and perform a variety of functions in different parts of the nervous system. The major features of a neuron are Soma (the cell body), Dendrites (signal receiving ends), Axon (signal transmitter lines) and Synapses (chemical or electrical connectors). Neurons have a wide variety of shapes, sizes and electrochemical properties. The cables enclosing bundles of long and thin projections of neurons, peripheral axons are called as nerves.

The internal features of a typical neuron are similar to those of all eucaryotic cells (or all cells other than bacteria). They contain a nucleus and organelles, each of which is bound by membrane [Arms and Camp(1995)]. The organelles or substructures within a neuron maintain all basic life processes and, in addition, support the specialized functions of receiving, conducting, and transmitting electrochemical signals [Arms and Camp(1995)].A membrane covering the entire neuron isolates it from the environment and is responsible for the information transmission. The study

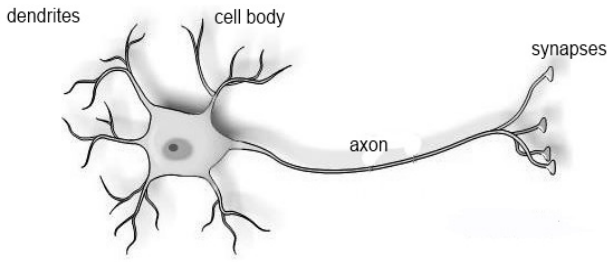

Figure 2.1: Neuron structure with the parts labelled. The direction of pulse propagation is from left to right.

of these action potentials (AP) is useful to understand the information exchange between nerve cells.

2.2 Membrane Potential

The plasma membrane is the border of a neuron and controls the movement of substances into and out of the cell. The membrane is composed of two layers of lipid (fat) molecules (phospholipids, in general). The water-repelling tails of these molecules are pointed towards the middle of the membrane and away from the extracellular and intracellular fluid. Therefore the water-attracting heads of the phospholipid molecules are in contact with extra and intracellular fluid. Proteins are embedded into this bi-lipid membrane (See Fig. 2.2). The extra and intra-cellular fluid typically consists

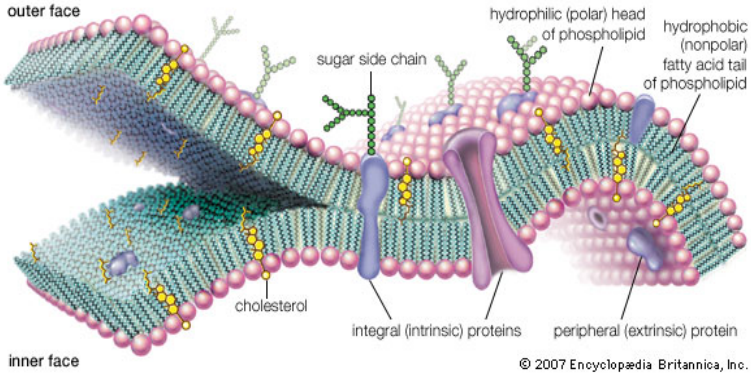

Figure 2.2: Molecular view of the cell membrane. [Art]. In Encyclopdia Britannica. Retrieved from http://www.britannica.com/EBchecked/media/45550/Intrinsic-proteins-penetrate-and-bind-tightly-to-the-lipid-bilayer.

of Na^+, K^+ and Cl^- ions. Sodium (Na^+) and Chloride (Cl^-) are at high concentrations in the extra-cellular region and low in the intracellular regions whereas Potassium (K^+) is at a high concentration inside the nerve cell and low at outside. The differences in the concentration of ions on each side of the membrane leads to a voltage called *Membrane potential*. The proteins act as selective ion transporters and lead to this concentration difference. Membrane potential can also stem from diffusion and electric force other than the active transport due to proteins. Diffusion is the process of compensating the lower concentration region by ion transport from high concentration region to attain neutral state. The unbalanced sodium charges outside the cell and potassium charges inside the cell line up on the membrane surface and attract each other across membrane. Electric force arises from the separation of these charges across the membrane and leads to membrane potential. A point at which the electric field completely counteracts the force due to diffusion is called as equilibrium potential or resting potential or Nernst potential. At this point, the net flow of a specific ion is zero. Figure 2.3 shows a section of the membrane acting as a barrier between positive and negative ions resulting in voltage across the membrane.

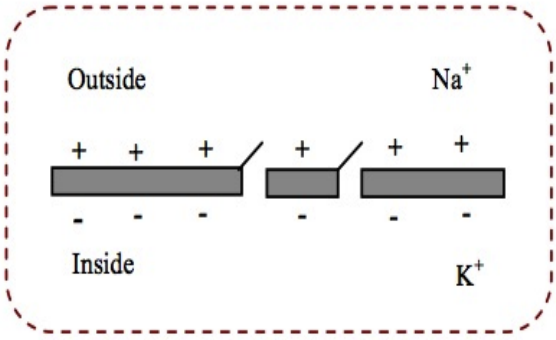

Figure 2.3: The nerve membrane separates the charge carrying ions and the potential difference results in membrane potential (modified from [Gerstner(2002)]).

The resting potential of a neuron is -70 mV. This varies for different type of cells.

Definition 1 (Membrane Potential) *The potential difference between the inner and outer of membrane is Membrane potential (V_m)*

$$V_m = V_i - V_o \tag{2.1}$$

where V_i is the potential at inner side of membrane and V_o is the potential at outer side of membrane.

The membrane potential depends on the ion movement across the membrane. This can be explained by the Goldman equation:

$$V_m = \frac{g_{Na}E_{Na} + g_K E_K + g_{Cl}E_{Cl}}{g_{Na} + g_K + g_{Cl}} \tag{2.2}$$

where g_{Na}, g_K, g_{Cl} are the conductivities of ions and E_{Na}, E_K, E_{Cl} are the Nernst potentials for involved ions (Na, K, Cl) denoted by j.

$$E_j = \frac{RT}{z_j F} ln\left(\frac{{c_j}^o}{{c_j}^i}\right) \tag{2.3}$$

with temperature as T, gas constant R, Faraday's constant F, z_j is the valence of ions j, ${c_j}^o$ is the concentration of ions outside the membrane and ${c_j}^i$ is the concentration of ions inside the membrane. For example, the membrane potential for sodium and potassium ions at equilibrium, when measured from outside to inside is

$$E_{Na} = \frac{RT}{z_{Na}F} ln\left(\frac{{c_{Na}}^o}{{c_{Na}}^i}\right) = 55mV, \;\; E_K = \frac{RT}{z_K F} ln\left(\frac{{c_K}^o}{{c_K}^i}\right) = -75mV \tag{2.4}$$

These are the resting potentials of sodium and potassium ions and since the concentration of potassium ions is high inside the membrane, the resting potential of neuron is considered to be -70 mV.

2.3 Action Potentials and Propagation

The rapid rise and fall of membrane potential, following a consistent trajectory in the cell membrane is called action potential. As mentioned earlier, in neurons, the action potential plays a key role in information transmission. Action potential is often referred as *nerve pulse* or *spike* in neurons. The proteins which are embedded in the membrane are thought to be responsible for this event. They assume different conformations and allow specific ions to pass-through them, thus acting as voltage-gated ion channels. Their conformation transitions is dependent on membrane potential and vice versa.

The polarized membrane of the *soma (cell body)* receives the depolarizing stimulus from *dendrites* and the action potential is propagated along the *axon* mediated by the ion-channels distributed along it. At the synapse, the electrical signal is converted to a chemical signal and is then conducted to the post-synaptic neuron. The depolarization of membrane and the phases of action potential is as follows (see Fig. 2.4): The

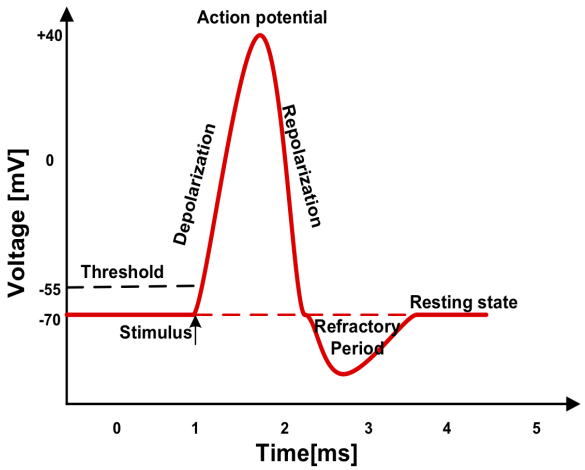

Figure 2.4: Action potential as a consequence of stimulus to the membrane potential and its phases.

membrane at rest when impinged by a stimulus opens up the Na^+ channels allowing sodium ions to enter the neuron. The increase in positive ions inside the cell depolarizes the membrane potential and brings it to reach the threshold potential. This opens up more sodium channels and voltage across the membrane rapidly reverses and reaches its most positive value. This phase is called *rising/depolarization* phase. At the peak of the action potential, many of the voltage-gated sodium channels begin to close and simultaneously, many more K^+-channels open allowing positive charges to leave the cell. This causes the membrane potential to fall back to its resting state. This phase is termed as *re-polarization*. The membrane re-polarizes beyond the resting state as a consequence of more number of open potassium channels. The return to steady state continues as the potassium channels close. This phase is known as *refractory period/recovery phase*.

2.4 The electrical model : Hodgkin-Huxley Model

The current understanding of neural excitability is remarkably influenced by the phenomenal work of Hodgkin and Huxley [Hodgkin and Huxley(1952a)]. Their five articles published in 1952 demonstrated the key properties of ionic conductances underlying the nerve action potential. For this outstanding achievement, Hodgkin and Huxley were awarded the 1963 Nobel Prize in Physiology and Medicine. The first four papers of Hodgkin and Huxley summarize the new experimental techniques for characterizing membrane properties. In the final paper, the complex experimental data was placed into an extensive theoretical framework. This theoretical framework that forms the cornerstone of our present-day views of neural excitability will be discussed in this section.

Hodgkin and Huxley studied the conductance properties of nerve axons from squid in voltage-clamp experiments [Hodgkin and Huxley(1952a)]. In such experiments an electrode is inserted into a nerve axon such that the voltage difference between inside and outside is constant along the whole axon. Under such conditions no pulse can propagate. The voltage-clamp experiments by Hodgkin and Huxley showed that a stepwise depolarization (reduction of trans-membrane voltage) of the membrane by electrodes first triggered an inward current (against the applied field) followed by an outward current (along the external field). With the aid of ionic substitution, they demonstrated that the net current could be separated into two distinct components: a fast inward current carried by Na^+ ions, and a more slowly activated outward current carried by K^+ ions. They concluded that these two currents result from independent permeation mechanisms for Na^+ and K^+ involving time and voltage dependent conductances of particular objects in the membrane. This new concept was named the 'ionic hypothesis' [Haeusser(2000)].

In the Hodgkin-Huxley picture, three different ion currents contribute to the voltage signal of the neuron, i.e., a sodium current, a potassium current, and a leak current that consists mainly of Cl^- ions. The flow of these ions through the cell membrane is controlled by their respective voltage-dependent ion channels. The leak current also takes care of other channel types which are not described in particular. The most remarkable achievement of this theory was the self-consistent agreement of the experimental voltage-clamp data (in the absence of a pulse) with a quantitative model for the propagating nerve pulse [Hodgkin and Huxley(1952b)], which made it the very first complete description of the excitability of a single neuron.

The schematic diagram for the electrical circuit in the voltage-clamp experiment is shown in Fig. 2.5. The lipid membrane is considered an insulator that acts as a capacitor with constant capacitance, C_m. The proteins are considered being resistors

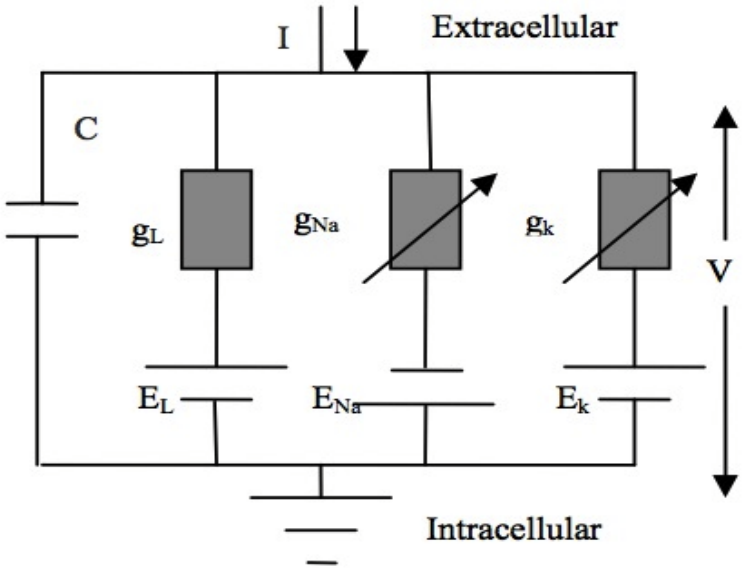

Figure 2.5: Schematic diagram of Hodgkin-Huxley circuit.

described by conductances g_i (i being the index for a particular channel and ion). Upon change of voltage, V_m, two currents can be observed - a capacitive current charging the capacitor and Ohmic currents through the protein. The total current through the membrane, I_m, is the sum of these two currents. The time-dependent membrane current I_m is given by following equation:

$$I_m(t) = C_m \frac{\mathrm{d}V_m}{\mathrm{d}t} + g_{Na}(V_m - E_{Na}) + g_K(V_m - E_K) + g_L(V_m - E_L) \tag{2.5}$$

The last term in this equation accounts for small leak currents and will be omitted in the following. The quantities E_{Na}, E_K (and E_L) are the Nernst potentials of the different ions. The concentrations of ions on the inner and outer side of the cell (c_{in} and c_{out}) are different (K^+ concentrations of the giant squid are 400 mM inside and 20 mM outside. Na^+ concentrations are 50 mM and 440 mM, respectively [Johnston and Wu(1995)]). As a consequence, currents flow even in the absence of an external voltage due to diffusion along the gradients. This is taken into account by the Nernst potentials by the Eq. (2.3). If the external voltage is equal to the Nernst potential, no current flows. The Nernst potentials are different for different ions.

The functions g_{Na} and g_K are the conductances of the ion channel proteins for the respective ions. They are assumed to be functions of voltage and time. Hodgkin and Huxley parametrized these conductances by using their voltage clamp data in

the following manner:

$$\begin{aligned} g_{Na} &= g_{Na,0} \cdot m^3 \cdot h \\ g_K &= g_{K_0} \cdot n^4 \end{aligned} \tag{2.6}$$

introducing the functions $m(V_m, t)$, $h(V_m, t)$ and $n(V_m, t)$ that depend on voltage and time. These functions range between zero and one and are related to the likelihood that the channel is open. If $m^3 \cdot h = 1$, the sodium channel is open and conducts with the characteristic conductance $g_{Na,0}$. If $n^4 = 1$, the potassium channel is open and conducts with its characteristic conductance $g_{K,0}$. The functions m, h and n are called 'gating variable'. Each of them follows a simple linear differential equation after changing voltage yielding an exponential relaxation in time:

$$\begin{aligned} \frac{dm}{dt} &= \alpha_m(V_m)(1-m) - \beta_m(V_m)m \\ \frac{dn}{dt} &= \alpha_n(V_m)(1-n) - \beta_n(V_m)n \\ \frac{dh}{dt} &= \alpha_h(V_m)(1-h) - \beta_h(V_m)h \end{aligned} \tag{2.7}$$

The newly introduced functions $\alpha_m(V_m)$, $\alpha_h(V_m)$, $\alpha_n(V_m)$ and $\beta_m(V_m)$, $\beta_h(V_m)$ and $\beta_n(V_m)$ are voltage dependent rate constants that cannot be derived by any theory. Instead, they are fitted to experimental data. Each of the rate constants requires several parameters to obtain an empirical fit. All together, one has more than 20 empirical fit parameters. This indicates that the Hodgkin-Huxley model is not a theory based on first principles but rather a parametrization of the electrical features of the membrane.

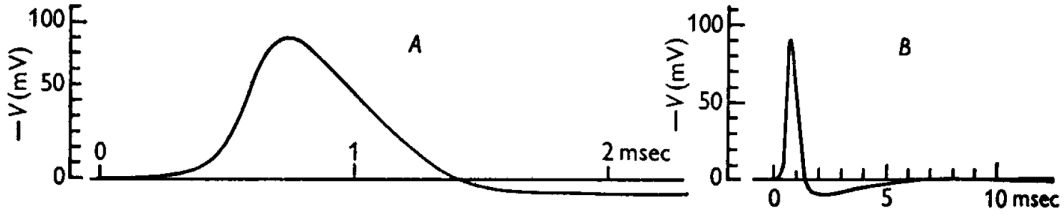

Figure 2.6: Action potential in squid axons as simulated by Hodgkin and Huxley in 1952. The pulse in two different time windows is shown. From [Hodgkin and Huxley(1952b)].

The propagating action potential is now calculated by combining Eq. (2.5) with cable theory (Fig. 2.6). Using Kirchhoff's laws, cable theory describes the spreading

of a voltage along a cylindrical membrane as a function of distance x, the specific resistance of the membrane (R_m) and the specific inner resistance of the intracellular medium along the cable (R_i). A central equation originating from cable theory [Tuckwell(1988)] is

$$\frac{\partial^2 V_m}{\partial x^2} = \frac{2R_i}{a} I_m \tag{2.8}$$

for a cable with radius a, which together with Eq. (2.5) yields

$$\frac{\partial^2 V_m}{\partial x^2} = \frac{2R_i}{a}\left(C_m \frac{\mathrm{d}V_m}{\mathrm{d}t} + g_{Na}(V_m - E_{Na}) + g_K(V_m - E_K)\right) \tag{2.9}$$

Finally, it is assumed that a pulse exists that propagates with constant speed θ independent of voltage. This implies that the wave equation

$$\frac{\partial^2 V_m}{\partial t^2} = \theta^2 \frac{\partial^2 V_m}{\partial x^2} \tag{2.10}$$

can be used. Combining Eq. (2.10) with Eq. (2.9) yields the final equation for the propagation of the electrical pulse:

$$\frac{a}{2R_i\theta^2}\frac{\partial^2 V_m}{\partial t^2} = C_m \frac{\mathrm{d}V_m}{\mathrm{d}t} + g_{Na}(V_m - E_{Na}) + g_K(V_m - E_K) \tag{2.11}$$

This partial differential equation has to be solved and yields the Hodgkin-Huxley action potential.

The HH model can reproduce a wide range of data from squid axon, for instance the shape and propagation of the action potential (see Fig. 2.7), its sharp threshold, its refractory period and the hyper-polarization. However, it has to be noted that the model contains a hidden complexity since the conductances are empirical functions of voltage and time that were parametrized from experiment (see above).The HH model can also describe many channel types with small parameter changes indicating the generality of the approach. Thus, the HH model links the microscopic level of ion channels to the macroscopic level of currents and action potentials. The detailed dynamics of HH model can be read in Hodgkin and Huxley series of papers. However due to the non-linearity and 10 differential equations, this model takes greater computational time and power to simulate.

The Hodgkin-Huxley description of dynamics of membrane potential and voltage-gated conductances can be reduced to one-dimensional and two-dimensional systems. When all the trans-membrane conductances have fast kinetics then the system is said to be one-dimensional. Such systems establish a bridge between electro-physiology

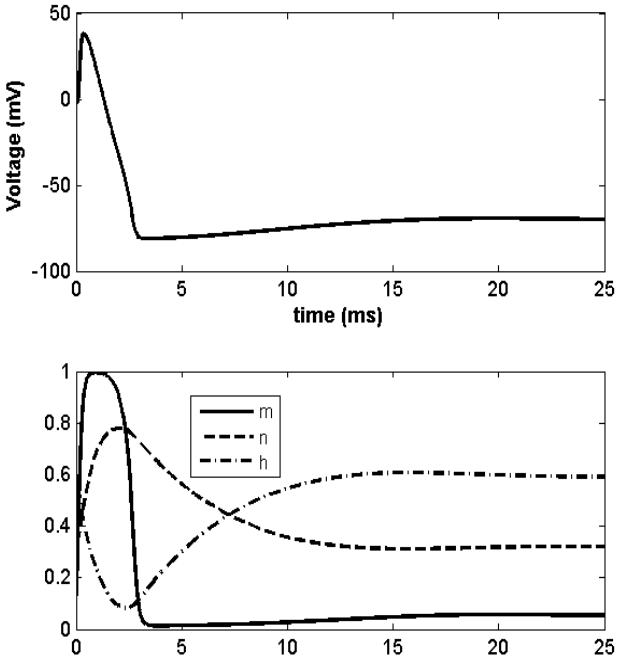

Figure 2.7: Hodgkin-Huxley action potential solved by using Matlab with membrane capacitance C =1 $\mu F/cm^2$, g_{Na}=120 m^3h, g_K=36 n^4 and with data and definitions as in [Hoppensteadt1997].

and dynamical systems. While the two-dimensional systems are useful for mathematical analysis using phase-portraits and capture the essence of neuronal behavior. In all these systems, the parameters (having biophysical meaning) must be measured experimentally for different neurons, they should be averaged and then arbitrary choices have to be made. This is a major drawback and there is no guarantee that the model exhibits the same kind of behavior as the type of neuron under consideration. In addition, it is not always possible to measure these parameters for specific neuron to have a conductance-based model. Thus, a general model that reproduces all the neurocomputational features of the neuron is feasible. With this motivation, several simplified models have been derived from Hodgkin-Huxley model depending on their neuron of interest such as FitzHugh-Nagumo model [FitzHugh(1961), Nagumo et al.(1962)], Hindmarsh-Rose model [Hindmarsh and Rose(1984)], Morris-Leccar Model [Morris(1981)] and Rajagopal-model [Rajagopal(1983)]. Such models are widely used in simulating the neural networks in order to rationalize experimental data.

Simplest models like *Integrate-and-fire* and *Resonate-and-fire* [Keener and Sneyd(1998)] neurons capture the essence of integrators and resonators respectively. These models are idealization of neurons only having leakage current and all the voltage-gated currents are de-activated at rest. Both models are linear and are useful in analytical analysis. These models are not quite useful fo computational neuroscientists who want to simulate network of neurons [Keener and Sneyd(1998)].

Therefore, in the context of our project we need computationally efficient, as simplest models, yet as biophysically plausible as Hodgkin-Huxley type model. In the next chapter, such model based on the FitzHugh-Nagumo model will be presented in detail.

2.5 Digest

- Neurons are the core-components of nervous system. They are specialized cells performing variety of functions in different parts of nervous system.
- The plasma membrane forms the envelope of a neuron. The difference in the concentration of ions on each side of the membrane leads to membrane potential.
- A nerve pulse is the rapid rise and fall of the membrane potential often called as action potential.
- Hodgkin and Huxley conceptualized the ionic hypothesis for the action potential propagation in nerves.
- This model was the very first complete description of the excitability of a single neuron.
- The complexity of the model lead to several simplifications in the time-line.
- One- and two-dimensional systems can be deduced from the Hodkin-Huxley model depending on the kinetics of conductances.

Model building is the art of selecting those aspects of a process that are relevant to the question being asked.

– J.H Holland

3

3D Field Simulation of Single Axon

3.1 Introduction

The behavior of the Hodgkin-Huxley model (Eq. (2.5) and Eq. (2.7)) can be understood by having a closer look onto the model variables: V, m, n and h. Some of the model variables have fast kinetics, while others are much slower [Keener and Sneyd(1998)]. Precisely, as the membrane potential changes quickly and Na^+ channel activates fastly, V and m are the fast variables. Where as Na^+-channel inactivation and K^+-channel activation are slow processes, n and h are slow variables. These slow variables stay constant in the initial phase of the action potential, while the fast variables are varying.

Based on this fact, FitzHugh fixed the slow variables and considered the model's behavior as a function of the two fast variables which led to a two variable model, called the *fast-slow phase plane model*. In the following sections, we will discuss the FitzHugh-Nagumo model in detail and proceed to simulate a single axon and the electric field during action potential propagation.

3.2 Analysis of Neuron Models

Neuron models are dynamical systems. The basic definitions and classical methods that are used in the analysis of neuron models are listed below for better understanding [Izhikevich(2007)].

- *Dynamical System*: A mathematical concept in which a set of variables describe the state and a law/function describes the evolution of the state variables with time.

For example, activity of a single neuron for the state variables (i) membrane potential, (ii) excitation variable and (iii) recovery variable and the evolution rule can be either HH model, FHN model and so on.

- *Dimensions*: The number of state variables identified for an application decides n (dimension number) in the n-dimensional system of ordinary differential equations.

Example: If the state of neuron is described by membrane potential (V_m) and activation variable, m, of the persistent Na^+ current then the evolution law would be a 2-dimensional system of ordinary differential equations describing the dynamical system.

- *Phase diagrams*: A mathematical technique for studying the dynamical systems. The axes of phase diagram are the *state variables*. The solutions of ordinary differential equations describe the trajectories in the phase space. Units of *time* is plotted along the trajectory. The phase portrait helps in understanding the dynamics of the system.

For the example given above, the phase diagram for a neuron at rest will have stable equilibrium point usually denoted as an attractor. Where-as for an active neuron, shows the response of state variables for input stimuli as shown in following figure 3.2. For a spiking neuron, the phase portrait exhibits a periodic spiking activity known as stable perioidic orbit. The neuron can be switched from equilibrium to periodic spiking by a transient input and this transition is called *bifurcation* which corresponds to a qualitative change of phase portrait. Neurons are excitable as they are near bifurcations from resting state to spiking activity. The type of bifurcation determines the excitable properties of the neuron. For further details on types of bifurcations refer to [Izhikevich(2007)].

3.3 FitzHugh-Nagumo Model

In his papers [FitzHugh(1961), FitzHugh(1962)], Richard FitzHugh has given elegant qualitative description of HH model that allows a better understanding of the model's behavior. He pioneered such two-dimensional neuronal models and their phase plane analysis which helped in better understanding of neuronal behavior. His approach of fast and slow variables is useful to study the excitation processes and the propagation. Let us look into the simplification of HH model through FitzHugh's point of view.

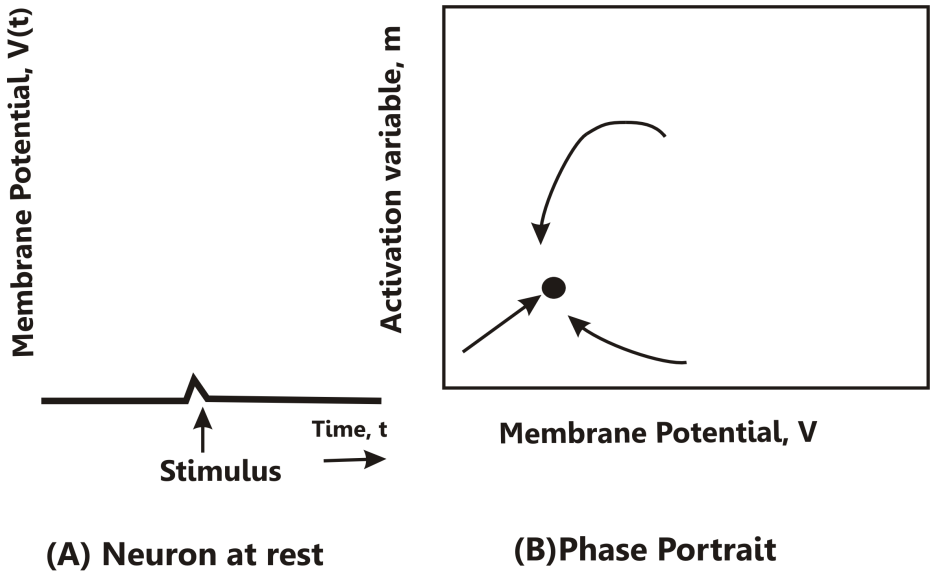

Figure 3.1: A neuron at rest with its phase portrait showing the equilibrium point (Adapted from [Izhikevich(2007)]).

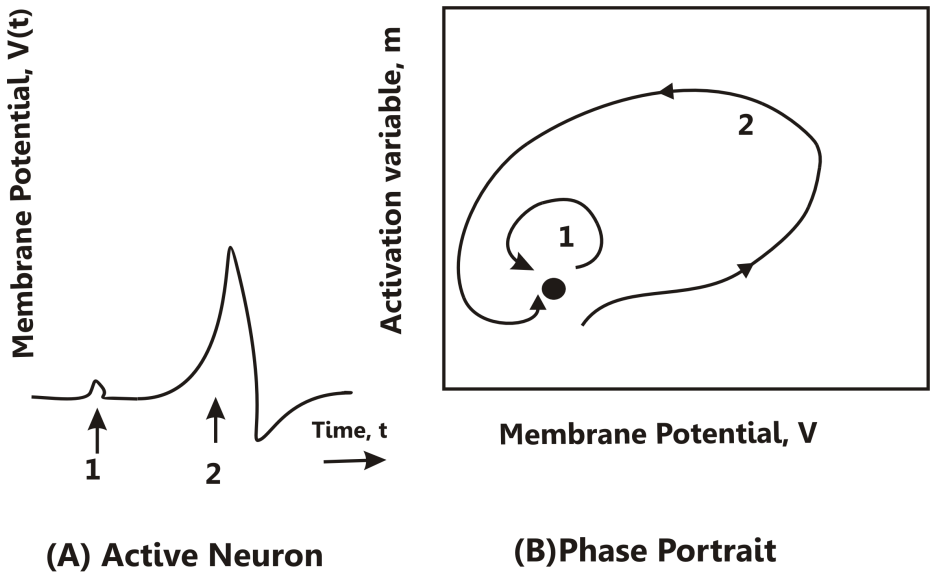

Figure 3.2: A neuron with external stimuli leading it to spike along with its phase portrait (Adapted from [Izhikevich(2007)]).

3.3.1 The Fast-Slow Phase-Plane Model

[Keener and Sneyd(1998)] When the slow variables, n and h are fixed at their resting states, say n_0 and h_0 then the HH model's differential equations (Refer Eq. (2.5),

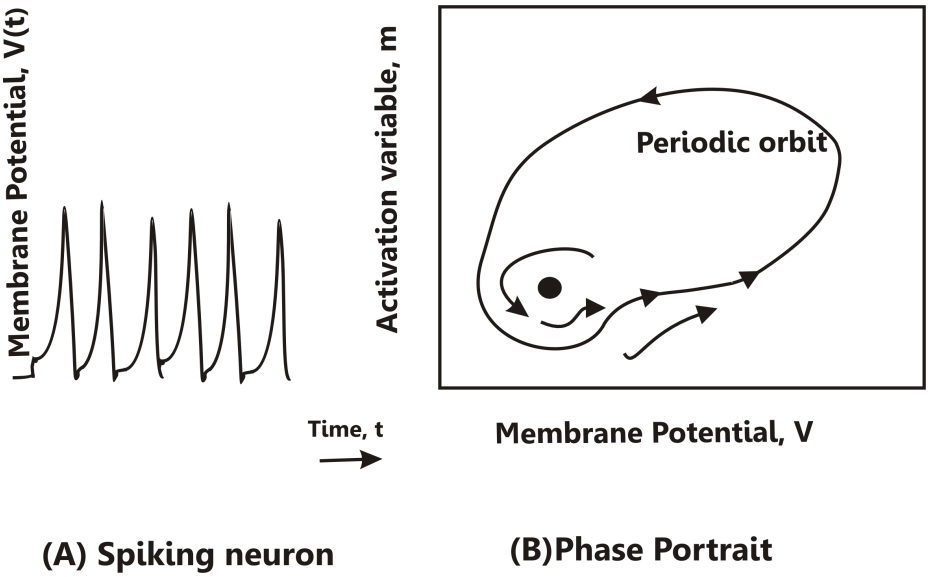

Figure 3.3: A spiking neuron with constant current input and its phase portrait showing the periodic orbit (Adapted from [Izhikevich(2007)]).

(2.7), (2.8)) shows how m and V behave in response to the stimulation. These are then the equations for *fast phase-plane* given by

$$\begin{aligned} C_m\frac{dV}{dt} &= -g_{Na}m^3h(V_m - E_{Na}) + g_K n_{0^4}(V_m - E_K) + g_L(V_m - E_L) \\ \frac{dm}{dt} &= \alpha_m(1-m) - \beta_m m \\ \equiv \tau_m\frac{dm}{dt} &= m_\infty - m \end{aligned} \tag{3.1}$$

where m_∞ is m-nullcline curve. This is now a two-dimensional system and can be studied on the (m, V) phase-plane. [1] However, if we take a different cross-section involving one fast-variable and one-slow variable we can highlight the other aspects of the action potential. This will result in a description of HH model that has been proven extremely useful, FitzHugh-Nagumo model. Assume that the activation of Na^+ conductance acts on a faster time scale than that of voltage, then we can extract a single fast variable by taking m as an instant function of V, thereby $m = m_\infty$ at all the times. FitzHugh also observed that during the course of an action potential, $h + n \approx 0.8$. Using this h can be eliminated by setting $h = 0.8 - n$. Now the *fast-slow*

[1] Detailed analysis of the phase plane portrait of this system is beyond the scope of this work. Please refer [Keener and Sneyd(1998)] for more details about this model.

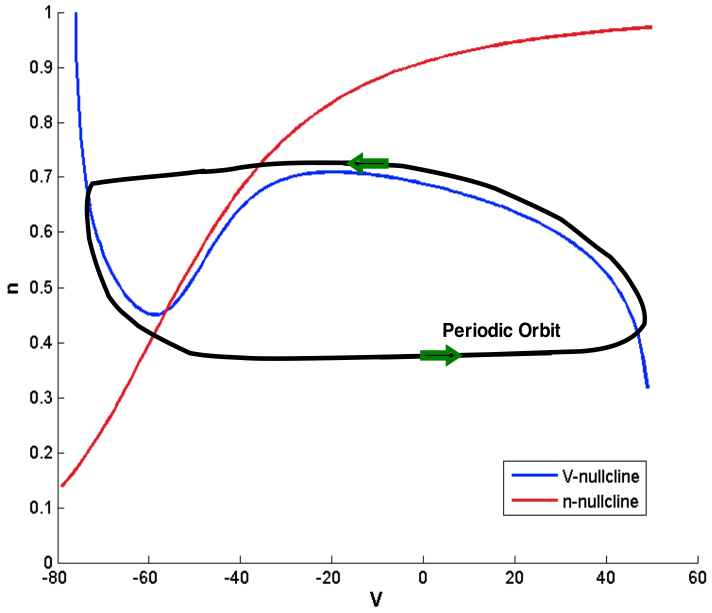

Figure 3.4: The nullclines for fast-slow system. The V-nullcline is in blue and n-nullcline in red.

model is given by (with added stimulating current on RHS):

$$C_m \frac{dV}{dt} = I - g_{Na^-} m_\infty^3(V)(0.8-n)(V_m - E_{Na}) - g_{K^-} n_{0^4}(V_m - E_K) - g_{L^-}(V_m - E_L)$$
$$\frac{dn}{dt} = \alpha_n(1-n) - \beta_n n \tag{3.2}$$

A plot of the nullclines of the fast-slow system is given in Fig. 3.4. The V-nullcline, defined by $f(V,n) = 0$ and has a cubic shape, while the n-nullcline is $n_\infty(V)$ and is linearly increasing. The nullclines intersect each other once and thus there is a single steady state. The V-nullcline is called the *"slow-manifold"* along which the solution moves slowly in the direction depending on the sign of dn/dt. Away from the slow-manifold the solution moves quickly in horizontal direction. This representation of the HH model in terms of fast-slow variables is the basis of the FitzHugh-Nagumo (FHN) model. FHN model presents the fast-slow phase-plane in a simplified form. The two variables of FHN model are fast(V) and slow(w). Here V mimics the membrane voltage and the recovery variable w mimics the activation of an outward current. I mimics the injected current. Parameter a describes the shape of cubic parabola and

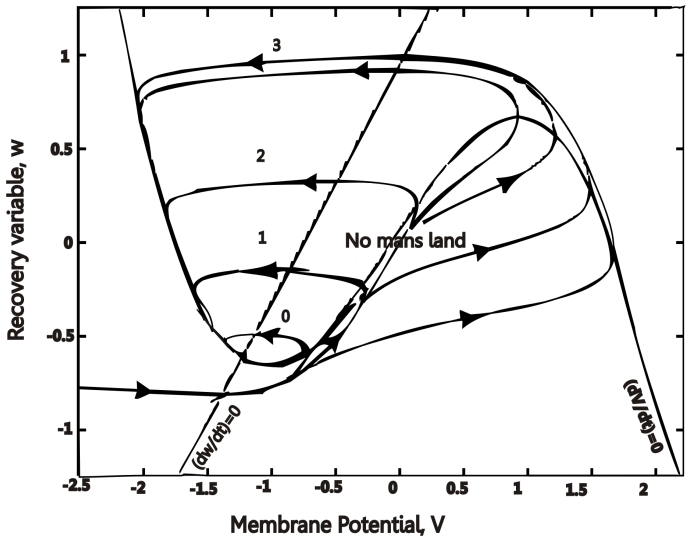

Figure 3.5: Phase plane protrait of FHN model(modified from [FitzHugh(1961)]).

parameters $b > 0$ and $c \geq 0$ describe the kinetics of recovery variable.

$$\frac{dV}{dt} = V(a - V)(V - 1) - w + I$$
$$\frac{dw}{dt} = e(bV - cw) \tag{3.3}$$

The nullclines of FHN model are given by

$$\frac{dV}{dt} = 0 \rightarrow w = V(a - V)(V - 1) + I$$
$$\frac{dw}{dt} = 0 \rightarrow w = \frac{b}{cV} \tag{3.4}$$

There are many equivalent forms of the system Eq.(3.3) [Izhikevich(2004),Keener and Sneyd(1998)].The fast variable (V) has a cubic nullcline and is called the excitation variable, while the slow variable (w) is called the recovery variable and has a nullcline that is monotonically increasing. The nullclines of FHN model are shown in the figure 3.5. They have a single intersection point at the origin $(0, 0)$ when $I = 0$ [Keener and Sneyd(1998)]. The intersection may occur on the left or middle branch of the cubic V-nullcline depending on the sign of parameter a. Figure 3.5 depicts the phase portrait of the FHN with its nullclines and some typical trajectories emerging due to various initial conditions. The trajectories with numbering $0, 1$ and 2are the result of a weak stimulus (I), whereas the trajectories 3, 4 are the result of stronger stimulus. When I is weak or zero, the equilibrium is on the left branch (stable) of V-nullcline and the

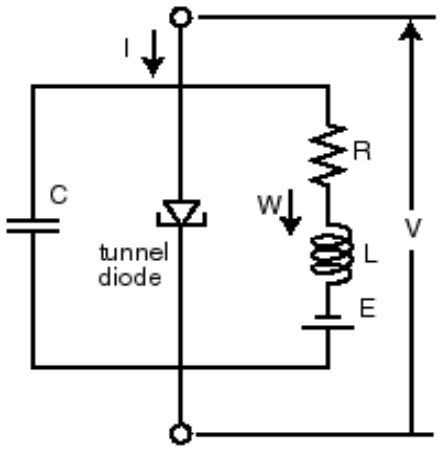

Figure 3.6: Circuit diagram of FHN neuron model from [Nagumo et al.(1962)].

neuron is at resting state. An increase in I shifts the V-nullcline upwards along the w-nullcline and shifts the equilibrium onto the middle branch of the nullcline. This phase space is called as the *no man's land* and is unstable. The neuron exhibits periodic spiking in this region. Further increase in I shifts the equilibrium onto the right stable branch of V-nullcline and the spiking is blocked. The simplicity of this model allows to view the entire solution at once. An electronic circuit using a tunnel diode (see Fig.3.6) serves as an equivalent circuit for the model. This was built by Nagumo in 1962 [Nagumo et al.(1962)] thereby the model named as FitzHugh-Nagumo Model.

3.4 Spatial FitzHugh-Nagumo Model

The FHN model explained above are expressions of inward and outward currents (radial currents) for any arbitrary point along the axon. Radial currents are due to voltage gated ion channels. The current in the direction of axon, axial current is not taken into account. The propagation pulse can be achieved by combining FHN equations with cable theory, as explained in the previous chapter for HH model Eqs.(2.8), (2.9). The radial currents and axial current are related and the propagating FHN is given as:

$$\frac{\partial^2 V}{\partial z^2} = \frac{2R_i}{a}(C_m \frac{\mathrm{d}V}{\mathrm{d}t} + V(a - V)(V - 1) - w) \tag{3.5}$$

It describes the spreading of a voltage along a cylindrical membrane as a function of distance z, the specific inner resistance of the intracellular medium along the cable

(R_i) for a cable with radius a. Assuming capacitance minimally dependent on membrane potential ($C_m = 1$) and setting the expression $2R_i/a = 1$ yield the spatially distributed FHN model with voltage variable $V(z,t)$ and recovery variable $w(z,t)$ and time $t > 0$ [FitzHugh(1962)]

$$\frac{\partial V}{\partial t} = D_1 \Delta V + V(a - V)(V - 1) - w \tag{3.6}$$

$$\frac{\partial w}{\partial t} = D_2 \Delta w + e(bV - cw - d) \tag{3.7}$$

with $\Delta V, \Delta w$ as diffusion terms, a- excitation threshold, e- excitability, b, c, d are the parameters effecting the resting state and dynamics of the system. The quantities e, c, D_1 and D_2 are positive and usually considered to be constants, although they could vary with both space variables and t. The parameter d can be positive or negative. Initial and boundary conditions must also be specified. Note that the input signal $I(z,t)$ is not considered in the equation. In many applications, $D_1 = 1$ and $D_2 = 0$. Note that the model is a dimensionless system [FitzHugh(1962)]. This model is useful in realizing different traveling waves depending on the choice of parameters of the system.

3.4.1 Significance

The FHN equations qualitatively show the action potential course as the HH equations. In addition, the spatial extension of FHN equation describes the propagation of action potential. The model exhibits traveling pulses in 1D, spiral waves in 2D as well as other phenomena in 3D. Moreover, it serves as a generalized biological model of neuron when compared to Morris-Lecar model [Morris(1981)] which is particularly useful for fast-spiking neurons like pyramidal neurons of neocortex (bursting neurons). It is obvious from the previous material that mathematical modeling of a real neuron is a quite challenging task, depending on the details we intend to show. Table 3.1 provides a comparison of HH and FHN model in the context of model selection for the simulation of action potential propagation.

Table 3.2 give a synopsis of models considered for action potential propagation in an axon.

The methods and parameters used to simulate the action potential propagation using system Eq.(3.4) will be explained in the following section.

Table 3.1: Comparison of HH and FHN models for the simulation of action potential propagation in an axon

Model	HH	FHN
Type	Detailed, conductance based	Detailed, conductance based
Dimensions	Four	Two
Solution on Phase-plane	No	Yes
Non-linearity	Highly	Comparitively less
Numerical simulation	Not effective	Effective
Neural network	Not plausible	Plausible

Table 3.2: Comparison of FHN, Morris-Lecar(M-L) and Hindmarsh-Rose (H-R) models for the simulation of action potential propagation in an axon

Model	FHN	M-L and H-R
Type	Detailed, conductance based	Specific, conductance based
Dimensions	Two	Two
Solution on Phase-plane	Yes	Yes
Non-linearity	Comparatively less	Linear
Numerical simulation	Effective	Possible
Neural network	Plausible	Plausible

3.5 Methods

The spatial FHN model of the following form is used for the numerical simulation of action potential propagation in an axon.

$$\frac{\partial V}{\partial t} = \Delta V + V(a - V)(V - 1) - w$$
$$\frac{\partial w}{\partial t} = e(bV - cw - d) \tag{3.8}$$

with axon's radius taken into consideration. The commercial software tool, Comsol Multiphysics 4.2a® is used to solve the system of partial differential equations. This software is based on the computational technique of Finite Element Method (FEM). FEM is a method of piecewise approximation, i.e. the bounded domain is divided into finite number of non-overlapping elements, usually triangular or rectangular in 2D and tetra- or hexahedral elements. Over these elements the functions are approximated by trial functions (usually polynomials). The boundary conditions are applied both locally and at the edge of the element and globally along the continuum boundary. The variational form of the system, involving an integral of differential equation

over the domain is approximated by the linear combination of a finite set of trial functions. The steps involved in solving a partial differential system by Galerkin FEM are [vanRienen(2001)]:

- *Discretization*: The partitioning of computational domain into finite set of elements. Each element possesses a set of distinguishing points called *nodes*.
- On each element a trial function is assigned and the approximate solution is supposed to be the linear combination of these trial functions.
- Weighted-integral formulation of the differential equation over the finite element is derived using "Galerkin method", the method of weighted residuals.
- *Assembly*: The global system of algebraic equations is obtained by assembling the equations on each element.
- The boundary conditions are imposed onto the assembly.
- Lastly, the system of algebraic equations is solved to find the approximate values of global partial differential system.

The FHN system Eqs.(3.5) were solved in the partial differential equation (pde)-mode of Comsol Multiphysics 4.2a® using the time dependent direct solver PARDISO. The subdomain equation in the general pde-mode of Comsol Multiphysics® is:

$$e_a \frac{\partial^2 u}{\partial t^2} + d_a \frac{\partial u}{\partial t} + \nabla \cdot \Gamma = f \tag{3.9}$$

with e_a as mass coefficient, d_a as damping coefficient, f is source term and Γ is the conservative flux. This equation is modified to adapt the FHN system. The axon's geometry (Fig. 3.7) is taken as a three-dimensional cylinder with a radius (a) of $0.5mm$ (squid-giant axon [Hodgkin and Huxley(1952a)]) and length (L) of $8mm$(along z-axis) with all the other parameters and variables in dimensionless form. For reducing the complexity of fitting parameters, an axon of such a diameter is chosen as a first step. Due to the inclusion of membrane dynamics, biological parameters like axon-diameter is neglected in this simulation. In a standard one-dimensional approach the axon radius should be definitely considered. The FHN system is rearranged in the form of the subdomain equation (3.5) by taking $e_a = 0, d_a = 1$ and right hand side of FHN system as the source term f.

The simulations are performed with a time dependent solver assuming zero flux (insulation) as the boundary condition of the axon i.e. there is no current flowing into or out of the axon. The initial condition defining the initial potential distribution,

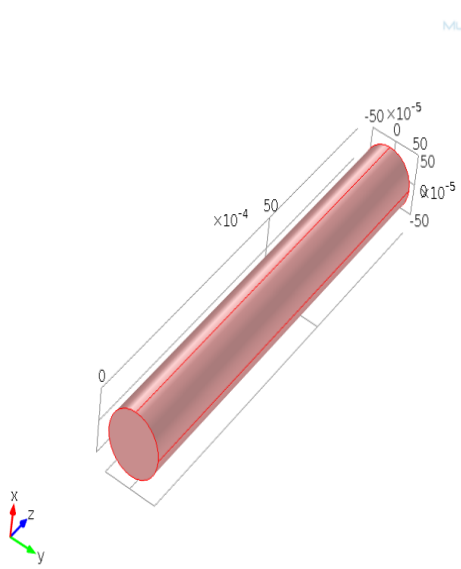

Figure 3.7: Geometry of the axon used to implement the FHN model in Comsol Multiphysics 4.2a®.

.

with elevated values of $V_0 = 1$, $w_0 = 0.5$ are distributed at a position $z = 7.9\ mm$ on the length of the axon. This is implemented with the following logical expression in the initial distribution, where TRUE evaluates to 1 and FALSE to 0.

$$\begin{aligned} V(0, x, y, z) &= V_0(z > 7.9 \times 10^{-3}) \\ w(0, x, y, z) &= w_0(-z > 7.9 \times 10^{-3}) \end{aligned} \tag{3.10}$$

The propagation of the action potential is along the length of the axon (z-axis in the simulation model). Diffusion is considered only in this direction.The cylindrical structure is in 3D, therefore the mesh has tetrahedral elements. The cylinder was discretized by using free tetrahedral mesh consisting of $41,290$ elements in the volume and $6,146$ triangular elements at the end planes (Fig. 3.8).

The relation among the parameters b, c and d is given by [Phillipson(2005)], [Zhao(2010)], [FitzHugh(1962)]

$$\begin{aligned} 0 \leq a \leq \frac{1}{2} \\ 0 < b \leq 1 \\ c \geq 0 \\ c = 2.54b \end{aligned}$$

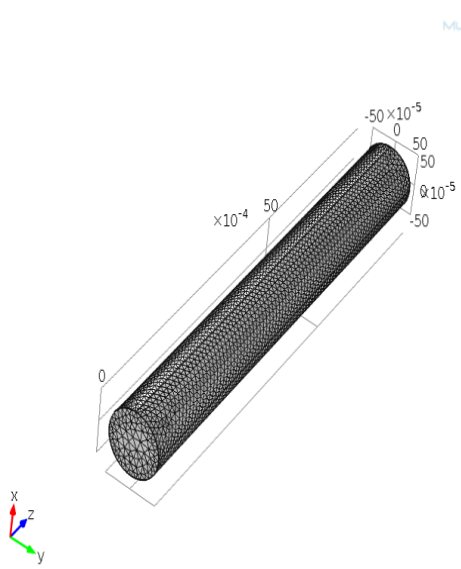

Figure 3.8: Simulation model with the finite element discretization.

(3.11)

Parameter b is essentially in the range of 0.001 to 0.007 [Zhao(2010)]. The list of parameters used in the simulation of action potential propagation without diffusion are

Table 3.3: Parameters used in the model

Name	Value	Description
a	0.01	Excitation threshold
b	0.002	System parameter
c	2.54 b	System parameter
d	0	System parameter
e	1.8	Excitability

3.6 Simulation Results

Numerical simulations were carried out without external input signal and without spatial diffusion with respect to the boundary conditions. The action potential propagation with and without diffusion term in the FHN model is explained in section

3.6.1. In Sect. 3.6.2 the influence of the parameters on the characteristics of action potential pulse is analyzed. Section 3.6.3 demonstrates the characteristics of pulse propagation in branched structures and collision studies.

3.6.1 Action potential propagation

The time dependent solver with a time step of $\Delta t = 5$ is chosen for the computation (depending on Δz to yield numerical stability) with a relative tolerance of 10^{-2}. Two instants of measurement $t_1 = 190$ and $t_2 = 490$ are defined to record the position of action potential. Please note that the equation system is dimensionless. These instants are chosen so that the full profile of action potential can be viewed. The

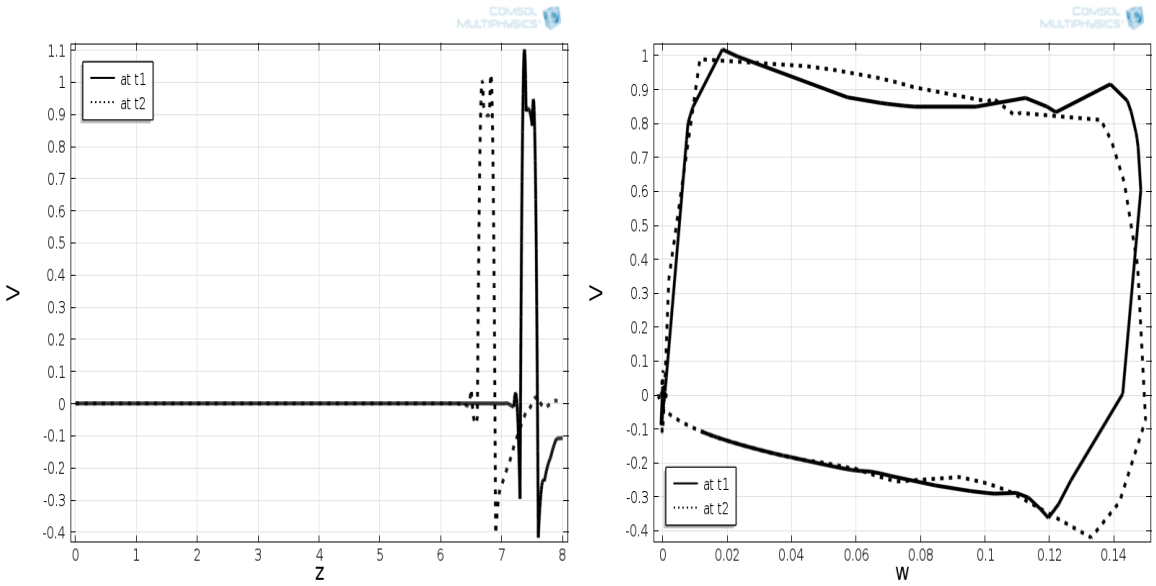

Figure 3.9: (Left) Action potential profiles without diffusion at times t_1 and t_2 and corresponding phase portraits (Right).

speed of the pulse propagation in this case of no diffusion is found to be 0.0003 with the parameters listed in table 3.3.

3.6.2 Action potential propagation with diffusion

The following result shows the effect of radial diffusion on the pulse properties of action potential. In principle, the propagation of action potential along the length of

the axon gives the axial diffusion. So, the simulation model reads as

$$\frac{\partial V}{\partial t} = (\frac{\partial^2 V}{\partial x^2} + \frac{\partial^2 V}{\partial y^2}) + V(a - V)(V - 1) - w\frac{\partial w}{\partial t} = e(bV - cw - d) \tag{3.12}$$

The inclusion of radial diffusion into the spatial FHN model results in a propagation profile as shown in Fig.3.10. It is observed that the pulse propagates five times faster

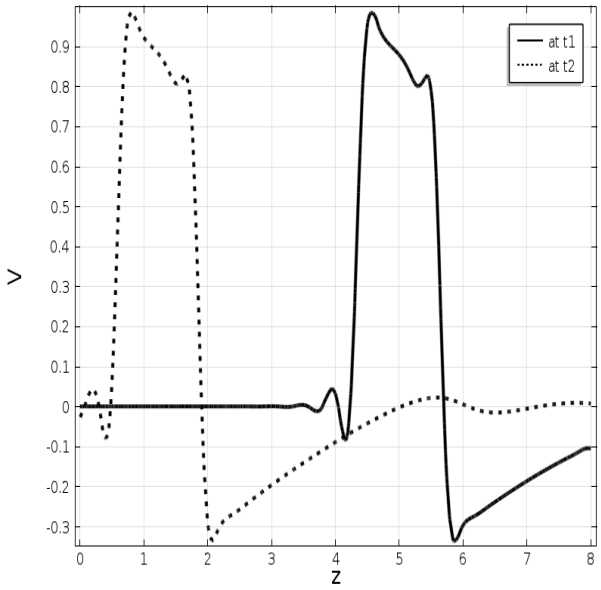

Figure 3.10: Action potentials with radial diffusion at times t_1 and t_2.

than the pulse with 'no diffusion'. Also the width of the wave front is double the width of pulse with no diffusion. Biophysically, it represents the increase in number of ion channels along the length of the axon, thereby the speed of propagation increases. It also affects the pace of de-polarization and re-polarization, thereby affecting the course of wave. Several studies on the parametric variation, radius of the axon are reported in the literature [Izhikevich(2004)]. In the context of our aims we restrict ourselves for further analysis in these directions. Indeed we proceed onto simulating a meaningful, predictive model of action potential propagation which can be coupled with an electrode.

3.6.3 Pulse Properties-Branching

Generally, axons showcase branching behavior. A branched Y-structure of axon geometry will be a realistic representation. So we adapt the geometry of simulation model from a cylindrical axon to a Y-shaped cylindrical axon to study the branching

behavior. Figure 3.12 shows the geometry used for the computation. Furthermore, a realistic value of the axon radius is incorporated into the model by adjusting the parameters. It is expected that the action potential flows through these branches undivided and without or with minimal loss of energy. The following sequence of figures represent the action potential propagation in two types of branched structures.

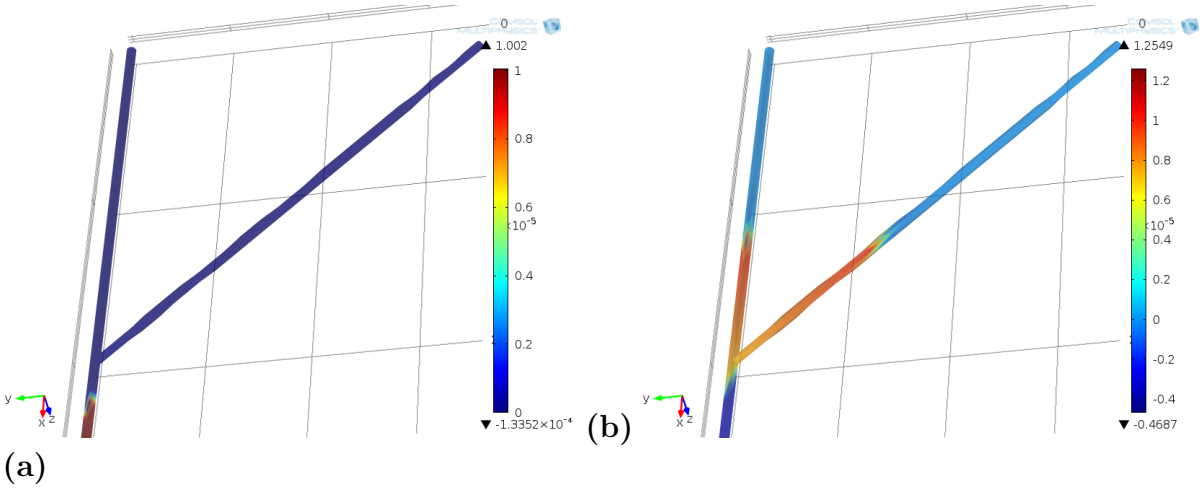

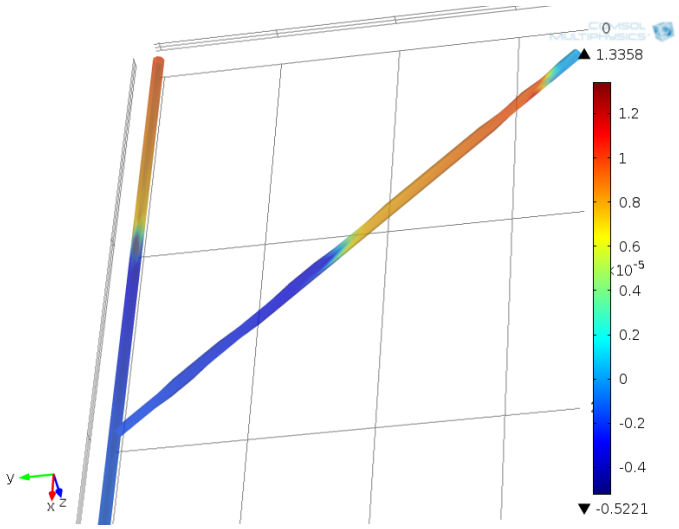

Figure 3.11: Propagation of AP through branches of a small Y-structured axon for time steps (a) 0 (b) 0.2 and 0.4.

The following figures shows the branching scheme of action potential in an extended Y-structure, roughly approximated as a network of axons.

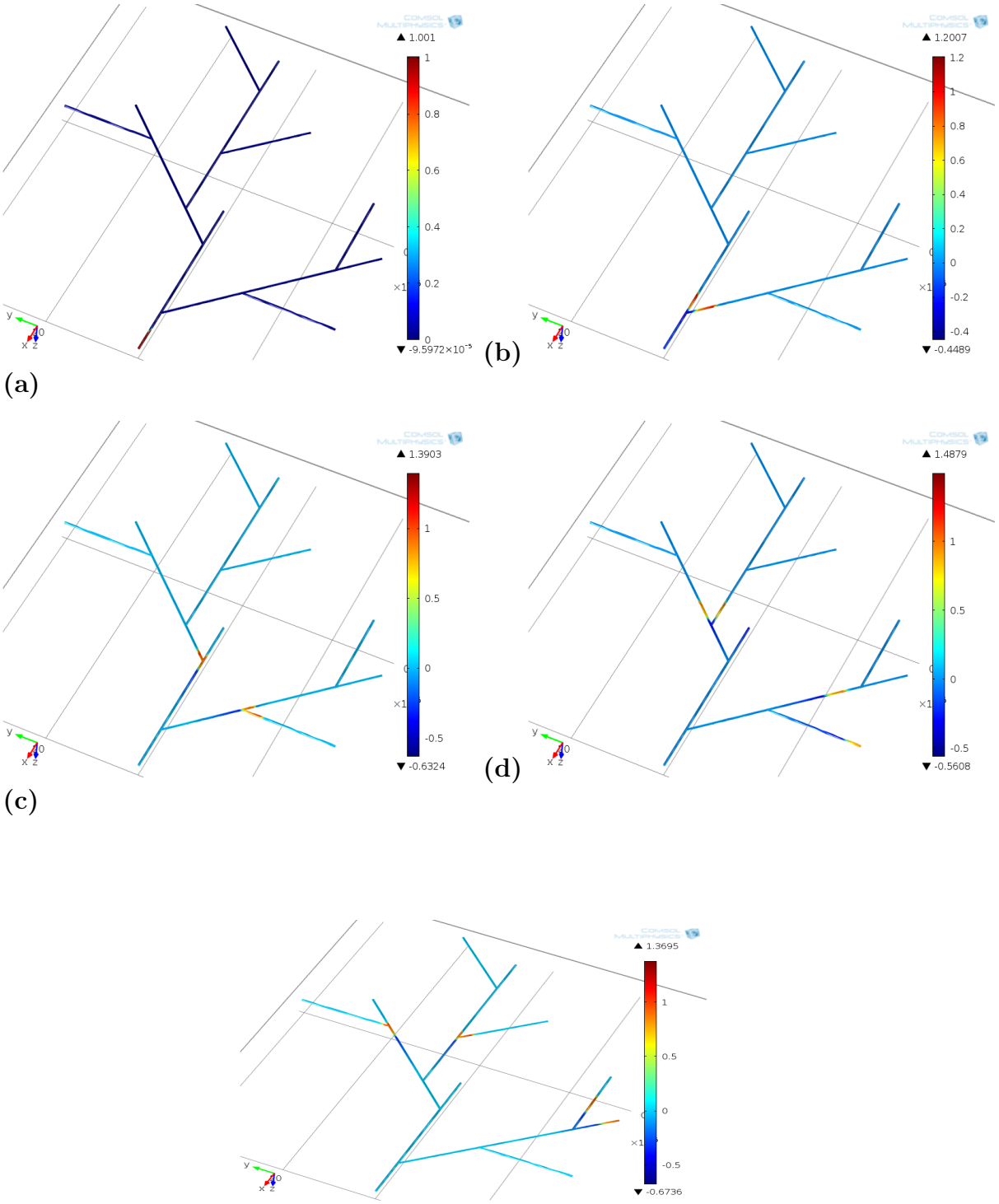

Figure 3.12: Propagation of action potential along the branched structures of an axon at times (a) 0 (b) 2 (c) 4 (d) 6 and (e) 8.

Signal splitting at the branch points has been also demonstrated in [Xylouris(2010)]. It can be concluded that such biological neuron models are well suitable for the fundamental investigations of neural networks.

3.6.4 Collision

The branching nature of action potential is an interesting feature that can be explored to model the networks of axon. Consequently, it also raises the question of what happens when two action potentials traveling in opposite directions collide head-on. It has been known since the 1940s that the nerve pulses are blocked upon collision [Tasaki(1949)]. In the Hodgkin-Huxley model, the cause of the decay in signal amplitude upon collision is the refractory period. This is the minimum distance between two pulses that travel in the same direction. It is caused by the finite relaxation times of the protein conductances of the stimulation of a pulse. In the so-called refractory zone a nerve fiber is unexcitable, and the existence of these zones prevents two colliding pulses from passing through each other. Simulations by [Aslanidi and Mornev(1997), Argentina et al.(2000)] based on the Hodgkin-Huxley equations support this view. Our simulations using the FHN model lead to the same results. Fig. 3.13 shows that the pulses eliminate each other upon collision.

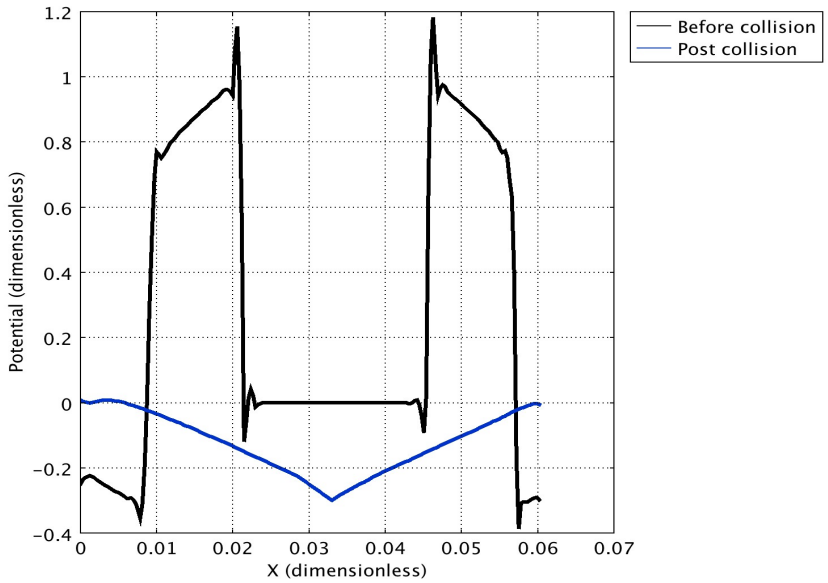

Figure 3.13: Collision of nerve pulses calculated with the FitzHugh-Nagumo equations. Two pulses traveling in opposite directions are shown before (black) and after the collision (blue). The pulses are annihilated after the collision.

3.7 Discussion

In this chapter, a detailed explanation on 2-dimensional excitable systems emerging from the HH model is given. It is also emphasized that FHN model can act like "simple- model of choice" [Izhikevich(2004)] and fitting of parameters according to the phase-space portraits is not complicated. Then the traveling pulse solutions are presented for a three-dimensional cylindrical axon using FEM approach. The main idea of this work is to realize an action potential propagation qualitatively with proper dynamics of the system. It is achieved through an adaptation of spatial FHN model by fitting the parameters. The effect of radial diffusion on the traveling speed and the wave front width is shown through the numerical simulation. This model finds its application in DBS-simulation studies as the mimic of traveling action potential must be of biophysical origin in such studies. There is always a possibility of improvisation to the system of equations by performing dimensional analysis, parametric analysis, accounting passive conduction and so on, which can be foreseen in the future work.

3.8 Digest

- A neuron is an excitable media and mathematically a neuron models are dynamical systems.
- The fast and slow variables of HH model can be simplified into two-variable systems, the pioneer of such models is FHN model.
- The FHN model can be called as a general model since its parameters, having bio-physical meaning are not specific to single type of cell.
- Thus, FHN model is chosen to simulate the action potential propagation (qualitatively) in three dimensional cylindrical axon using FEM technique on Comsol Multiphysics 4.2a® platform.
- The parameters are fitted for the given size of axon according to the established relations between parameters.
- Furthermore the effect of radial diffusion on the physical attributes of pulse like speed and width of wave front is studied.
- The action potential propagation properties such as branching and collision are studied and the results are found to be in good agreement with the literature.

Swiftly the brain becomes an enchanted loom, where millions of flashing shuttles weave a dissolving pattern always a meaningful pattern though never an abiding one.

—C. Sherrington

4 Application to a Neurochip

In this chapter, the spatial FHN model for action potential propagation and the branching property of axon structures are exploited to simulate a neurochip environment. In the first section an introduction to neurochips will be presented.

4.1 Introduction

Single neurons, dissected from the brain, attached to the bottom of a *Petri dish* isolate from their tissue and regrow their axons and dendrites to form networks in cultured medium. In 1972, researchers have explored the use of planar electrode arrays to record from the cultured neurons without making any damage to the cells. Over the years, the method of extracellular measurement of neuronal signals has evolved [Gross(1977), Pine(1980)]. A neurochip is an electronic micro-machined device with metallic planar electrodes upon which cultured neurons are monitored, stimulated both continuously and individually [Maher(1999)]. This device helps in detecting the action potentials in the external medium surrounding the cell. This device plays a key role in the fields of basic and medical research aiming at the development of electrically active implants. The specifications of a neurochip and its model design in Comsol Multiphysics 4.2a ® are explained in the next section.

4.1.1 Neurochip

A Glass Neuro Chip (GNC) consisting of Pt- Micro-Electrode Arrays (MEA) of 52 electrodes is considered for our numerical study. Such GNC's have been realized at Biophysics group of University Rostock [Baumann(2004),Koester(2010)]. Living cells are directly cultured on the neuro-sensor chip.

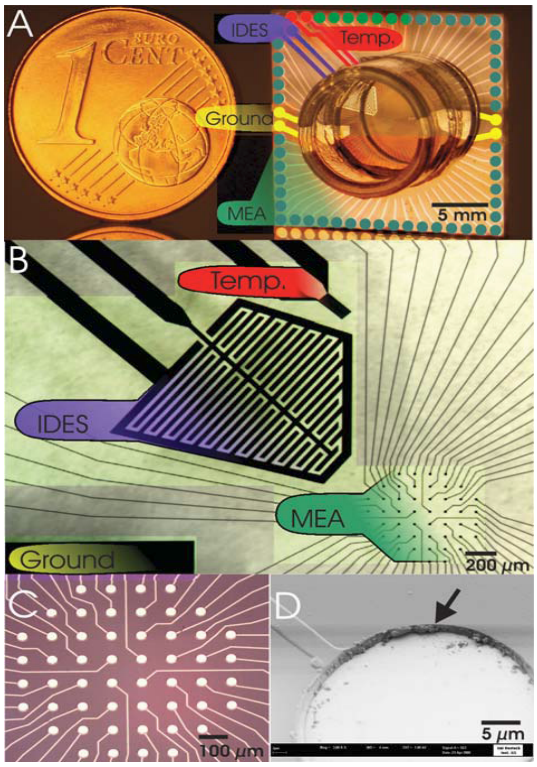

Figure 4.1: Example of GNC structures: (A) GNC with a side length of 16 mm. 52 electrode pads of the GNC are used to contact the MEA (green); (B) overview of cell culture area and the sensor structures; (C) MEA and (D) single Pt-electrode of the MEA. The arrow indicates the 2 μm thick Si_3N_4- passivation (Courtesy of Dr. Phillip. J. Koester, Biophysics group, University of Rostock, with permission [Koester(2010)]).

A 50 μm high, 0.16 mm diameter glass ring forms the cell culture trough. Fig. 4.1B gives an overview of the platinum structures. The Si3N4-passivation (thickness 2 μm) was opened above the active electrodes areas (like in Fig. 4.1D). The glass ring that is glued onto the GNC provides a culture volume. The MEA is located in the center of the GNC. The inner diameter of the ring ensures that the ground electrodes are in electrical contact with the medium. The MEA electrodes have a diameter of 25 μm and an inter-electrode distance of 0.15 mm.

4.2 Coupling of action potential and electrode

The electric field due to the action potential propagation is captured by the micro electrodes of neurochip. In order to model the coupling between the action potential and electrode, the spatial FHN equations are coupled with Maxwell's equations [van-Rienen(2001)].

Maxwell's Equations and the Quasi-Electrostatic model

The electromagnetic field simulation is based on the Maxwell's equations. The differential form of Maxwell's equations are Gauss's law for electricity:

$$\nabla \cdot \mathbf{D} = \rho$$

Gauss's law for magnetism:

$$\nabla \cdot \mathbf{B} = \mathbf{0} \tag{4.1}$$

Faraday's induction law:

$$\nabla \times \mathbf{E} = -\frac{\partial \mathbf{B}}{\partial \mathbf{t}}$$

Ampere's law with Maxwell's extension:

$$\nabla \times \mathbf{H} = \frac{\partial \mathbf{D}}{\partial \mathbf{t}} + \mathbf{J} \tag{4.2}$$

and the constitutive material equations:

$$\begin{aligned} \mathbf{D} &= \epsilon \mathbf{E} \\ \mathbf{B} &= \mu \mathbf{H} \end{aligned} \tag{4.3}$$

where **D**-electric displacement, **E**-electric field, **B**-magnetic flux, **H**-magentic field, ρ-charge density, ϵ-permittivity, μ-permeability. To model static electric fields and currents, requires a basic understanding of the charge dynamics in conductors. If the wavelength of the electromagnetic fields is large compared to the extension of the studied object, then either electric or magnetic field are considered [vanRienen(2005)]. These slow-varying fields are called as electro- and magneto-quasistatics. According to electro-quasistatics the electric field **E** is free from eddy currents and is described by a scalar potential function.

$$E = -\nabla \phi, \tag{4.4}$$

The fundamental equations involved are Ohm's law:

$$\mathbf{J} = \sigma \mathbf{E} \tag{4.5}$$

with **J**-total current flux Gauss's law:

$$\nabla \cdot (\epsilon \mathbf{E}) = \rho \tag{4.6}$$

and the equation of continuity can be given as:

$$\frac{\partial \rho}{\partial t} + \nabla \cdot \mathbf{J} = \mathbf{0} \tag{4.7}$$

By combining these fundamental relations, the space charge density in a homogenous medium can be deduced:

$$\frac{\partial \rho}{\partial t} + \frac{\sigma}{\epsilon}\rho = 0 \tag{4.8}$$

This has a solution of

$$\rho(t) = \rho_0 \exp(\frac{-t}{\tau}) \tag{4.9}$$

where $\tau = \epsilon/\sigma$ is the charge relaxation time which determines the conductivity of material. It is the external time scale t, i.e. the observation time of the system which determines whether the system can be solved for Electro-Quasi-Statics (EQS) or electrostatics. If $\tau \gg t$, then the system can be solved for stationary/electrostatics. If $\tau \ll t$ then the system can be solved for stationary electric currents. Otherwise, if $\tau \approx t$, then the frequency or time dependent study of electric currents can be carried out. The governing equation for EQS with time variant and locally constant material can be be given by [vanRienen(2003)]

$$\Delta \left[\epsilon \frac{\partial \phi(\mathbf{r}, \mathbf{t})}{\partial t} + \sigma \phi(\mathbf{r}, \mathbf{t}) \right] = \nabla \cdot \mathbf{J_E}(\mathbf{r}, \mathbf{t}) \tag{4.10}$$

where ϵ and σ are permittivity and conductivity tensor, respectively. While for frequency domain the governing equation becomes:

$$\Delta \left[\epsilon j\omega \phi(\mathbf{r}, \mathbf{t}) + \sigma \phi(\mathbf{r}, \mathbf{t}) \right] = \nabla \cdot \mathbf{J_E}(\mathbf{r}, \mathbf{t}) \tag{4.11}$$

where $\omega = 2\pi f$ is the angular frequency.

4.3 Simulation Model

For the numerical calculations, the area consisting of MEA's on which the neurons are grown in a cultured medium is considered. The geometry of the model is shown in the figure 4.2. The glass trough of above given specifications is built with the MEA of Pt-electrodes with passivation.

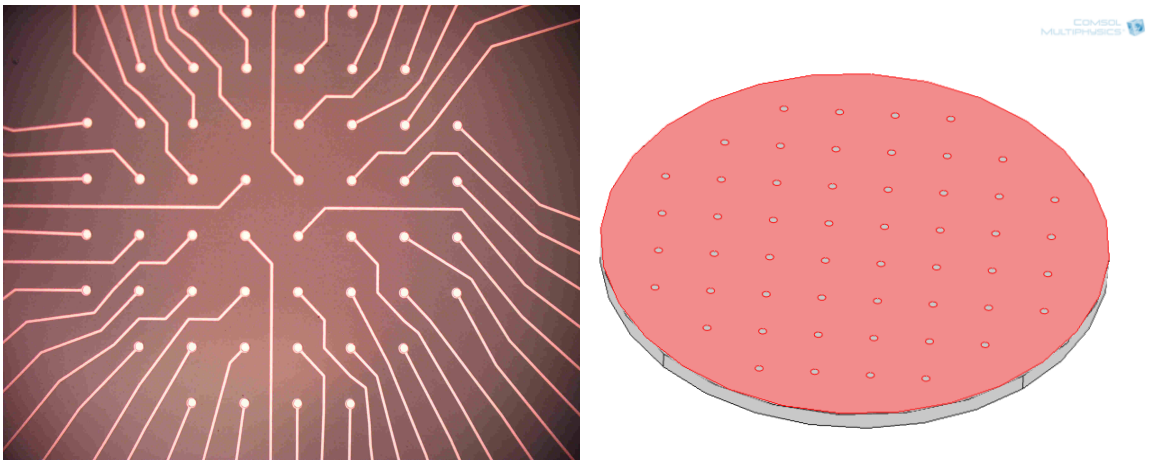

Figure 4.2: Arrangement of planar electrodes of MEA in a neurochip (left) and the MEA in the simulation model (Right).

The material parameters are listed in table 4.1. Physiological saline is taken as the medium. A network of axons is laid in the culture medium. The network is chosen to be not too big nor small, with respect to the available computational resources.

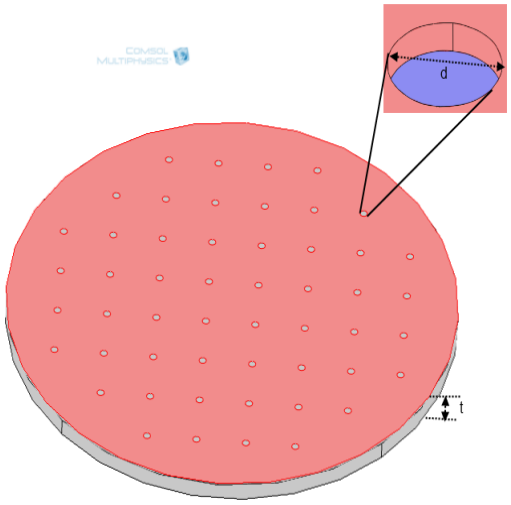

Figure 4.3: 3D simulation geometry of MEA and trough of GNC.

Table 4.1: Material parameters of neurochip components

Component	Material	σ
Electrodes	Pt	8.9×10^6 S/m
Trough	Glass	$1 \times 10^{-}14$ S/m
Passivation	Si_3N_4	0
Medium	Saline	1.2 S/m

4.3.1 Simulation of EQS model coupling with FHN equations

Different approaches that are used for the numerical solution of electromagnetic field problems are Boundary Element Methods (BEM), FEM, Finite Difference Methods or Finite Integration Technique (FIT) [Weiland(1977)]. The FEM is used for the application of neurochip using Comsol Multiphysics 4.2a®. The FEM equation is coupled with the frequency domain computation of the EQS potential ϕ through the current flux vector $\mathbf{J}$ by the so-called thin layer approximation. The boundary conditions assumed for the neurochip simulation are summarized in the following table.

Table 4.2: Boundary conditions of neurochip simulation

Component	Condition
Electrodes	Continuity
Trough	Insulation
Passivation	Insulation
Medium	Saline
Bottom of trough	Ground
Neural network	Distributed impedance

The FHN output variable V is coupled with the frequency domain EQS electrodes through a thin layer, distributed impedance boundary condition which reads as:

$$n \cdot (\mathbf{J_1} - \mathbf{J_2}) = \frac{\mathbf{1}}{\mathbf{d_s}}(\sigma + \mathbf{j}\omega\epsilon_\mathbf{0}\epsilon_\mathbf{r})(\phi - \phi_\mathbf{ref}) \tag{4.12}$$

with $\phi_{ref} = V$ and d_s being the surface thickness of thin layer.

4.4 Results

The neurochip environment simulated in FEM based Comsol software is shown in the following figure.

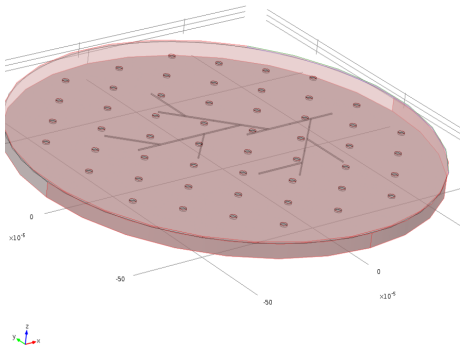

Figure 4.4: Simulation model of neurochip environment with a network of axons.

A free tetrahedral mesh has been used to discretize the system with 79, 713 elements (see Fig. 4.5). An iterative multigrid solver has been employed to solve the nonlinear coupled system and to make sure the solution is stable a time step of $\Delta t = 0.0002$ is chosen and solved for $t = 0.006$. A convergence of 10^{-6} has been achieved with the chosen time step and took a solution time of about 5 hours on a standard PC (64 Bit, Intel Core 2 Duo, 4 GB RAM).

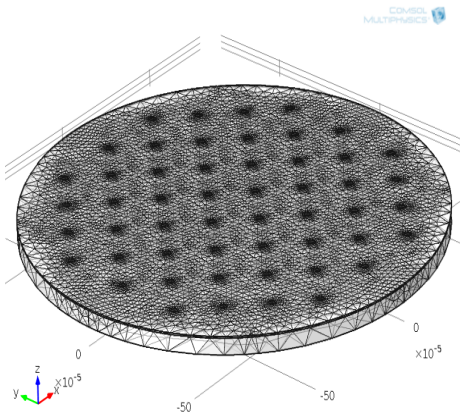

Figure 4.5: Mesh model of 3D neurochip simulation.

The action potential of axons has been recorded by the electrodes of MEA. Figure 4.6 shows the propagating action potential and its field near the electrodes at various times.

The action potential in the axon at a point and its recorded value on electrode

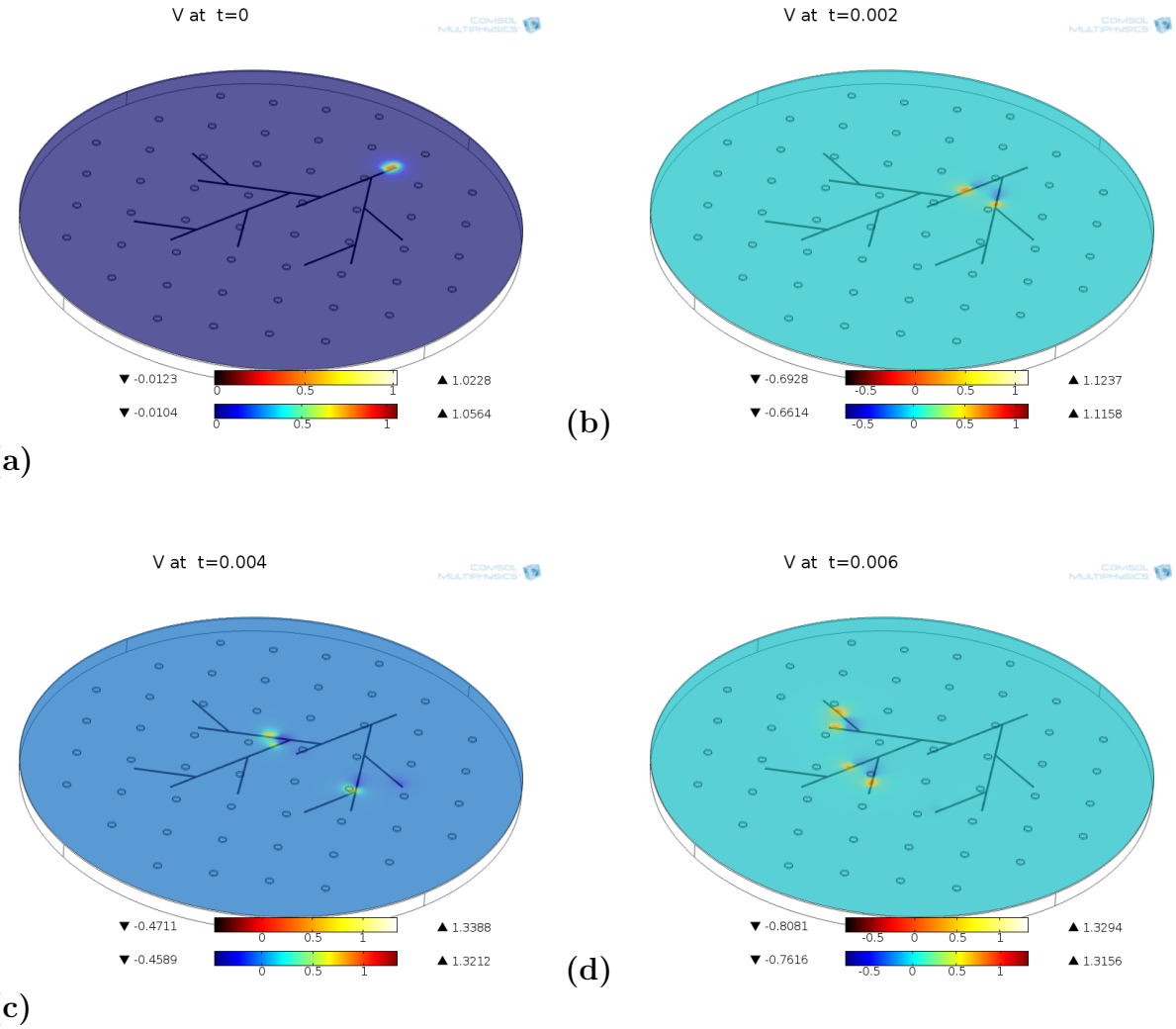

Figure 4.6: Action potential and recorded potentials in the neurochip at times (a) 0 (b) 0.002 (c) 0.004 (d) 0.006.

is depicted in the Fig.4.7. It shows that the electrode perfectly records the action potential profile. The electrodes that are near to the network record the maximum of field than that of the farther ones. It is obvious from the *inverse square law* of electricity [Feynman(1963)] that the field intensity decreases with the distance from source.

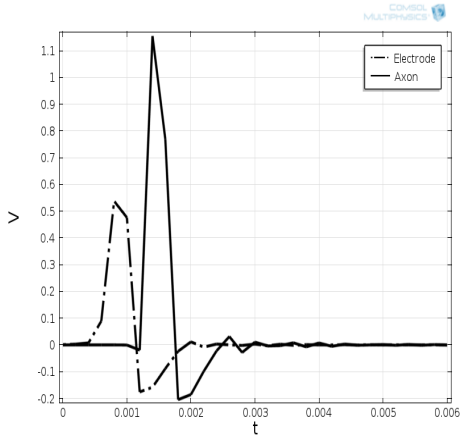

Figure 4.7: Action potential and a single electrode recording on MEA.

The graph (Fig. 4.8) shows the action potentials recorded on the electrodes at different instants of time. It has to be noted that the results are qualitatively arguable

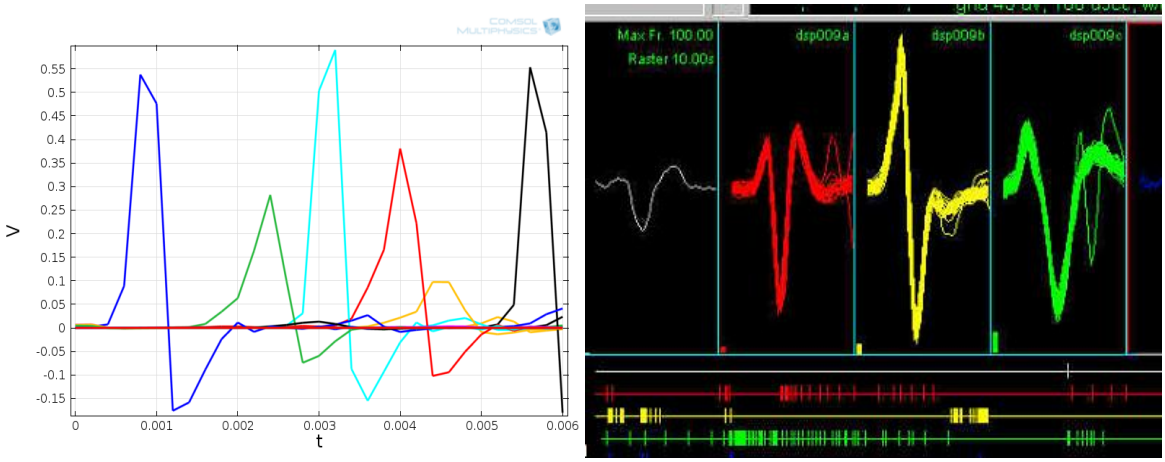

Figure 4.8: The propagating action potential on the MEA electrodes and its comparison with MEA experimental recordings.

as the FHN model mimics a dimensionless action potential and thereby the recorded electric field is also dimensionless.

4.5 Discussion

The goal is to achieve 3-D simulations of neuronal networks on neurochip as shown in Fig.. For which, FEM based Comsol multiphysics 4.2a® has been used. The coupling of Maxwell's equations in EQS approximation to the FHN equations is achieved by using Electric currents mode and PDE mode of Comsol platform. Neurons are approximated as cylinders with branched structures and planar trough electrodes are approximated in the 3-D environment. The model simulates the pulse propagation in the neuronal structures. While FHN equations provide the information only about the potential difference across the neuron's membrane, the 3-D model also considers the extra-cellular region and provides freedom to choose the materials outside the neuron. The MEA with extended neuronal network is simulated. In comparison with the work in [Flehr(2006)], the 3D model of axon with its extracellular and intracellular environment is coupled with electrodes of MEA, the results are quite comparable. It is the underlying equations that used to simulate the action potential are different in [Flehr(2006)]'s work. A complete 3D environment is achieved with our simulation model, due to the simplicity of FHN model when compared to Flehr's electrodynamic equations based on HH model. This model can be used for analysis of stimulation and recording of electrodes qualitatively. It is a good compromise of computational power and model predictibility. However, the model can be further improved by working on the large networks of neurons firing continuously which requires greater computational power. Furthermore, stimulation of neurons can also be studied using this model with an inclusion of external stimuli in FHN equations.

4.6 Digest

- Neurochip is a micromachined device used to record the neuronal signals as well as to stimulate the neurons.
- Neurochips are proven to be essential in basic neuronal research and pharmaceutical studies.
- Coupling of action potential with electrodes of MEA.
- 3D simulation of action potential propagation using FHN equations and branching axons are made use of to mimic a network of neurons.
- EQS simulation model using FEM method has been implemented.
- 3D simulation of a simple neuronal network on a neurochip has been achieved using FHN model for action potential propagation.

Part II

Alternative Modeling

Classical thermodynamics..is the only physical theory of universal content which I am convinced...will never be overthrown.

—A. Einstein

5 Membrane Properties

In the introduction of this thesis, during the discussion of internal structure of the nerves it has been considered that the membranes of each nerve fiber are responsible for the signal transmission. Let us know more about the physical properties of the membranes.

5.1 Physical Properties

The phospholipid structure of the plasma membrane is key to gain better understanding of how the membrane functions [Arms and Camp(1995)]. The typical thickness of a lipid bilayer is about 5nm [Heimburg(2010)]. In this section we will briefly go through the membrane's constituents: lipids, proteins and their physical properties.

Lipids

The lipids are bipolar in nature. The tip of the molecule is denoted as the "head". The head contains phosphorous and is polar and hydrophilic. The other end referred to as "tail" contains the phospholipid molecule and is non-polar and hydrophobic. Two lipid layers form a membrane. The hydrophilic heads of lipids orient themselves outwards in contact with the water in the extracellular fluid and inwards with the water in the intracellular fluid. The hydrophobic tails of lipids orient themselves to the inside of membrane, away from the extracellular and intracellular fluid. Lipids tend to agglomerate and guard the apolar chains from water and uncover the head

groups to water. Figure 5.1shows the phospholipid structure which has two parts: a polar phosphate head and two non-polar fatty acid tails. The chain colored in red shows the polar region.

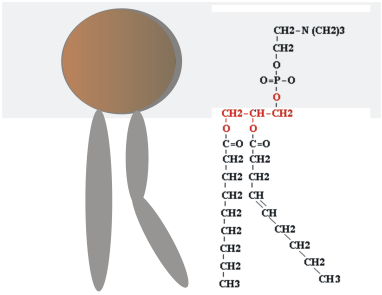

Figure 5.1: Lipid monomer showing the head group and hydrocarbon chains (Adapted from textbooks).

Proteins

Proteins are genetically coded molecules. Membrane proteins have various functions of which the prominent is the transport processes, both active and passive across the membrane. Thus, proteins are thought to be the reason behind the pulse propagation in nerves.

The membranes are flexible, heterogeneous and permeable. However, these properties depend on the conditions, for example on temperature, pressure, electrical field, pH, salt concentration, but also the presence of proteins and protein conformation. This basically means that the state of a biological membrane depends on all thermodynamic variables.

5.2 Thermodynamic Properties

One of the important features of membranes is melting transitions. The order transition between two states of different physical properties is known as the melting process. At low temperatures, lipid chains are ordered into an all-trans configuration, i.e., straight arrangement. At high temperatures these chains are disordered due to rotations around the Carbon-Carbon (C-C) bonds within the lipid chains. The membranes are in an ordered gel phase at low temperature while they are in a disordered fluid phase at high temperature.

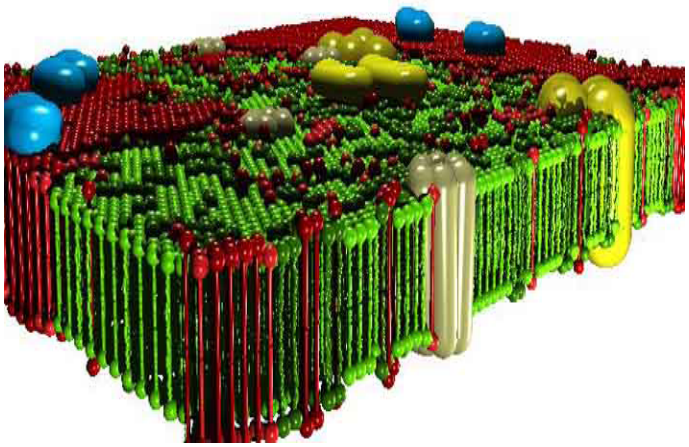

Figure 5.2: Membrane with proteins and lipids: by Heiko Seeger/T. Heimburg (Used with permission from [Heimburg(2009a)]). Lipid domains in solid-ordered (red) and liquid disordered (green) state. The lipid composition of the two monolayers might vary. Membrane proteins can aggregate and interact with the lipid components in various ways, altering physical state of the membrane.

Phases

The thermodynamics of ensembles of molecules allows for the formation of quite different phases. If the conditions are right more than one phase may coexist. This happens in temperature, pressure or concentration intervals well defined by the thermodynamic parameters of the system. The graphical representation of the co-existence of such phases is called a phase diagram'.

The most common phases found in artificial and biological membranes are the solid ordered (SO) phase, the liquid ordered (LO) phase and the liquid disordered (LD) phase. Solid means that the lipids arrange on a (typically triangular) lattice in the membrane plane while liquid indicates the loss of lateral packing. The attributes ordered and disordered indicate the internal order of the lipid chains. The transition between ordered and disordered states is linked to the uptake of significant amounts of enthalpy (i.e., heat). The SO phase is also often called the gel phase and the trivial name of the LD phase is the fluid phase. Typically, the different phases differ in their physical properties. For instance, they may display very different elasticities, auto-diffusion constants or electrostatic potential. Under most circumstances biological membranes seem to exist in the LD phase due to the proximity to melting transitions, however, this can be fine tuned by the organism.

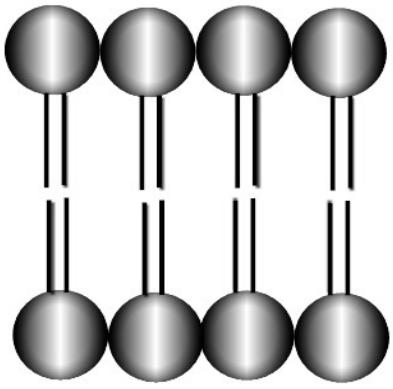

Figure 5.3: SO phase of lipid bilayer.

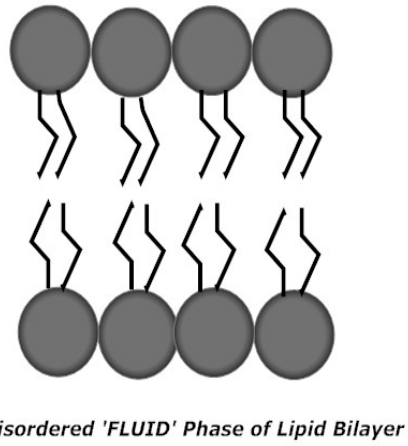

Figure 5.4: LD phase of lipid bilayer.

Temperature and pressure dependence

The membrane is an electrochemical and a thermodynamic system. The change in the internal energy of the membrane depends on the exchange of heat, work, ion flow and so on. This can be given as

$$dE = dQ + dW + dI \tag{5.1}$$

where dQ is the change in heat and is a reversible process in the membranes, which can be given by

$$dQ = TdS \tag{5.2}$$

In which, T is the temperature and S is the entropy. dW gives the mechanical work done on the system related to pressure p and volume V. That is

$$dW = -pdV \tag{5.3}$$

The charges (q) on the membrane result in surface potential (ψ) and it is

$$dI = \psi dq \tag{5.4}$$

Therefore the change in the internal energy is

$$dE = TdS - pdV + ..\psi dq + ... \tag{5.5}$$

In the chain melting process, the molecules absorb heat (enthalpy) and the entropy increases due to the increase in the number of possible chain configurations. The

melting processes is cooperative, meaning that the lipids do not melt independently of each other. The absorption of heat is typically monitored by measuring the heat capacity, that is the amount of heat absorbed per degree temperature increase. The heat capacity at constant pressure is defined by $C_p = (dH/dT)p$, with H as enthalpy. At the melting temperature, T_m it displays a pronounced maximum.

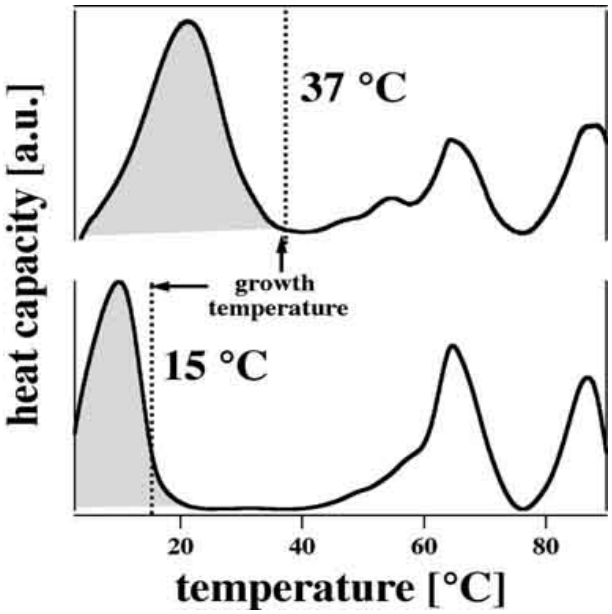

Figure 5.5: Heat capacity profiles of native cell membranes of E.coli bacteria by Thomas Heimburg (Use with permission from [Heimburg(2009b)]). They display chain melting (shaded region) at temperature slightly below their growth temperature (dotted line).

It is obvious from the above equation that there are changes in the physical properties of the membrane due to change in the temperature, pressure and vice versa. During the melting process membranes also change their volume and area [Heimburg(2009a)]. Typically, the volume changes by about 4% and the area by about 25% [Heimburg(2009a)]. Thereby, the melting temperature is pressure-dependent. An increase in the hydrostatic pressure by 40 bars increases the melting temperature by 1 degree [Heimburg(2009a)]. Similarly an increase in the lateral tension within the membrane also changes the melting temperature. This effect can be studied on a *Langmuir trough* in which the lipid monolayers are compressed by changing the film area and the lateral pressure is monitored simultaneously [Heimburg(2009a)].

5.3 Electrical Properties

Membranes contain zwitterionic and charged lipids. The zwitterionic lipids have a head group that is an electric dipole. Thus, a monolayer of lipids possesses a strong dipole potential across that layer that can be of the order of 500 mV. Upon area changes in a monolayer experiment one finds that the lateral pressure changes in close relationship to this dipole potential. This implies that similarly to a change in pressure, voltage changes can induce a transition in the lipid monolayers. Since a membrane consists of two monolayers, these potentials partially compensate. The membranes additionally possess a net electrostatic potential due to ion concentrations on both sides of the membrane. As discussed in the previous chapters, the quantifiable property of the membranes so far is the electrical potential.

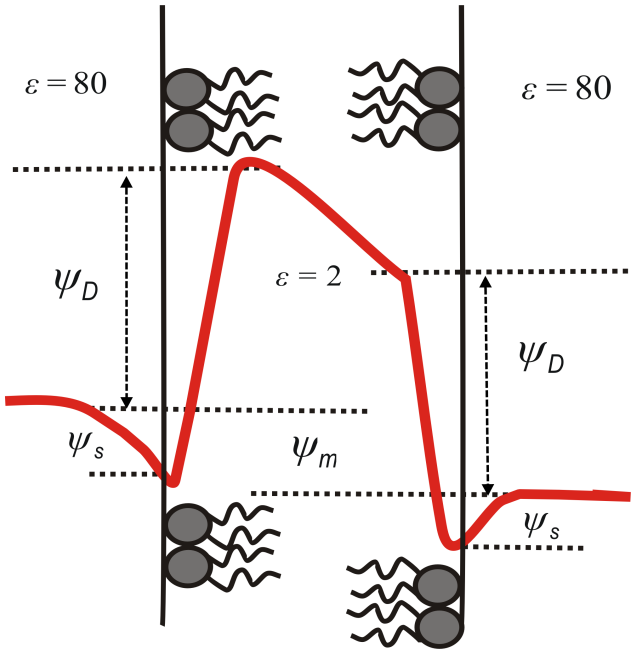

Figure 5.6: Schematic sketch of potential gradients across a phospholipid bilayer. The transmembrane potential ψ_m is caused by different concentration of ions on each side of the membrane. Charged head groups define the surface potential ψ_s and dipole potential ψ_D arises from the dipoles present in the bilayer.

Electrostatic Potential

On an average, 10% of lipids in a bio-membrane are negatively charged. The relative amount of negative charge is very different depending on the particular organelle of

a cell. The charges often distribute asymmetrically such that the inner membranes of cells and organelles are more charged. The electrostatic potential at a membrane surface also depends on the number of charged molecules that form the membrane. The potentials across the membrane are often named in text books as:

- *Transmembrane potential* ψ_m generated by ion gradients across the membrane.
- *Surface potential* ψ_s arising from fixed charges at the lipid head groups and membrane proteins.
- *Dipole potential* ψ_D of the dipoles at the lipid-water interface.

  Please refer to the sketch in Fig. 7.14.

Transmembrane potential

The transmembrane potential ψ_m facilitates the accumulation of proteins on the membrane. It is of order 10-100 mV [Kroon(1989)] and leads to trans-membrane movement of ions down their concentration gradients. The transmembrane potential is measured using Patch-Clamp method developed by Neher and Sakmann in 1976 [Sakmann(2009)]. This method is widely used for single channel analysis. More details on the transmembrane potential have been discussed in chapter 2.

Surface potential- Ionic strength dependence

The surface potential ψ_s of a membrane depends on the charge density and on the ionic strength of the salt solution in contact with the membrane. The surface potential decays as a function of the distance from the membrane and the characteristic decay length is called the *Debye length*. The Debye length for a solution depends on the its molar concentration. For example, for a 100 mM solution of NaCl, the Debye length is 0.97 nm and it is 3.1 nm, 9.7 nm for 10 mM, 1 mM concentrations respectively. Which indicates that the Na^+ concentration is increased at the membrane surface while the Cl concentration is reduced. The surface potential ψ_s of a membrane consisting of 40% negatively charged lipids in a biological environment of a ionic strength of 150 mM NaCl has a magnitude about -50 to -100 mV [Heimburg(2007)]. The surface potential decays exponentially with the distance from the charged surface and can further be reduced by binding of ions [Brockman1994] [Heimburg(2007)]. This electrostatic theory of surfaces has originated from Gouy and Chapman. A detailed treatment of the theory will be carried out in Chapter 8.

Dipole potential Dependence on charged lipid concentration

Dipole potentials ψ_D of membranes arise from the polar head groups on the lipids. For these lipids the dipole moment p is oriented from the negatively charged phosphate

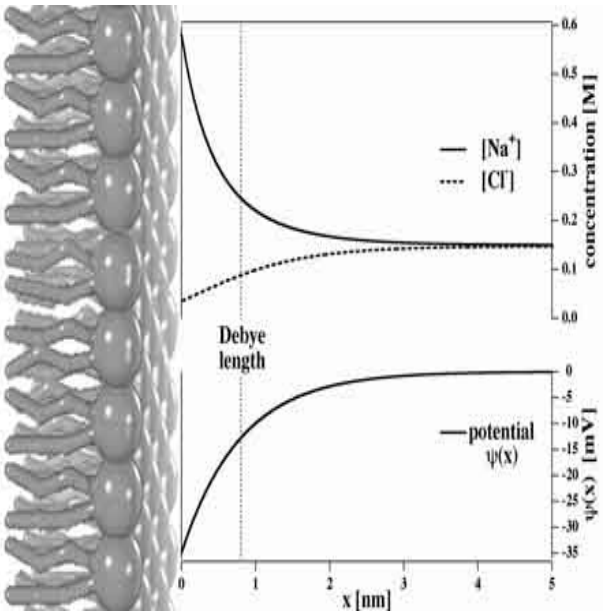

Figure 5.7: Distribution of Na^+ and Cl^- ions. Electrostatic potential (ψ) as a function of distance from the membrane containing anionic lipids (By T. Heimburg, Used with permission from [Heimburg(2009a)]).

to a positively charged group directed away from the membrane surface. In the case of monolayers, the terms dipole potential (ψ_D) and surface potential (ψ_s) are put together into the collective term surface potential and the actual measurement depends on the composition of monolayer.

ψ_D can be measured with the *Black Lipid Membrane* (BLM) technique in which two small containers with buffer solution are separated only with an artificial membrane. The basis in such ψ_D measurement is the rate-constants of transporting large hydrophobic anions and cations across the membrane. It appears that hydrophobic anions are transported across membranes, of typical phospholipids, at rate constants faster than the equivalent cations. Thus, in the center of the membrane ψ_D must assume positive values relative to the aqueous phase which for DPPC bilayers ψ_D varies between 200mV and 280mV [Flewelling(1986)]. Monolayers are treated in more detail in chapter 8.

Proteins and permeability

Proteins as 'voltage gated channels' are not only permeable to ions but also carry positive charge to interact with the negatively charged lipid membranes, which reduces the overall electrostatic potential. Whereas the lipid membranes are considered as impermeable to ions, molecules and water. However this may not be true as the lipid

membranes are very thin and the molecular fluctuations can lead to instantaneous pores [Heimburg and Jackson(2005)]. The probability of formation of such pores increases in the phase transition regimes of lipid membrane i.e., slightly below the body temperature in bio-membranes [Heimburg(2009a)]. Therefore, the permeability is also related to the thermodynamic property of membranes i.e., heat capacity.

Protein and Lipid Ion Channels

The embedded proteins are held responsible for the permeation events through the membranes, as the permeability of lipid membranes is always thought to be small. The patch clamp and BLM measurements suggest the same by the quantized ion currents through the membrane indicating localized events. For detailed mechanism of protein ion channels see [Heimburg and Jackson(2007)] and references therein.

Further, the lipid membranes are also permeable to molecules if they are close to their phase transition temperature [Heimburg and Jackson(2005)]. This effect is not as well known as the protein conductance but has been described in the literature [Antonov et al.(1980)]. The protein ion channels are always embedded in membranes and the biological membranes are close to their transition temperature. The quantized channels can be due to events in the lipid membrane. Therefore, it is complicated to distinguish between the protein and lipid conductances.

5.3.1 Signal Transmission

The primary function of nerves is to transmit information in form of signals. In the previous chapters, the electrical model for signal propagation is explained in detail. The transient charging of membrane (capacitor) and the cascading effect of it is believed to be the nerve signal propagation. The Hodgkin-Huxley model explains a wide range of data from squid axon, like the shape of the action potential. However the model is not *the only* description of pulse propagation and it only addresses the voltage-related aspects of nerve pulse. Hodgkin and Huxley themselves mentioned it in their article [Hodgkin and Huxley(1952a), Hodgkin and Huxley(1952b)]:
"The agreement must not be taken as evidence that our equations are any- thing more than an empirical description of the time-course of the changes in permeability to sodium and potassium. An equally satisfactory description of the voltage clamp data could no doubt have been achieved with equations of very different form, which would probably have been equally successful in predicting the electrical behaviour of the membrane. It was pointed out in Part II of this paper that certain features of our equations were capable of a physical interpretation, but the success of the equations is no evidence in favour of the mechanism of permeability change that we tentatively had in mind when formulating them". Furthermore, a number of unanswered questions about action potential propagation such as geometric changes, reversible heat changes

and effect of anesthesia on the membranes declares the Hodgkin-Huxley model as *a posteriori* description of the measurements [Heimburg(2010)].

In fact, many aspects of the nerve pulse conduction can be deduced from the cooperative properties of membranes discussed in the previous sections of this chapter. This forms the basis for an alternative theory of nerve pulse propagation called 'Soliton Model'. The details of the model will be presented in the next chapter.

5.4 Digest

- The plasma membrane consists of a lipid bilayer with embedded proteins.
- Lipids are bipolar molecules that exhibit melting transitions.
- The properties of the lipid layers depend on the thermodynamic variables such as temperature, pressure and presence of proteins.
- The charged lipids, saline environment and lipid-water interface constitute the electrical properties of the membrane and lead to various potentials across the membrane.
- Proteins and lipid conductances contribute to the electrical properties of the membrane.

The difficulty lies, not in the new ideas, but in escaping the old ones, which ramify, for those brought up as most of us have been, into every corner of our minds.

—J. M. Keynes

6 The Soliton Model and Collision Study

Note: Parts of this chapter are excerpt from a book chapter authored by me in Advances in Planar Lipid Bilayers and Liposomes (APLBL) [Appali(2012)] and a contribution to an article [Lautrup et al.(2011)].

6.1 Introduction

In 2005, Thomas Heimburg and Andrew Jackson proposed a thermodynamic theory of nerve pulse propagation in which the action potential is a reversible electromechanical soliton [Heimburg and Jackson(2005), Heimburg and Jackson(2007), Heimburg and Jackson(2007), Andersen et al.(2009), Villagran Vargas et al.(2011)]. It is based on thermodynamics and in particular on the phase behavior of the lipids, that has been discussed in the previous chapter. The Heimburg-Jackson theory is often referred to as the *soliton model*. A central prerequisite of this theory is the chain melting transition of the lipid membranes (see Fig. 6.1, [Heimburg and Jackson(2005), Heimburg(2007)]). The biological membranes are in fluid state at physiological temperatures. When a biological membrane is compressed, the fluid membrane reaches the ordered, denser gel phase. It is known from the previous chapter that the melting transition is associated with the changes in enthalpy, entropy, but also to changes in volume, area and thickness. Which means that the state of the membrane can also be influenced by hydrostatic pressure, lateral pressure in the membrane plane along with temperature.

Local compression of the membrane creates a wave or pulse by increasing the

local density. The lipid membranes have the properties required for the generation and propagation of solitons [Andersen et al.(2009)]. In the melting transition phase, the fluctuations in enthalpy, in volume and area are at a maximum as indicated by fluctuation-dissipation theorem. Thereby, the heat capacity (refer Fig. 6.1), the volume compressibility all reach maxima. Simultaneously, the relaxation time scale reaches a maximum. This implies that the lateral compression of a fluid membrane leads to an increase in compressibility. This effect is known as a 'non-linearity'. From experiment it is known that the compressibility is also frequency-dependent, an effect that is known as 'dispersion'. These two phenomena are necessary conditions for the propagation of solitons. It can be shown that the features of lipid membranes slightly above a transition are sufficient to allow the propagation of mechanical solitons along membrane cylinders [Heimburg and Jackson(2005)]. The solitons consists of a reversible compression of the membrane that is linked to a reversible release of heat, mechanical changes in the membrane. Furthermore, the soliton model also implies a mechanism for anesthesia that lies in the well-understood influence that anesthetics have on the lipid phase transition [Heimburg and Jackson(2007)].

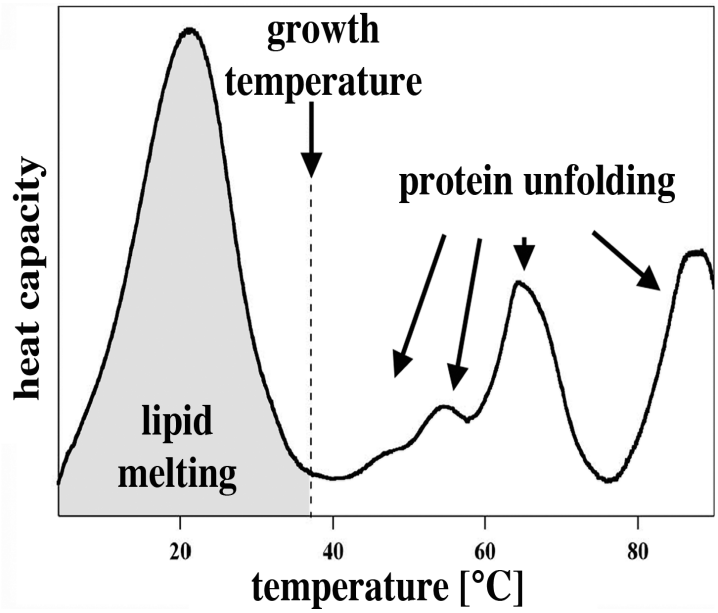

Figure 6.1: Heat capacity profile of native *E. coli* membranes showing a lipid melting peak below physiological temperature (by T. Heimburg, used with permission from [Heimburg(2009a)]).

A mini review of [Heimburg and Jackson(2005)] which explains the experimental facts behind the thermodynamic theory of pulse propagation and the model (soliton model) are described in detail in the next sections.

6.2 Theory

The soliton model derives from several experimental results on membranes close to the thermal melting transition. A short review of [Heimburg and Jackson(2005)] which leads to the thermodynamic and mechanical equations of the model will be presented in this section. It is known that the lipid membranes display order transitions in the temperature regime slightly below body temperature. In this transition regime, the elastic constants of the membrane such as compressibilities, bending elasticity and relaxation times are at their maximum. The peripheral and integral proteins of membrane can influence the lipid melting caused by molecular interactions and thereby impact the cooperative nature of the membrane fluctuations as a whole [Heimburg and Jackson(2005)]. The fluctuations in volume and area and related functions in curvature, pronounce the changes in elastic constants. Which means that the membranes become more compressible and easier to bend in the transition region. The experimental and theoretical work of [Halstenberg et al.(1998), Grabitz(2002), Ebel et al.(2001] suggest that these response functions of elastic constants are simple functions of *heat capacity*.[1]

Therefore in the work of [Heimburg and Jackson(2005)], the biological membranes *Escherichia coli (E.coli), Bacillus subtilis (B. subtilis)* and artificial unilammelar DPPC vesicles were subjected to pressure calorimetry to distinguish the melting peaks and protein unfolding and heat capacity profiles were obtained (See Fig. 6.2). In Fig. 6.2 the transition peaks associated with protein unfolding are shaded in gray. The dotted line indicates $T = 37\,\mathrm{deg}\,C$, which is the bovine body temperature and the growth temperature of E. coli and B. subtilis. From the heat capacity profiles in Fig. 6.2, the temperature dependence of elastic constants was estimated. The heat capacity (C_p), the isothermal volume compressibilty (κ_T^V) and the lateral compressibility (κ_T^A) are related to fluctuations in enthalpy, volume and area as

$$\begin{aligned} C_p &= \frac{< H^2 > - < H >^2}{RT^2} \\ \kappa_T^V &= \frac{< V^2 > - < V >^2}{< V > .RT} \\ \kappa_T^A &= \frac{< A^2 > - < A >^2}{< A > .RT} \end{aligned} \tag{6.1}$$

[1]Heat capacity (C) is the measurable physical quantity (but dimensionless when measured under constant pressure (C_p) or constant volume (C_v)) that gives the amount of heat required to change a substance's temperature to a given amount.

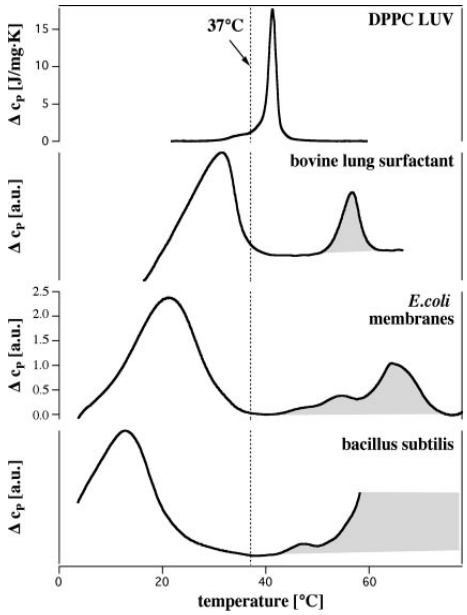

Figure 6.2: Heat capacity profiles of artificial unilamellar DPPC vesicles, bovine lung surfactant extract, E. coli membranes, and B. subtilis membranes (by T. Heimburg, used with permission from [Heimburg and Jackson(2005)]).

The excess enthalpy change (ΔH), excess volume change (ΔV) and excess area change (ΔA) of the lipid melting transitions obey the relations

$$\begin{aligned} \Delta V(T) &= \gamma_V \Delta H(T) \\ \Delta A(T) &= \gamma_A \Delta H(T) \end{aligned} \tag{6.2}$$

with the constants $\gamma_V = 7.8 \times 10^{-4} cm^3/J$ and $\gamma_A = 8.9 \times 10^3 cm^2/J$ for all the lipid membranes considered in [Heimburg and Jackson(2005)]. These relations were used to calculate the elastic constants from the heat capacity using

$$\begin{aligned} \kappa_T^V &= \kappa_{T,0}^V + \Delta\kappa_T^V = \kappa_{T,0}^V + \frac{\gamma_V^2 T}{< V >} \Delta C_p \\ \kappa_T^A &= \kappa_{T,0}^A + \Delta\kappa_T^A = \kappa_{T,0}^A + \frac{\gamma_A^2 T}{< A >} \Delta C_p \end{aligned} \tag{6.3}$$

where $\kappa_{T,0}^V$ and $\kappa_{T,0}^A$ are the compressibilities outside the transition temperature which are taken from the literature. Furthermore it is also shown in [Heimburg and Jackson(2005)] that these elastic constants close the melting region vary significantly with density as can be seen in Fig. 6.3. Some consequences of this fact are that the sound propagation velocities are related to isentropic/adiabatic compressibilities in elastic

media i.e., $c_0 = \sqrt{\rho\kappa_S}$ where c_0 is the sound velocity, κ_S is isentropic compressibility and ρ is the density.

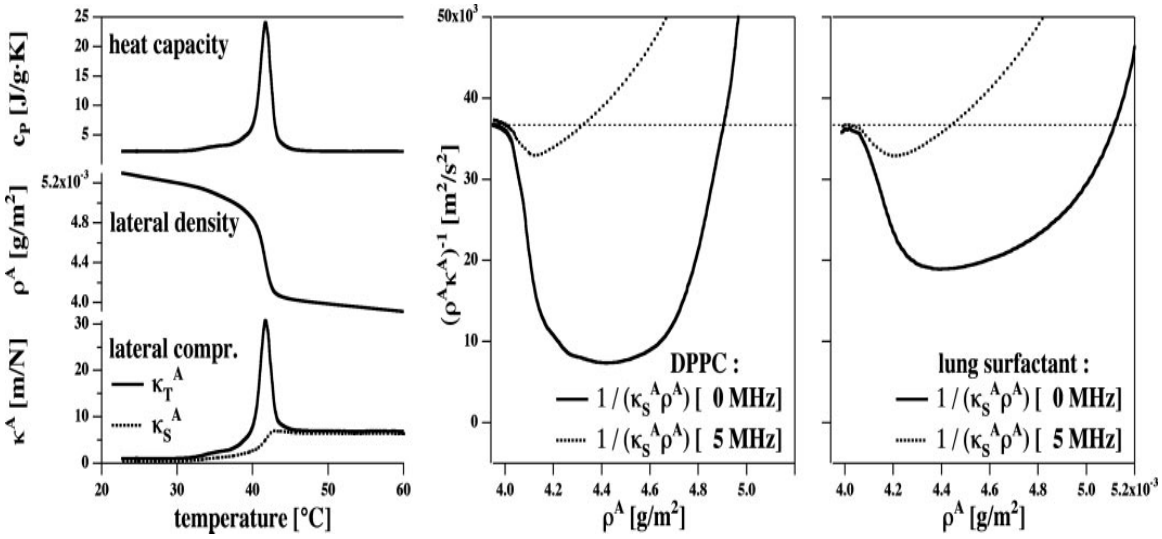

Figure 6.3: Thermodynamic data for DPPC vesicles and lung surfactant (by T. Heimburg, used with permission from [Heimburg and Jackson(2005)].

Figure 6.3 (Left) Heat capacity(C_p) of DPPC large unilamellar vesicle (top), lateral area density (ρ^A) (middle) and the corresponding lateral compressibility (bottom) Thermodynamic data for DPPC vesicles and lung surfactant. (Left) Heat capacity of DPPC large unilamellar vesicle (Top), lateral area density, A (Middle), and the corresponding lateral compressibility (Bottom) (isothermal area compressibility, solid curve, corresponding to a low-frequency case and adiabatic area compressibility, dotted line, corresponding to a 5-MHz ultrasonic experiment), as calculated from the heat capacity. (Center) The lateral sound velocity $c^2 = 1/\kappa_S^A \rho^A \;\; [m^2/s^2]$ for the low-frequency and the 5-MHz case, as a function of membrane area density, ρ^A $[g/m^2]$ at $T = 45\,\mathrm{deg}\,C$. (Right) c^2 profiles for lung surfactant at $T = 37\,\mathrm{deg}\,C$ calculated from the heat capacity in Fig. 6.2.

If the nerve membrane is considered as a long and narrow cylinder, the propagation of sound in one direction, z, in the absence of dispersion is governed by the equation

$$\frac{\partial^2}{\partial\tau^2}\Delta\rho^A = \frac{\partial}{\partial z}\left(\frac{1}{\kappa_S^A.\rho^A}\left(\frac{\partial}{\partial z}\Delta\rho^A\right)\right) \tag{6.4}$$

where $\Delta\rho^A = \rho^A - \rho_0^A$ is a function of z andτ. If the compressibility is approximately

constant and if $\Delta\rho^A \ll \rho_0^A$, this reduces to the initial equation (6.5) of the model. [2]

6.3 The Soliton Model

The soliton model starts with the well-known wave equation for area density changes $\Delta\rho^A$

$$\frac{\partial^2}{\partial\tau^2}\Delta\rho^A = \frac{\partial}{\partial z}\left(c^2\frac{\partial}{\partial z}\Delta\rho^A\right) \tag{6.5}$$

that originates from the Euler equations of compressible media (e.g., [Landau and Lifshitz(1987), Sommerfeld(1992)]). Here, τ is the time, z is the position along the nerve axon, and c is the sound velocity. If $c = c_0$ is constant, one finds the relation for sound propagation.

$$(\frac{\partial^2\rho}{\partial\tau^2}) = c_0^2(\frac{\partial^2\rho}{\partial z^2}) \tag{6.6}$$

However, it has been shown that close to melting transitions in membranes the sound velocity is a sensitive function of density [Halstenberg et al.(1998), Schrader et al.(2002)]. As shown in Fig. 6.1, such transitions are found in biomembranes. This is taken into account by expanding the sound velocity around its value in the fluid phase

$$c^2 = c_0^2 + p\Delta\rho^A + q(\Delta\rho^A)^2 + ... \tag{6.7}$$

up to terms of quadratic order. The parameters p and q describe the dependence of the sound velocity on density close to the melting transition and are fitted to experimental data [Heimburg and Jackson(2005)].

It is further known, that the speed of sound is frequency-dependent. This effect is known as 'dispersion'. In order to take dispersion into account, a second term is introduced into Eq. (6.5) that assumes the form

$$-h\frac{\partial^4}{\partial z^4}\Delta\rho^A \tag{6.8}$$

where h is a constant. For low amplitude sound, this term leads to the most simple dispersion relation $c^2 = c_0^2 + (h/c_0^2)\omega^2 = c_0^2 + \text{const}\cdot\omega^2$. Lacking good data on the frequency-dependence of sound in the kHz regime, the term given by Eq. (6.8) is the most natural expression of a dispersion term.

Combining Eqs. (6.5)-(6.8) leads to the final time and position-dependent partial

[2] It has to be noted that all the details of experiments and establishment of relations between quantities are not discussed in this mini review of section 6.2

differential equation [Heimburg and Jackson(2005), Lautrup et al.(2011)]:

$$\frac{\partial^2}{\partial\tau^2}\Delta\rho^A = \frac{\partial}{\partial z}\left[\left(c_0^2 + p\Delta\rho^A + q\left(\Delta\rho^A\right)^2 + ...\right)\frac{\partial}{\partial z}\Delta\rho^A\right] - h\frac{\partial^4}{\partial z^4}\Delta\rho^A \tag{6.9}$$

which describes the propagation of a longitudinal density pulse in a myelinated nerve. In this equation

- $\Delta\rho^A$ is the change in lateral density of the membrane $\Delta\rho^A = \rho^A - \rho_0^A$.
- ρ^A is the lateral density of the membrane.
- ρ_0^A is the equilibrium lateral density of the membrane in the fluid phase.
- c_0 is the velocity of small amplitude sound.
- p and q are the parameters determined from density dependence of the sound velocity. These two constants parametrize the experimental shape of the melting transition of the membrane and are given in [Heimburg and Jackson(2005)].
- h is a parameter describing the frequency dependence of the speed of sound, i.e., the dispersion.

All parameters except h are known from experiment. The empirical equilibrium value of ρ_0^A *is* 4.035×10^{-3} g/m^2 and the low frequency sound velocity c_0 is 176.6 m/s. The coefficients p and q were fitted to measured values of the sound velocity as a function of density. The parameter h is not known experimentally due to difficulties to measure the velocity of sound in the kHz regime. The article by Mosgaard, Jackson and Heimburg [Mosgaard(2012)] attempts to derive this parameter theoretically from relaxation measurements.

The non-linearity and dispersive effects of the lipids can produce a self-sustaining and localized density pulse (soliton) in the fluid membrane (see Fig. 6.4). The pulse consists of a segment of the membrane that locally is found in a solid (gel) state. It preserves its amplitude, shape and velocity while it is propagating along the nerve axon. Further, the pulse propagates over long distances without loss of energy.

In the following we work with the dimensionless variables u (dimensionless/normalized density change), x and t defined in [Lautrup et al.(2011)] as

$$u = \frac{\Delta\rho^A}{\rho_0^A} \qquad x = \frac{c_0}{h}z \qquad t = \frac{c_0^2}{\sqrt{h}}\tau \qquad B_1 = \frac{\rho_0}{c_0^2}p \qquad B_2 = \frac{\rho_0^2}{c_0^2}q \tag{6.10}$$

Equation (6.9) now assumes the following form

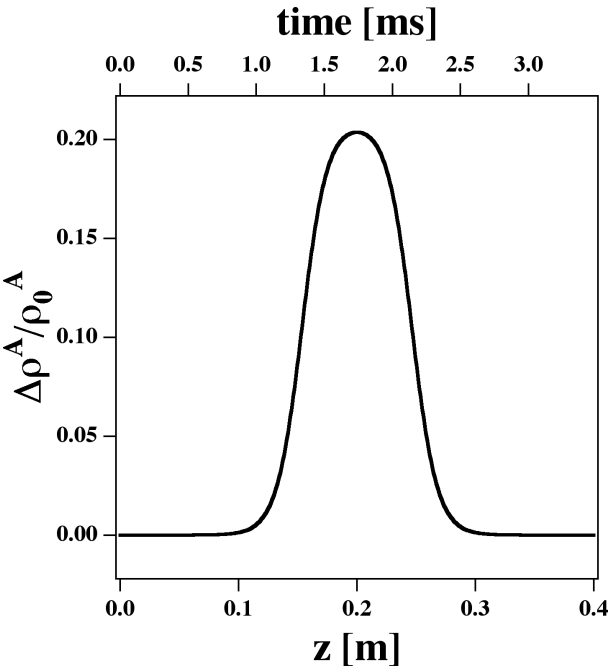

Figure 6.4: Calculated solitary density pulse as a function of lateral position using experimental parameters for a synthetic membrane. The pulse travels with about 100 m/s (by T. Heimburg, used with permission from [Heimburg and Jackson(2008)]).

$$\frac{\partial^2 u}{\partial t^2} = \frac{\partial}{\partial x}\left(B(u)\right)\frac{\partial u}{\partial x} - \frac{\partial^4 u}{\partial x^4} \tag{6.11}$$

with

$$B(u) = 1 + B_1 u + B_2 u^2 \,. \tag{6.12}$$

$B_1 = -16.6\,,\ B_2 = 79.5$ were determined experimentally for a synthetic lipid membrane in [Heimburg and Jackson(2005)]. If we consider a density pulse u propagating with constant velocity we can use the coordinate transformation $\xi = x - \beta t$ (where β is the dimensionless propagation velocity of the density pulse). This yields the following differential equation

$$\beta^2 \frac{\partial^2 u}{\partial \xi^2} = \frac{\partial}{\partial \xi}\left(B(u)\frac{\partial u}{\partial \xi}\right) - \frac{\partial^4 u}{\partial \xi^4} \,. \tag{6.13}$$

Equation (6.12) displays exponentially localized *solitary* solutions which propagate without distortion for a finite range of sub-sonic velocities [Heimburg and Jackson(2005), Lautrup et al.(2011)].

The above differential equation possesses analytical solutions given by

$$u(\xi) = \frac{2a_+a_-}{(a_+ + a_-) + (a_+ - a_-)cosh(\xi\sqrt{1-\beta^2})} \tag{6.14}$$

where $u = a_\pm$ is given by

$$a_\pm = \frac{-B_1}{B_2}\left(1 \pm \sqrt{\frac{\beta^2 - \beta_0^2}{1-\beta_0^2}}\right) \tag{6.15}$$

for the velocity range $\beta_0 <\mid \beta \mid< 1$ (with 1 being the normalized low amplitude sound velocity). There exists a lower limit for the propagation velocity of the pulse given by $\beta_0 = 0.649851$ for a synthetic membrane. No solitons exist for slower velocities. The density change $u(\xi)$ describes the shape of the propagating soliton, which depends on the velocity β. A typical soliton generated by Eq. (6.13) is shown in Fig. 6.4. The minimum propagation velocity β is about 100 m/s, very similar to the measured propagation velocity of the action potential in myelinated nerves. Since the pulse describes a reversible mechanical pulse, it possesses a reversible heat production, a thickening and a simultaneous shortening of the nerve axon, in agreement with observation. Due to the electrostatic features of biomembranes, the pulse possesses a voltage component. Thus, the traveling soliton can be considered a piezoelectric pulse. To seek the energy density that yields in Eq. (6.13), the dimensionless displacement, $s(x,t)$ has to be introduced which is defined as $u = \partial s/\partial x$. The energy density can be written as

$$\mathcal{E} = \frac{1}{2}\left(\frac{\partial s}{\partial t}\right) + \left[\frac{1}{2}u^2A(u) + \frac{1}{2}\left(\frac{\partial u}{\partial x}\right)^2\right], \tag{6.16}$$

with

$$A(u) = 1 + \frac{1}{3}B_1u + \frac{1}{6}B_2u^2. \tag{6.17}$$

The first term in the above equation represents the kinetic energy density and the second term represents the potential energy density. The total energy associated with an arbitrary solution, $u(x,t)$ of Eq. (6.13) is given by the integral over all space of the energy density, $\mathcal{E}$, of Eq. (6.3). It is made use of in the numerical study.

One feature of the soliton model not discussed here in detail is that it provides a mechanism for general anesthesia. It has been shown that general anesthetics lower the melting points of lipid membranes. At critical dose (where 50% of the individuals are anesthetized), the magnitude of this shift is independent of the chemical nature of the anesthetic drugs [Kharakoz(2001), Heimburg and Jackson(2007)]. From this one can deduce quantitatively how much free energy is required to trigger a soliton. In the presence of anesthetics this free energy requirement is higher. As a result, nerve

pulse stimulation is inhibited. In this respect it is interesting to note that hydrostatic pressure reverses anesthesia. For instance, tadpoles anesthetized by ethanol wake up at pressures around 50 bars [Johnson and Flagler(1950)]. It is also known that hydrostatic pressure increases melting temperatures of lipid membranes due to the positive excess volume of the transition [Ebel et al.(2001]. The effects of anesthetics and hydrostatic pressure are known quantitatively. Therefore, one can also quantitatively calculate at what pressure the effect of anesthetics is reversed. The resulting pressures are of the order of 25 bars at critical anesthetic dose, which is of same order as the observed pressure reversal of anesthesia [Heimburg and Jackson(2007), Heimburg and Jackson(2007)].

Another important aspect discussed elsewhere is that melting of membranes results in quantized conduction events in lipid membranes due to thermal fluctuations. The conduction events are indistinguishable from protein ion channel traces [Antonov et al.(1980), Blicher et al.(2009), Heimburg(2010), Laub et al.(2012)]. Any change in a thermodynamics variable that is able to trigger a soliton in a nerve membrane is also able to generate lipid ion channel opening.

6.4 Stability Analysis

A good model for a biological process is the one with high predictive power. From a theory of given system it should be possible to explain how the system functions and predict how it will respond to perturbations. In order to study the intrinsic properties of the solitons, specifically the stability of solitons in the presence of noise and dissipation a numerical study has been carried out [Lautrup et al.(2011)]. Such studies are necessary to demonstrate that the solitary pulses Eq. (6.13) can propagate under realistic physiological conditions over the length scales of nerves in the presence of viscosity and lateral inhomogenities [Lautrup et al.(2011)]. A brief discussion on the results of the analysis will be presented in the following. The propagation of sound in the lipid membranes is described by equation (6.13). This equation has a strong similarity with the Boussinesq equation [Boussinesq1872] which in dimensionless form is given as

$$\frac{\partial^2 f}{\partial t^2} = \frac{\partial}{\partial x}\Big[(1+f)\frac{\partial f}{\partial x}\Big] + \frac{\partial^4 f}{\partial x^4}. \tag{6.18}$$

The solutions to the above equation, with the boundary condition that f should vanish at spatial infinity are of the form

$$f(x,t) = 3(v^2-1)sech^2\Big[\sqrt{(v^2-1)}(x-vt)/2\Big], \tag{6.19}$$

with $v > 1$ [Lautrup et al.(2011)]. The significance of these solitonic equations are enhanced by the powerful mathematical tools in all areas of physics. Solitons play an

important role in hydrodynamics, quantum field theory, antiferromagnetism, Bose-Einstein condensates, non-linear optics and biological systems [Lautrup et al.(2011)]. In the next paragraphs, a precise model for the numerical study will be stated. The numerical methods used to probe the stability of solitons will be described.

6.4.1 Numerical model

Although there exists the analytic form of the solitons, we elect to consider the problem numerically to solve for infinitesimal stability. Inorder to do so, Eq. (6.13) is re-written as two first-order equations. We get

$$\frac{\partial u}{\partial t} = \frac{\partial v}{\partial x}, \qquad \frac{\partial v}{\partial t} = \frac{\partial f}{\partial x}, \tag{6.20}$$

with

$$f = u + \frac{1}{2}B_1 u^2 + \frac{1}{3}B_2 u^3 - \frac{\partial w}{\partial x}, \tag{6.21}$$

where $w = \partial u/\partial x$ and thereby $v = \partial s/\partial t$.

The first of equations (6.20) ensures that the spatial integral of u is independent of time if v is chosen to be periodic. These equations are well suited for numerical solution using a variant of the two-step Lax-Wendroff method. Please see the appendix for the algorithm. This algorithm is both fast and stable in practice. For periodic boundary conditions and the choice of spatial step size $\Delta x = 0.1$ and time step $\Delta t = 0.001$, used below, it was possible to follow 10^6 time steps without discernible loss of accuracy. The energy is not rigorously conserved by this numerical algorithm. The energy was found to decrease at a roughly constant rate proportional to Δx^2. This fact was used to make an appropriate choice of spatial size. The corresponding value of temporal step size was selected to yield full numerical stability.

In [Lautrup et al.(2011)], a detailed study on small amplitude perturbations, genesis of solitons, consequences of dissipation on soliton propagation was performed. The results of colliding nerve pulses using numerical simulations are presented in the following. Please refer [Lautrup et al.(2011)] for the results of other stability studies. It has to be noted that the main interest of this study is physical rather than mathematical. A parallel comparison with the Hodgkin-Huxley model will also be carried out.

6.4.2 Collision Study

In-order to study this aspect in soliton model we have considered the head-on collison of two solitary pulses with identical amplitudes and opposite velocities. Our model is based on adiabatic and reversible physics with no detailed mechanism for dissipation

other than the inclusion of viscous friction. This means that the right hand side of equation (6.11) now consists the viscosity in the Navier-Stokes velocity

$$\frac{\partial^2 u}{\partial t^2} = \frac{\partial}{\partial x}\Big(B(u)\Big)\frac{\partial u}{\partial x} - \frac{\partial^4 u}{\partial x^4} + \kappa\frac{\partial^3 u}{\partial x^2 \partial t} \tag{6.22}$$

This term is readily incorporated in our numerical approach into Eq. (6.21)

$$f = u + \frac{1}{2}B_1 u^2 + \frac{1}{3}B_2 u^3 - \frac{\partial w}{\partial x} + \kappa\frac{\partial v}{\partial x} \tag{6.23}$$

The numerical results are performed with the value $\kappa = 0.05$. Here we investigate collisions in the absence of friction.

In contrast, the soliton model doesn't exhibit a complete annihilation. The pulses pass through each other almost undisturbed with the generation of some small amplitude noise. Thus, soliton model contradicts the description of the cancellation of pulses suggested in the biology literature. Fig. 6.5 (left) shows two identical small

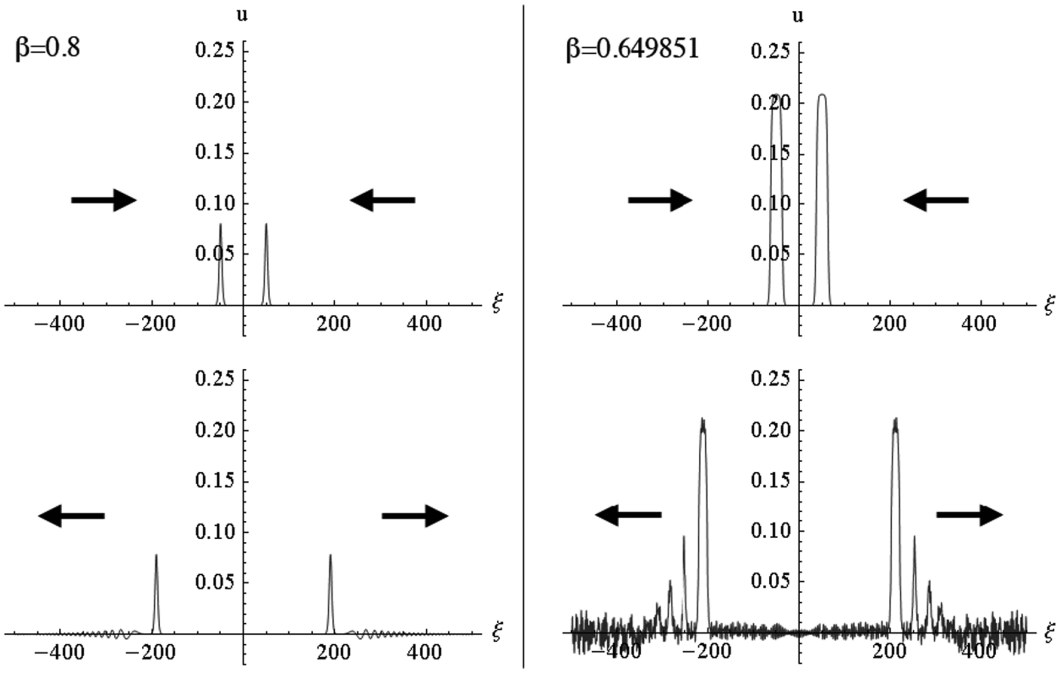

Figure 6.5: Collision of two solitons before (top panels) and after collision (bottom panels) for two different velocities (left and right panels). Left: soliton velocity of $\beta = 0.8$. Small amplitude noise is traveling ahead of the post-collision pulses. This indicates some dissipation during the collision. Right: soliton velocity $\beta = 0.649850822$ (close to maximum amplitude). Adapted from [Lautrup et al.(2011)].

amplitude solitons traveling in opposite directions at a velocity of $\beta = 0.8$ (80% of the lateral speed of sound in fluid membranes) before and after a collision. Small amplitude noise travels ahead of the post-collision pulses indicating a small dissipation of energy of the order of $\ll 1\%$ compared to the soliton energy. The same was found for solitary pulses with different velocities and amplitudes. However, when the maximum amplitude solitons collide, Eq. (6.12) allows the density transiently to exceed the density of the solid phase ($u = 0.25$). Since we regard this as unphysical, a "soft barrier" is introduced at the density of the solid phase:

$$B(u) = (1 + B_1 u + B_2 u^2)(1 + e^{\alpha(u-u_{max})}). \tag{6.24}$$

This modification of Eq. (6.24) is valid only at the moment of collision of two large-amplitude solitons. We used $\alpha = 100$ and as maximum density $u_{max} = 0.26$, which is close to the maximum change of density for the particular synthetic membrane discussed. The result of such a collision of solitons approaching the minimum velocity (maximum amplitude) is shown in (Fig. 6.5, right). The solitons fall apart in a sequence of lower amplitude solitons and some high frequency noise. This effect is more pronounced the closer the velocity is to the minimum velocity [Lautrup et al.(2011)]. Such a decomposition of larger pulse into several pulses was not seen in the absence of this soft barrier. Comparison of energy of the largest amplitude pulse after the collision with the energy before collision is shown in Fig. 6.6. Only for the case of solitons approaching minimum velocity and maximum amplitude, the fraction of energy lost into smaller amplitude solitons and small amplitude noise is significant (Fig. 6.6). Thus, we observed that most of the energy of the major soliton was conserved in collisions even if a maximum density was enforced.

6.5 Discussion

Interestingly, soliton-like regimes can be also found in the Hodgkin-Huxley model [Aslanidi and Mornev(1997)]. The term soliton is used here in a more mathematical sense meaning that one can generate pulses that reflect or penetrate each other when using certain parameters. Since the HH and the FHN model are based on dissipative processes, these are not solitons in a physical sense as in the soliton model.
Aslanidi and Mornev demonstrated that in excitable media under certain conditions, one can expect the emergence of a soliton-like regimes that corresponds to reflection (or loss-free penetration) of colliding waves. Fig. 6.7 shows for $E_K = -12mV$ that colliding pulses annihilate. In contrast, a soliton-like regime was found for $-2.50mV < E_K < 2.46mV$ (Fig. 6.7). Furthermore, the pulses can also collide with the fiber boundaries and be reflected [Aslanidi and Mornev(1997)]. The authors of this study concluded that the soliton-like regime is described by spatially

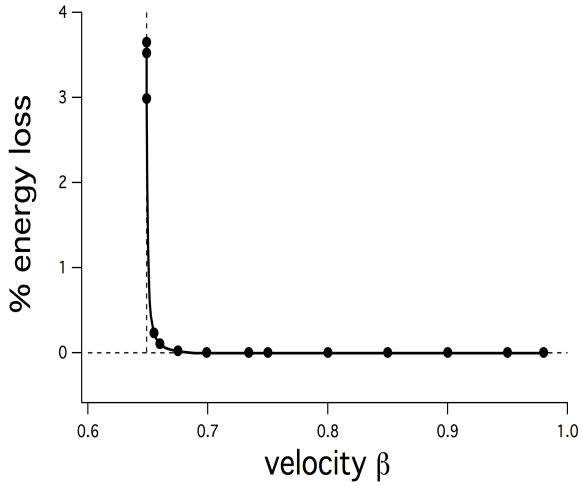

Figure 6.6: Energy loss of soliton after collision in %. The dissipation is significant only when the pulses reach their minimum velocity. From [Lautrup et al.(2011)].

nonuniform time-periodic solutions of the Hodgkin-Huxley equations. The mechanism of pulse reflection is explained as follows [Aslanidi and Mornev(1997)]. *"In the soliton-like regime the traveling pulse presents a doublet consisting of a high-amplitude pulse-leader and a low-amplitude wave following this pulse. When doublets interact, the leaders are annihilated, and the collision of the low-amplitude waves after a short delay leads to their summation. As a result of the summation, the potential V at the site of the collisions reaches a super-threshold value, causing regeneration of the doublets, which thereafter move apart in opposite directions. The process of reflection of excitation pulses from impermeable fiber ends evolves according to the same scenario."*

It was also noticed that low-amplitude waves can give rise to new extra pulses which also take part in interactions. When a doublet was initiated at the left end of a fiber, the amplitude of the following pulse rapidly increases while traveling. It reaches threshold value and initiates two "extra pulses". These pulses travel apart to the opposite ends of the axon and are reflected from them. This complex regime was observed for $-2.46mV < E_K < 2.40mV$. Such soliton regimes are also observed in the simplified models of Hodgkin-Huxley, [Kosek(1995), Petrov(1994)]. However, it is a challenge to search for any of these regimes in the experiments. Summarizing, the soliton model does not lead to annihilation of pulses, while the Hodgkin-Huxley model allows for both, annihilation and penetration depending on parameters.

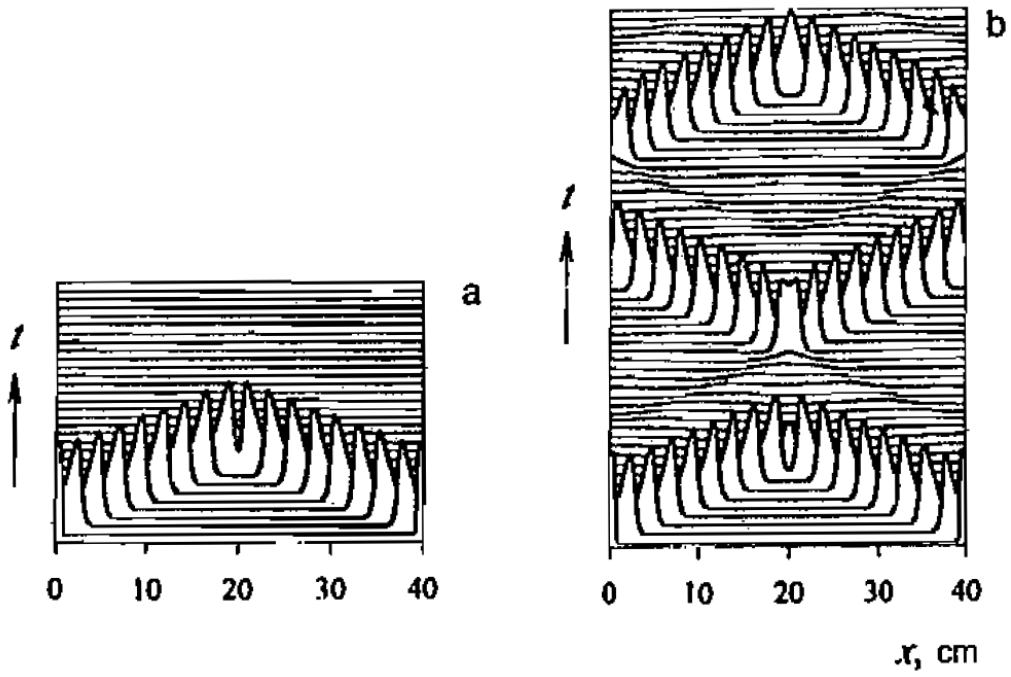

Figure 6.7: Collision of pulses in the HH model. Left: Annihilation of colliding nerve pulses at the standard value $E_K = -12.0mV$. Right: Reflection (or penetration) of pulses at $E_K = -2.5mV$. Use with permission from [Aslanidi and Mornev(1997)].

6.6 Comparison of Hodgkin-Huxley and Soliton Models

The Hodgkin-Huxley (HH) model of nerve pulse propagation is a remarkable achievement in the field of physiology. It has shaped the thinking of a complete discipline for decades and is in line with the emergence of ion channel proteins and the influence of many drugs on the excitability of a nerve membrane. However, as already mentioned above the HH-model cannot explain several nonelectrical phenomena such as the finding of reversible heat changes [Abbott et al.(1958), Howarth et al.(1968), Howarth(1975), Ritchie and Keynes(1985), Tasaki et al.(1989), Tasaki and Byrne(1992)], changes in nerve thickness and nerve contraction described in mechanical and optical experiments [Tasaki et al.(1968), Iwasa and Tasaki(1980), Iwasa et al.(1980), Tasaki(1982), Tasaki(1999)]. The soliton model is an alternative model that can convincingly describe some of the unexplained observations found in the experiments. It also generates ion channel-like events and provides a mechanism for general anesthesia [Heimburg and Jackson(2007)]. In the following, we list some of

the major features of the two neural models:
Hodgkin-Huxley Model :

- The action potential is based on electrical cable theory in which the pulse is the consequence of voltage- and time-dependent changes of the conductance for sodium and potassium.
- The nerve pulse consists of a segment of charged membrane capacitor that propagates driven by dissipative flows of ions.
- The model is consistent with quantized ion currents attributed to opening and closing of specific channel proteins.
- It is consistent with the channel-blocking effects of several poisons (such as tetrodotoxin).
- The underlying hypothesis is exclusively of electrical nature and does not refer to changes of any other thermodynamics variables other than charge and electrical potential.
- The HH model is based on ion currents through resistors (channel proteins) and is therefore of dissipative nature.
- Reversible changes in heat and mechanical changes are not explicitly addressed but heat generation would be expected.
- The propagating pulse dissipates a significant amount of free energy [Heimburg and Jackson(2008)].
- The HH model generates a refractory period (minimum distance between pulses) and hyperpolarization as a consequence of the complex time-dependence of channel conduction.
- The theory does not provide an explanation of anesthesia.

Soliton Model

- The nerve pulse is a solitary electromechanical soliton coupled to the lipid transition in the membrane.
- The solitary character is a consequence of the non-linearity of the elastic constants close to the melting transition of the lipid membrane, and of dispersion.
- The theory is based on macroscopic thermodynamics and implies role for all thermodynamics variables.

- It does not contain an explicit role of poisons and protein ion channels.
- However, the theory is consistent with channel-like pore formation in lipid membranes that is indistinguishable from protein conductance traces [Blicher et al.(2009), Heimburg(2010), Laub et al.(2012)].
- Additional to changes in the electrical potential and the charge of the membrane, the propagating pulse is associated to changes in all variables including temperature, lateral pressure, area and length. As found in experiments, the nerve pulse is coupled to changes in thickness and length.
- In agreement with experiment, the propagating pulse does not dissipate heat because it is based on adiabatic processes.
- The model generates a refractory period and a hyperpolarization that is a consequence of mass conservation [Villagran Vargas et al.(2011)].
- The soliton model implies a mechanism for general anesthesia [Heimburg and Jackson(2007), Heimburg and Jackson(2007)].

Both the theories describe the existence of voltage pulse in nerve pulse propagation. In the HH model the propagating potential-change itself is the signal, while in the soliton model it is only one inseparable aspect of a more generic adiabatic pulse that implies changes in all variables.

6.7 Digest

- The lipid membranes have the properties required for the generation and propagation of density/ sound pulse.
- Local compression of the lipid membrane creates a wave or pulse by increasing the local density.
- The "non-linearity " and "dispersion" phenomenon at the melting transition regime are necessary conditions for the soliton propagation.
- The soliton model is a modified Boussinesq equation and we have conducted tests of stability of the solitons numerically with periodic boundary conditions.
- These solitons were found to be stable with smallest possible perturbations inevitably induced by the finite size of the numerical mesh and to finite but small periodic perturbations (Refer [Lautrup et al.(2011)]).

- The solitons retain their characteristic properties even in the presence of relatively strong dissipation (See [Lautrup et al.(2011)]).
- Finally, the solitons pass through each other "almost undisturbed" with the generation of only small amounts of small-amplitude noise. Therefore this model does not offer a description of the cancellation of pulses upon collision in the nerve membrane as suggested in the literature.
- Thus this stable solitary wave model is viable in a realistic physiological nerve environment and may provide an immediate and reliable explanation of mechanical and thermodynamic effects associated with it.

At the heart of science is an essential balance between two seemingly contradictory attitudes- an openness to new ideas, no matter how bizarre or counterintuitive they may be, and the most ruthless skeptical scrutiny of all ideas, old and new. This is how deep truths are winnowed from deep nonsense.

—C. Sagan

7 Membrane Electrostatics

In the pursuit of translating the 'soliton' of nerve membrane to action potential, we proceeded to work on the electrostatic potential of the membrane. Since the lipid melting plays a key role in the soliton's generation and propagation, it is interesting to investigate the contribution of lipids to the electrostatic potential of membrane.

7.1 Introduction

Membrane electrostatics plays an important role in many intracellular and extracellular processes. Several lipid species found in natural membranes are charged. Phosphatidylethanolamine (PE), phosphatidylcholine (PC), sphingomyelin (SM) and phosphatidylserine (PS) are the four main phospholipids in membranes. Of which PE, PC and SM are considered neutral and PS is negatively charged. The electric properties of these lipids constitute to the membrane electrostatic potential by various phenomena. In a membrane, the amphiphilic phospholipids with hydrophilic head groups exposed to the aqueous environment and hydrophobic carbon chains directed into the interior of the membrane. This minimizes the contact of the carbon chains with ions, water and other polar molecules in the aqueous environment. Ion concentrations on both sides of the biological membrane and the high densities of charged and polar head groups, separated by membrane thickness produce high electrostatic potentials across the membrane. These potentials are

- Transmembrane potential (ψ_m) generated by ion gradients across the membrane

- Surface potential (ψ_s) arising from fixed charges at the lipid head groups and membrane proteins
- Dipole potential (ψ_D) of the dipoles at the lipid-water interface

A description on these potentials has been given in chapter 6. This chapter focuses on the dipole and surface potential of monolayers and also relates to the phases of lipids. The influence of ionic strength on these potentials will be also addressed. In the following subsection we will discuss about the electrostatics in general and terms involved in it in the context of diffuse double layer.

7.1.1 Electrostatic Problems

Let us recall Maxwell's equations [vanRienen(2001)] in differential form as described in Chapter 4.

$$\begin{aligned} \nabla \cdot \mathbf{D} &= \rho \\ \nabla \cdot \mathbf{B} &= \mathbf{0} \\ \nabla \times \mathbf{E} &= -\frac{\partial \mathbf{B}}{\partial \mathbf{t}} \\ \nabla \times \mathbf{H} &= \frac{\partial \mathbf{D}}{\partial \mathbf{t}} + \mathbf{J} \end{aligned} \tag{7.1}$$

In electrostatic problems, Maxwell's equations reduce to Gauss's law

$$\nabla \cdot \mathbf{D} = \rho \tag{7.2}$$

which relates the divergence of the electric displacement ($\mathbf{D}$) to the density (ρ) of free charges, and the static form of Faraday's law

$$\nabla \times \mathbf{E} = \mathbf{0} \tag{7.3}$$

In a dielectric, the electric displacement $\mathbf{D}$ is proportional to the electric field $\mathbf{E}$

$$\mathbf{D} = \epsilon_\mathbf{r}\epsilon_\mathbf{0}\mathbf{E} \tag{7.4}$$

where ϵ_r is the relative permittivity and ϵ_0 is the permittivity of vacuum. Substituting Eq.(7.4) in Eq.(7.2) gives

$$\nabla \cdot \mathbf{E} = \frac{\rho}{\epsilon_\mathbf{r}\epsilon_\mathbf{0}} \tag{7.5}$$

Because the electric field, **E** is irrotational (Eq.7.3) it can be expressed as the gradient of a scalar function,ϕ called the electrostatic potential.

$$\mathbf{E} = -\nabla\phi \tag{7.6}$$

Substituting the potential gradient for the electric field, Eq. (7.6) in Eq. (7.5), yields Poisson's equation:

$$\nabla \cdot \mathbf{E} = \nabla \cdot (-\nabla\phi) = -\nabla^{\mathbf{2}}\phi = \frac{\rho}{\epsilon_{\mathbf{r}}\epsilon_{\mathbf{0}}} \tag{7.7}$$

Therefore, the electrostatic potential ($\phi(x)$) of a charge distribution ($\rho(x)$) at location x is given by Poisson equation of the form:

$$\frac{\mathrm{d}^2\phi(x)}{\mathrm{d}x^2} = -\frac{\rho(x)}{\varepsilon_0\,\varepsilon_r} \tag{7.8}$$

where $\epsilon_0 = 8.854 \times 10^{-12}[C^2/Jm]$. Helmholtz was the first to create a double layer model in 1879 [Helmholtz(1879)]. This model conceptualized the charge separation at the interface of metallic electrode and an electrolyte solution. Gouy and Chapman were the next to consider the thermal motion of ions in contact with the charged surface. The surface and dipole potential of membranes in the aqueous environment can be modeled using this theory. In the following section, Gouy-Chapman theory is discussed in detail.

7.2 Gouy-Chapman Theory

The electrostatic surface charge of the lipid membrane in contact with the aqueous environment affects the ions. This electrostatic field along with the thermal motion of ions results in adsorption of counter-ions and screens the electric surface charge. These counter ions are not rigidly held instead they tend to diffuse into the aqueous environment until the counter potential set up by their departure restricts this tendency. Partly, the kinetic energy of the counter ions will also affect the thickness of the diffuse double layer. The change in concentration of the counter-ions near a charged surface follows the Boltzmann distribution. That is, the concentration of an ion n_i of species i with charge z_i at a location x is given by

$$n_i(x) = n_{i,0} exp\left(-\frac{z_i e\phi(x)}{kT} \right) \tag{7.9}$$

where $n_{i,0}$ is the concentration of ion species i at the location with the zero potential $\phi = 0$, i.e., infinite distance from the membrane. z_i may be positive or negative and elementary charge, $e = 1.602 \times 10^{-19}[C]$. k being the Boltzmann constant and T is

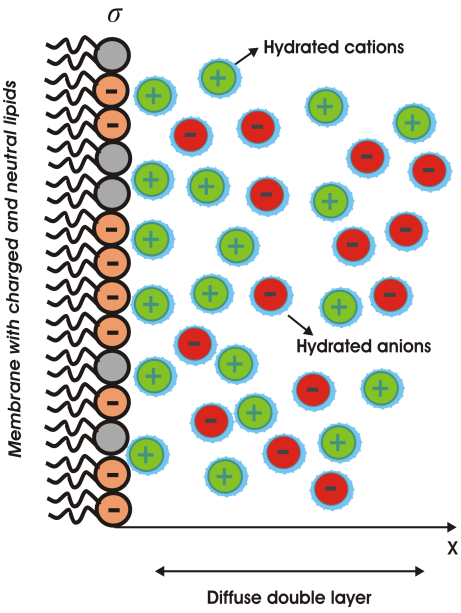

temperature. Since we have a diffuse double layer the total charge density per unit volume is given by

$$\rho(x) = \sum_i z_i \cdot e \cdot .n_i(x) \tag{7.10}$$

By inserting Eq. (7.9) in Eq. (7.10) and then inserting the result in Eq. (7.8) the coloumbic interaction between charges can be expressed as

$$\frac{\mathrm{d}^2\phi(x)}{\mathrm{d}x^2} = -\frac{e}{\varepsilon_0\,\varepsilon_r}\sum_i n_{i,0} z_i exp\left(-\frac{z_i e\phi(x)}{kT}\right) \tag{7.11}$$

This is called as *Poisson-Boltzmann equation*(PB) and can be solved numerically for given boundary conditions. It has to be noted that the concentration $n_{i,0}$ has to be given in mol/m^3 to be consistent with units. At infinite distance from the membrane the potential $\phi = 0$ and the charge density $\rho = 0$(electro-neutrality condition). This leads to the boundary condition

$$\text{at} \quad x = \infty: \quad \phi = 0 \quad \text{and} \quad \left(\frac{\mathrm{d}\phi}{\mathrm{d}x}\right) = 0 \tag{7.12}$$

For small potentials, $z_i e\phi \ll kT$, the PB equation can be expanded in Taylor series and linearized to obtain the *Linearized Poisson-Boltzmann (LPB) or Debye-Huckel*

Table 7.1: Debye lengths for varying concentrations of electrolyte

$n_0[mol/l]$	$\lambda_D[nm]$
0.15	0.78
0.1	0.96
0.05	1.3
0.01	3.03
0.001	10

equation

$$\begin{aligned}\frac{\mathrm{d}^2\phi}{\mathrm{d}x^2} &= \left(\frac{2e^2}{\varepsilon_0\,\varepsilon_r kT}\left[\frac{1}{2}\sum_i z_i^2 n_{i,0}\right]\right)\cdot\phi(x)\\ &= \left(\frac{2e^2}{\varepsilon_0\,\varepsilon_r kT}n_0\right)\cdot\phi(x)\\ &= \kappa^2\cdot\phi(x)\end{aligned} \tag{7.13}$$

where n_0 is the ionic strength and κ is the Debye constant and are given as

$$\begin{aligned}n_0 &= \frac{1}{2}\sum_i z_i^2 n_{i,0}\\ \kappa &= \sqrt{\left(\frac{2e^2}{\varepsilon_0\,\varepsilon_r kT}c_0\right)}\end{aligned} \tag{7.14}$$

For monovalent salt like $NaCl$ the ionic strength is nothing but salt concentration. $\lambda_D = 1/\kappa$ is called the Debye length. It has units of length and depends on the ionic strength. It is the screening distance of an electrostatic charge. It is clear from the above equation that the screening length is inversely proportional to ionic strength. The concentrations in this equation also carry the units of $[mol/m^3](1M = 6.023 \times 10^{26}/m^3)$. Here is a table of debye lengths for various concentrations of electrolyte.

Therefore for an infinitely extended planar membrane with homogenous charge density the LPB equation has a simple solution

$$\phi(x) = \phi_0 exp(-\kappa x) \tag{7.15}$$

with ϕ_0 as the potential at the membrane. For an infinitely planar membrane with

homogeneous charge density one can simplify the equation to solve it analytically. By using the property of derivatives

$$\frac{\mathrm{d}^2\phi(x)}{\mathrm{d}x^2} = \frac{1}{2}\frac{\mathrm{d}}{\mathrm{d}\phi}\left(\frac{\mathrm{d}\phi}{\mathrm{d}x}\right)^2 \tag{7.16}$$

the PB equation can be solved as

$$\mathrm{d}\left(\frac{\mathrm{d}\phi(x)}{\mathrm{d}x}\right)^2 = -\frac{2e}{\varepsilon_0\,\varepsilon_r}\sum_i n_{i,0} z_i exp\left(-\frac{z_i e\phi(x)}{kT}\right)\mathrm{d}\phi \tag{7.17}$$

Using the boundary conditions Eq. (7.12) and integrating from ∞ to x

$$\left(\frac{\mathrm{d}\phi(x)}{\mathrm{d}x}\right)^2 = \frac{2kT}{\varepsilon_0\,\varepsilon_r}\sum_i n_{i,0} exp\left(-\frac{z_i e\phi(x)}{kT} - 1\right) \tag{7.18}$$

For an electrolyte solution of monovalent ions ($z = +1$ or -1), like $NaCl$ the above equation has the form

$$\frac{\mathrm{d}\phi(x)}{\mathrm{d}x} = \left(\frac{8kTn_0}{\varepsilon_0\,\varepsilon_r}\right)^{1/2} sinh\left(\frac{e\phi(x)}{2kT}\right) \tag{7.19}$$

The surface charge density of the membrane is σ. The electro-neutrality gives the relation

$$\sigma = \epsilon_r\epsilon_0\left(\frac{\mathrm{d}\phi(x)}{\mathrm{d}x}\right)_{x=0} \tag{7.20}$$

By using Eq. (7.19) this transforms into

$$\sigma = \sqrt{8\epsilon_0\epsilon_r n_0 kT}\, sinh\left(\frac{e\phi_0}{2kT}\right) \tag{7.21}$$

This is called as the Grahame equation. The effect of ionic strength on the membrane surface potential is depicted in the following figure.

The above numerical results are obtained for a planar liquid phase lipid membrane with area per lipid taken for DPPC as $a_l = 4.96 \times 10^{-19}[m^2]$. The numerical calculations are carried out in FEM based Comsol Multiphysics 4.2a®. The numerical calculations of GC model are verified with the analytical solution using Grahame equation. These are shown in the following table.

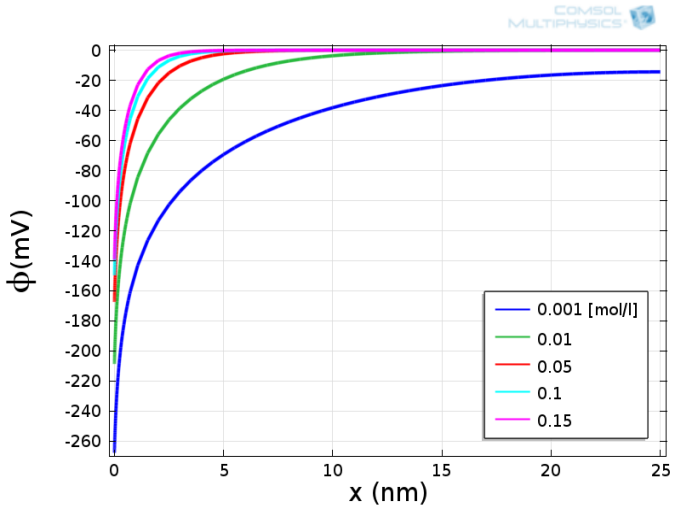

Figure 7.1: Potential distribution $\phi(x)$ of a fluid membrane for various concentration of $NaCl$ using Gouy-Chapman (GC) model.

Table 7.2: Comparison of numerical and analytical solutions of GC model

$n_0[mol/l]$	$Numerical\phi_0[mV]$	$Analytical\phi_0[mV]$
0.15	-136.5	-136.5
0.1	-147	-146.8
0.05	-164	-164.5
0.01	-206	-205.8
0.001	-265	-264.9

7.2.1 Limitations of GC theory

In the treatment of diffuse double layer, several assumptions were made [Cevc(1990)]

- The finite size of ions was neglected.
- Ions in the solution were considered as a continuous charge distribution.
- The surface charge was assumed to be homogeneous, instead it depends on the charged groups and adsorbed ions.
- All non-Coulombic interactions were not considered.
- The permittivity of the medium was supposed to be constant.

- The surface was assumed to be flat on the molecular scale. This is not a reasonable assumption for a biological membrane in a physiological buffer.
- Image forces between the ions and the surface were ignored.

7.3 Zwitterionic lipid layer in contact with water

Approximately 10-40% of the naturally occurring lipids carry a charge- usually one or two negative charges [Heimburg(2007)]. The rest of the lipids are neutral or zwitterionic. Such zwitterionic lipids in contact with water dipoles contribute to the surface and dipole potential of the membrane. This is due to the dipole-dipole interactions between them which effects the permittivity. Most of the theoretical models of [McLaughlin1989, Cevc(1990), KraljIglic(1996), Outhwaite(2002), Bazant(2009)] assume that the dielectric permittivity in the electrolyte solution or pure water being in contact with lipid surface is constant. The assumption of constant permittivity is the consequence of the constant number of water molecules distributed from the surface to bulk. But actually, close to the membrane surface the orientation and depletion of water molecules may result in strong spatial variation of permittivity. An explicit consideration of orientational ordering of water molecules in [Butt(2003), Outhwaite(1976), Outhwaite(1983), Iglic(2010), Gongadze(2011), GongadzeIglic(2012)] has shown its significance in such type of models. We model a zwitterionic lipid layer in contact with pure water (schematical representation in Fig.7.2) at saturation regime, in which the dielectric permittivity [Booth(1951), GongadzeRienen(2012)] is consistently related to the distribution of electric field strength and distribution of water molecules.

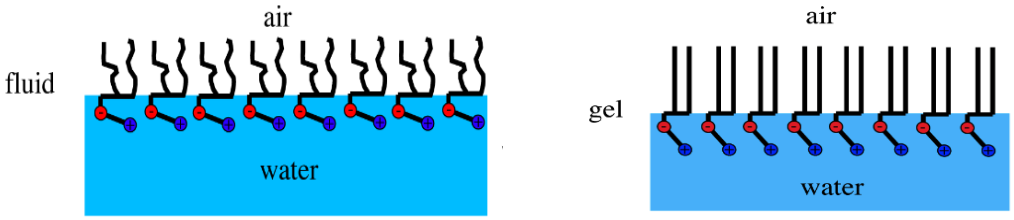

Figure 7.2: Schematic picture of zwitterionic lipid monolayers in contact with water (Left) lipid layer in fluid phase (Right) Lipid monolayer in gel phase.

7.3.1 Model

In the model the headgroup of zwitterionic lipid is described by two charges at fixed distance D, i.e. it is assumed that the headgroup has non-zero dipole moment. The

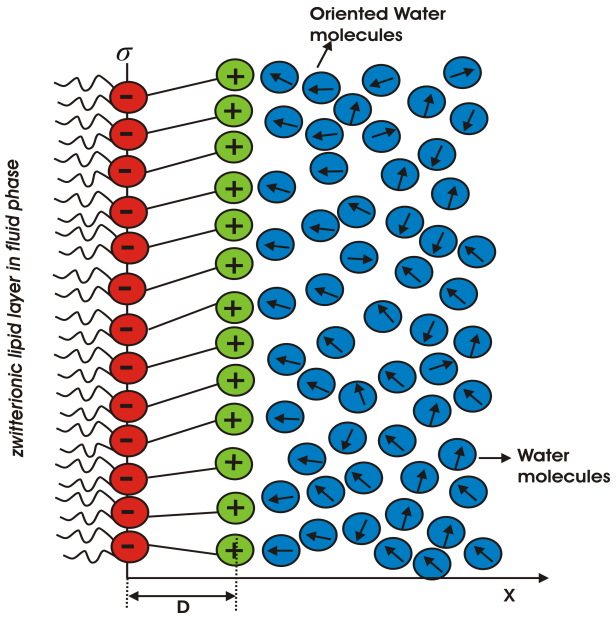

Figure 7.3: Schematic representation of zwitterionic lipid layer in contact with water.

negative charges of the phosphate groups of the lipids are described by negative surface charge density $\sigma = -e_0/a_0$ at $x = 0$ (see Fig. 7.3), where a_0 is the area per lipid. The orientational ordering of water is also taken into account assuming the spatial dependence of permittivity $\varepsilon(x)$ [Iglic(2010), GongadzeIglic(2012)]. The corresponding Poisson equation can be written in the form [GongadzeRienen(2012)] :

$$\nabla \cdot [\varepsilon_0 \, \varepsilon_r(\mathbf{r}) \nabla \phi(\mathbf{r}) \,] = -\rho_{Zw}(\mathbf{r}) \quad , \tag{7.22}$$

where $\rho_{Zw}(\mathbf{r})$ is the macroscopic (net) volume charge density of positive charges of zwitterionic ions (see Fig.1), ε_0 is permittivity of the free space, $\phi(x)$ is the electric potential and $\varepsilon_r(\mathbf{r})$ is the relative permittivity: [Booth(1951),GongadzeRienen(2012)]:

$$\varepsilon_r(\mathbf{r}) \; = \; n^2 + \; \frac{7 \, n_w(\mathbf{r}) \, p_0 \, (n^2+2)}{3 \, \sqrt{73} \, \varepsilon_0} \; \frac{\mathcal{L}(\sqrt{73} \, (n^2+2) \, p_0 E(\mathbf{r})/6kT)}{E(\mathbf{r})} \quad , \tag{7.23}$$

where $n = 1.33$ is the optical refractive index, $p_0 = 2.04$ Debye is the effective water dipole moment, $\mathcal{L}(u) = \coth(u) - 1/u$ is Langevin function, kT is the thermal energy, E is the magnitude of the electric field strength, $n_w(x)$ is space dependent number density of water and $p_{0,ef} = 4.8$ Debye [Gongadze(2011)] is the effective water dipole moment. Eq. (7.23) takes into account so called cavity field within generalized Kirkwood-Onsager-Fröhlich theory [Frohlich(1964)], where the water ordering is considered also in saturation regime [Booth(1951), GongadzeRienen(2012)]. In the

special case of planar geometry we can rewrite the above equations as:

$$\frac{\mathrm{d}}{\mathrm{d}x}\left[\varepsilon_0\,\varepsilon_r(x)\frac{\mathrm{d}\phi}{\mathrm{d}x}\right] = -\rho_{Zw}(x) \quad , \tag{7.24}$$

$$\varepsilon_r(x) \;=\; n^2 + \frac{7\,n_w(x)\,p_0\,(n^2+2)}{3\,\sqrt{73}\,\varepsilon_0}\;\frac{\mathcal{L}(\sqrt{73}\,(n^2+2)\,p_0E(x)/6kT)}{E(x)} \quad , \tag{7.25}$$

where $E = |\frac{\mathrm{d}\phi}{\mathrm{d}x}| = \frac{\mathrm{d}\phi}{\mathrm{d}x}$ (since $\sigma < 0$) is the magnitude of the electric field strength. The volume charge density due to positive charges of the lipid headgroups we can write in the form:

$$\rho_{Zw}(x) = \frac{e_0\,\mathcal{P}(x)}{D\,a_0} \quad , \tag{7.26}$$

where e_0 is the unit charge, $\mathcal{P}(x)$ is probability that the lipid headgroup dipole is oriented for the angle $\omega = \arccos(x/D)$, i.e. $\mathcal{P}(x)$ is the probability that the positive charge of the headgroup is located at the distance x from the negatively charged surface of phosphate groups (see Fig.7.3):

$$\mathcal{P}(x) = \Lambda\,\exp(-e_0\phi(x)/kT) \quad , \tag{7.27}$$

where $x \leq D$. The normalization condition

$$\frac{1}{D}\int_0^D \mathcal{P}(x)\,\mathrm{d}x = 1 \quad , \tag{7.28}$$

leads to :

$$\Lambda = \frac{D}{\int_0^D \exp(-e_0\phi(x)/kT)\,\mathrm{d}x} \quad . \tag{7.29}$$

Using Eqs. (7.26, 7.27 and 7.29) it follows from Eq. (7.24):

$$\frac{\mathrm{d}}{\mathrm{d}x}\left[\varepsilon_0\,\varepsilon_r(x)\frac{\mathrm{d}\phi}{\mathrm{d}x}\right] = -\frac{e_0\,\exp(-e_0\phi(x)/kT)}{a_0\,\int_0^D \exp(-e_0\phi(x)/kT)\,\mathrm{d}x} \quad , \tag{7.30}$$

where in Eq. (7.32) the surface charge density $\sigma = -e_0/a_0$. Note that the area per lipid a_0 is different in gel and liquid phase. The number density of water in $\varepsilon_r(x)$ is calculated as

$$n_w(x) \;= n_{0w}(1 - \alpha_i\mathcal{P}(x)) \quad , \tag{7.31}$$

where $0 < \alpha_{fl} < \alpha_{gel} \leq 1$ and $n_{0w}/N_A = 55\,\mathrm{mol/l}$ is the bulk number density of water. The boundary conditions are (see also [GongadzeRienen(2012)]) :

$$\left.\frac{\mathrm{d}\phi}{\mathrm{d}x}\right|_{(x=0)} = -\frac{\sigma}{\varepsilon_0\,\varepsilon_r(x=0)} \quad , \tag{7.32}$$

$$\left.\frac{\mathrm{d}\phi}{\mathrm{d}x}\right|_{(x=D)} = 0 \quad , \tag{7.33}$$

$$\phi\,|_{(x=D)} = 0 \quad . \tag{7.34}$$

7.3.2 Results

The governing equation of the model is second order partial differential equation, which was solved numerically in the 2D Electrostatics mode in the FEM based Comsol Multiphysics 4.2a®. The subdomain equation in the 2D Electrostatics mode in Comsol is:

$$-\nabla\cdot[\varepsilon_0\varepsilon_r\nabla V] = \rho_{free} \tag{7.35}$$

where the electric potential $V = \phi$ is the dependent variable in the FEM model. This equation is used for implementing our model. The planar zwitterionic lipid layer in pure water is presented as a rectangle with length as $D = 1nm$ and height of 2 nm (Fig. 7.4) and the boundary conditions are applied.

The poisson equation (7.30) is solved using the boundary conditions Eqs. (7.32, 7.34) considering the spatial variation of permittivity (Eq. 7.25). DPPC lipid data is used for the cross sectional area per lipid as $a_{0gel} = 4.96\mathring{A}^2$ and $a_{0fl} = 6.39\mathring{A}^2$. The bulk water dipole concentration (n_{0w}/N_A) is chosen as 55 mol/l, where N_A is Avogadro number. The number density of Langevin (water) dipoles $(n_w(x))$ is calculated according to Eq. (7.31). The α_{fl} is chosen as 0.02 and thereby $\alpha_{gel}$is calculated as

$$\alpha_{gel} = \alpha_{fl}\frac{a_{0gel}}{a_{0fl}} \tag{7.36}$$

A Direct (UMFPACK) stationary solver is employed to perform the simulations. The head group of lipid has a diameter of $0.5 - 1$ nm and since we are considering water dipole interaction in this region, the computation domain's width is set to 1 nm. The finite elements are triangular because the domain is 2D. The planar surface was discretized by use of free triangular mesh consisting of 40, 000 elements distributed

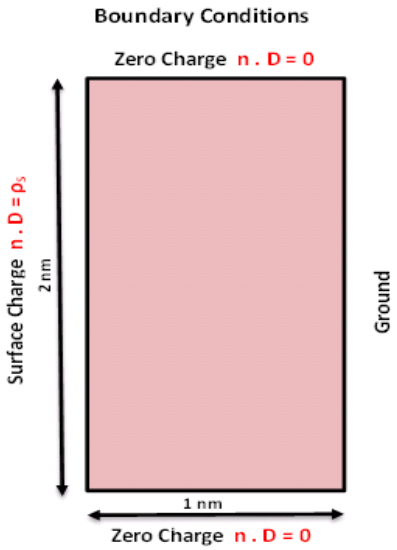

Figure 7.4: Geometry and boundary conditions of the planar structure used to implement the electrostatic model in Comsol Multiphysics 4.2a®.

exponentially with the denser mesh in the vicinity of fixed negative charges of head group. This saves the computational memory and reduces the computational time. Figure 7.5 shows the electric potential in the head group region of lipids in fluid and

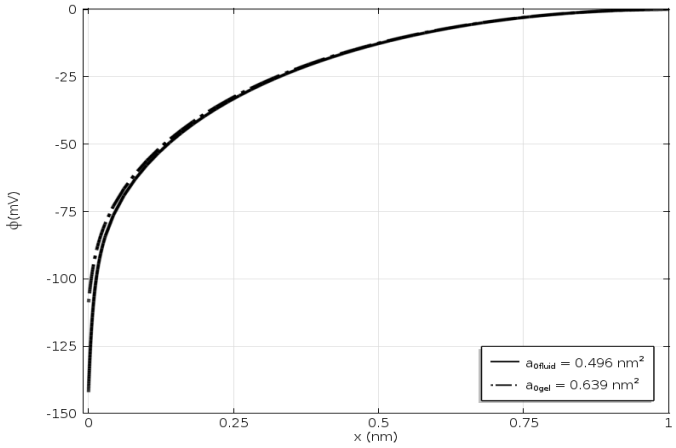

Figure 7.5: Calculated electric potential for the fluid and gel phase of zwitterionic lipid layer using Booth expression for spatial permittivity. Bulk concentration of water dipoles is $n_{0w}/NA = 55mol/l$ and α_{0fluid} is 0.02.

gel phases. The absolute value of the electrostatic potential is 140 mV in fluid phase and 100 mV in gel phase. Note that for the flat, large, homogeneous lipid layer in Fig. 7.9, the electrostatic potential $\phi = \phi(x)$ depends only on the x-direction. It is clear from the figure that in fluid phase of zwitterionic lipid layer, the surface is highly negatively charged when compared to the gel phase of the lipid layer.

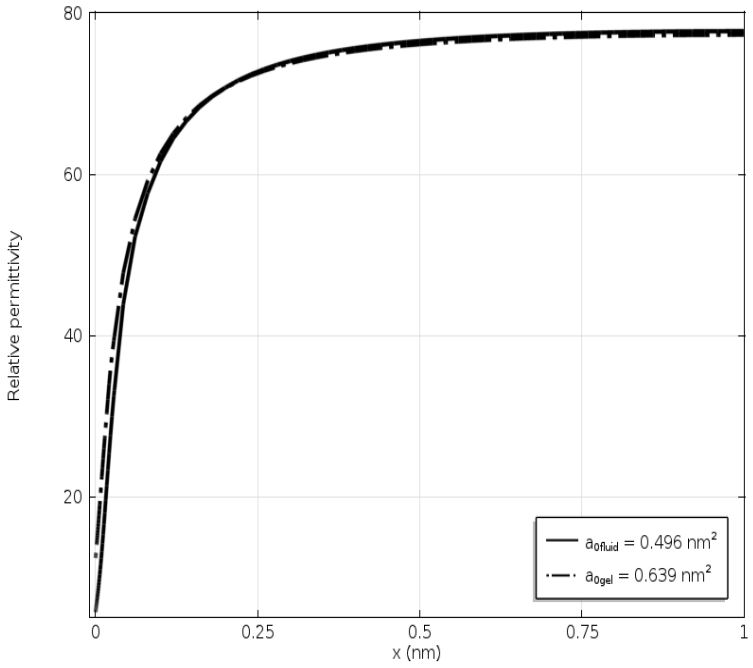

Figure 7.6: Calculated relative permittivity for the fluid and gel phase of zwitterionic lipid layer using Booth expression.

The spatially varying permittivity is depicted in Fig. 7.6. The effective water dipole moment is taken as $p_0 = 2.04$ Debye to reach the relative permittivity of pure water to 78.5 away from the head group region. An application of this model to the bilayers is presented overleaf. [1]

7.3.3 Application to the bilayer

The membrane's intrinsic potential regulates various biological phenomena such as protein binding, orientation of membrane proteins, transport processes, drug binding to membranes and so on [McLaughlin1989]. The origin of this potential is not clearly understood. It is believed that the potential difference is due to the ion imbalance across the membrane. It is interesting to consider pure lipid layers in the absence of

[1] Further in the script, this model will be referred as *Model-1*

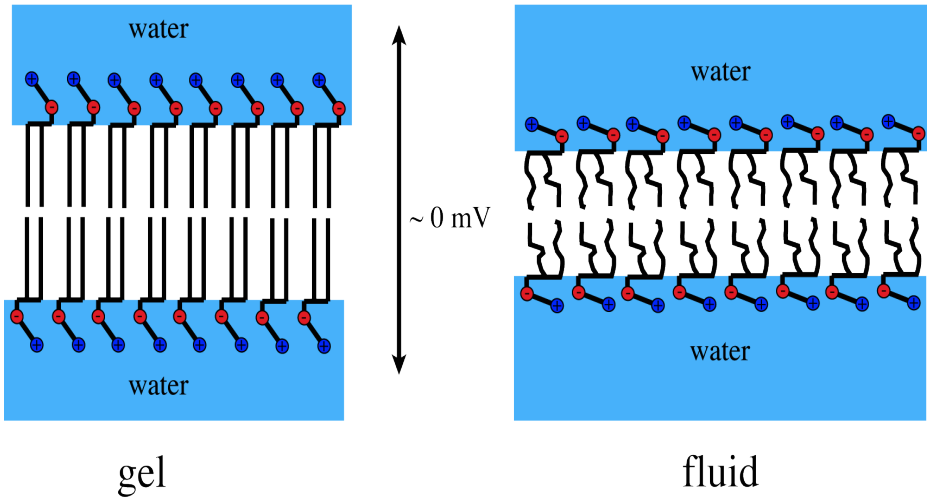

Figure 7.7: Schematic picture of lipid bilayers with lipids in same phase on both leaflets.

salt ions in the medium, to study the role of zwitterionic lipids in the transmembrane potential. For a bilayer of pure zwitterionic lipids (Fig. 7.7), the net electrostatic potential across the membrane is zero when both sides of bilayer are in same phase.

However, asymmetry of lipids is an inherent feature of membranes as depicted schematically in Fig. 7.8. In this context, our model of pure zwitterionic lipid layer

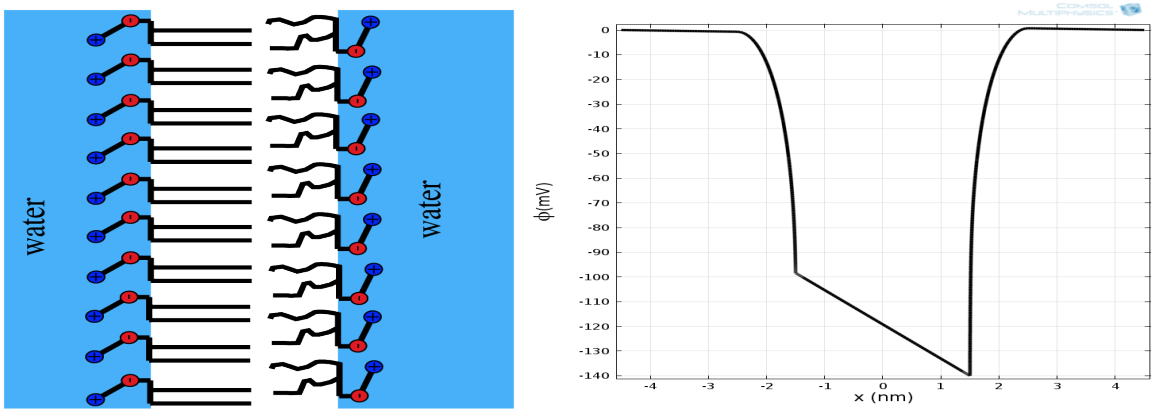

Figure 7.8: (Left) Schematic representation of asymmetric lipid membrane with gel phased lipids towards extracellular medium (Right) Calculated electric potential distribution across the membrane.

predicts the possibility of nonzero potential difference between the two sides of the membrane due to the asymmetric distribution of zwitterionic lipids between the membrane leaflets see Fig. 7.8. This implies that the orientation angle of zwitterionic lipids contibutes to the transmembrane potential of the membrane. A conceptual support to this result is provided by atomic-scale computer simulations communicated in [Gurtovenko(2007)]. Moving on to a realistic picture of membrane and its environment, in the next section, we model a mixed charged and zwitterionic lipid layer in monovalent electrolyte and water medium.

7.4 Mixed zwitter-anionic lipid layer in an electrolyte

In this work the Langevin-Poisson-Boltzmann (LPB) model [Gongadze(2011)] is generalized to take into account the cavity field [GongadzeRienen(2012), GongadzeIglic(2012)] in the saturation regime important in consideration of an electrolyte solution in contact with a highly charged surface. In addition, the electronic polarization is taken into account by assuming that the point-like rigid (permanent) dipole embedded in the center of the sphere with a volume equal to the average volume of a water molecule in the electrolyte solution [Frohlich(1964), GongadzeIglic(2012)] (Fig.7.9). The relative permittivity of the sphere is taken to be n^2, where $n = 1.33$ is the optical refractive index of water. The relative (effective) permittivity of the electrolyte solution (ε_r) can then be expressed as : [Velikonja(2013)]

$$\varepsilon_r(x) = n^2 + \frac{P(x)}{\varepsilon_0 E(x)}, \tag{7.37}$$

where $P = |\mathbf{P}|$ is the magnitude of the polarization vector due to a net orientation of permanent point-like water dipoles having dipole moment $\mathbf{p}$, ε_0 is the permittivity of the free space, while $E = |\mathbf{E}|$ is the magnitude of the electric field strength. The polarization $P(x)$ is given by [GongadzeIglic(2012)], [Velikonja(2013)]

$$P(x) = -\, n_w(x) \left(\frac{2+n^2}{3}\right) p_0 \, \mathcal{L}\left(\gamma p_0 E \beta\right) \ , \tag{7.38}$$

where $n_w(x)$ is space dependency of the number density of water molecules, p_0 is the magnitude of the external dipole moment $\mathbf{p}_e = (3/(2+n^2))\,\mathbf{p}$ [Frohlich(1964), GongadzeIglic(2012),Velikonja(2013)] (see also Fig.7.9), $\mathcal{L}(u) = (\coth(u) - 1/u)$ is the Langevin function, $\beta = 1/kT$, kT is thermal energy, while γ is [GongadzeIglic(2012),

Velikonja(2013)]:

$$\gamma = \frac{3}{2}\left(\frac{2+n^2}{3}\right) \quad . \tag{7.39}$$

In the following, for the sake of simplicity the number the finite volume of ions and water molecules is not taken into account as in [GongadzeIglic(2012)] and consequently the number density of water molecules is considered to be constant all over the solution and equal to its bulk value n_{w0}, i.e. $n_w(x) = n_{0w}$ from where it follows [Velikonja(2013)]:

$$P(x) = -\, n_{0w}\left(\frac{2+n^2}{3}\right) p_0\, \mathcal{L}\left(\gamma p_0 E \beta\right) \quad . \tag{7.40}$$

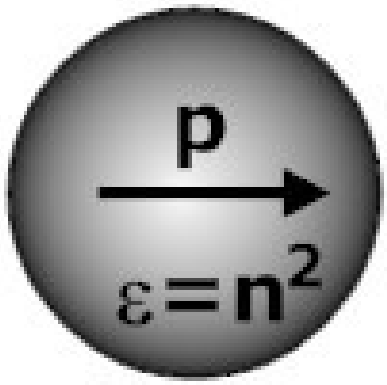

Figure 7.9: A single water molecule is considered as a sphere with permittivity n^2 and point-like rigid (permanent) dipole with dipole moment $\mathbf{p}$ at the center of the sphere [GongadzeIglic(2012)], where n is the optical refractive index of water (use with permission from [GongadzeIglic(2012)])

Combining Eq. (7.37) and Eq. (7.39) yields space dependency of permittivity within modified Langevin-Poisson-Boltzmann model (MLPB model) in the form:

$$\varepsilon_r(x) = n^2 + \frac{n_{0w}\, p_0}{\varepsilon_0}\left(\frac{2+n^2}{3}\right)\frac{\mathcal{L}\left(\gamma p_0 E(x)\beta\right)}{E(x)} \quad , \tag{7.41}$$

or

$$\varepsilon_r(x) = n^2 + \frac{3}{2}\left(\frac{2+n^2}{3}\right)^2 \frac{n_{0w} {p_0}^2 \beta}{\varepsilon_0}\frac{\mathcal{L}\left(\gamma p_0 E(x)\beta\right)}{\gamma p_0 E(x)\beta} \quad . \tag{7.42}$$

In the limit of vanishing electric field strength ($E(x) \longrightarrow 0$ everywhere in the solution) the above equation for relative permittivity $\varepsilon_r(x)$ gives the classical Onsager expression for bulk solution:

$$\varepsilon_x \cong n^2 + \left(\frac{2+n^2}{3}\right)^2 \frac{n_{0w} {p_0}^2 \beta}{2\,\varepsilon_0} \quad . \tag{7.43}$$

At room temperature with the value, $p_0 = 3.1$ Debye and $n_{0w}/N_A = 55\,\text{mol/l}$ for the bulk number density of water the above Eq. (7.43) give $\varepsilon_r = 78.5$ for bulk solution.

7.4.1 Modified Langevin-Poisson-Boltzmann (MLPB) Model

In the model the lipid layer is assumed to be composed of zwitterionic and anionic lipids. The percentage of zwitterionic lipid is described by parameter α, where in our case $0 < \alpha < 1$.

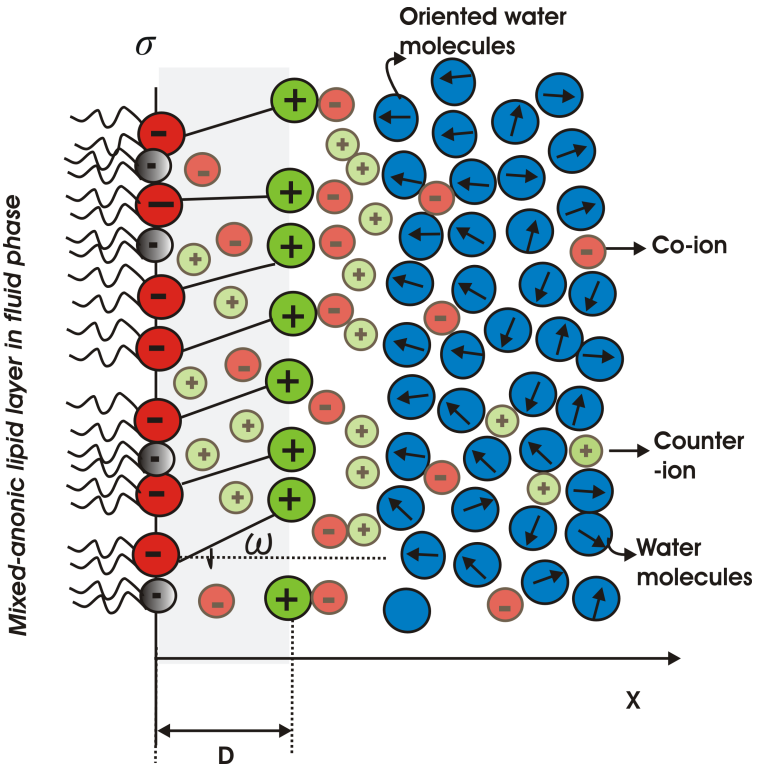

Figure 7.10: A schematic figure of mixed anionic-zwitterionic lipid layer in contact with monovalent salt solution and water dipoles.

The headgroup of zwitterionic lipid is described by two charges at fixed distance D, i.e. it is assumed that the headgroup has non-zero dipole moment. The negative charges of the phosphate groups of zwitterionic and anionic lipids are described by negative surface charge density $\sigma = -e_0/a_0$ at $x = 0$ (see Fig.7.10), where a_0 is the area per lipid. For simplicity a_0 is assumed to be equal for both kind of lipids, i.e. zwitterionic and anionic lipids.

The orientational ordering of water is taken into account assuming the spatial dependence of permittivity $\varepsilon(x)$ as described in the previous subsection. The corresponding Poisson equation in planar geometry can be written in the form (see also [GongadzeRienen(2012)], [Velikonja(2013)]) :

$$\frac{\mathrm{d}}{\mathrm{d}x}\left[\varepsilon_0\,\varepsilon_r(x)\frac{\mathrm{d}\phi}{\mathrm{d}x}\right] = -\rho_{ions}(x)\; - \rho_{Zw}(x), \tag{7.44}$$

where $\phi(x)$ is the electric potential, $\rho_{Zw}(x)$ is the macroscopic (net) volume charge density of positive charges of zwitterionic ions, $\rho_{ions}(x)$ is the macroscopic (net) volume charge density of co-$(-)$ and counter- $(+)$ ions of the electrolyte solution (see Fig.7.10) and $\varepsilon_r(x)$ is the relative permittivity determined by Eq. (7.42). Since we neglected the finite volumes of ions and water molecules [Gongadze(2011), GongadzeRienen(2012)] the co-ions and counter-ions are distributed according to Boltzmann distribution function [McLaughlin1989,Cevc(1990),KraljIglic(1996),Outhwaite(2002), Bazant(2009), Velikonja(2013)]:

$$n_+(x) = \; n_0\, \exp(-e_0\phi(x)\beta), \tag{7.45}$$

$$n_-(x) = \; n_0\, \exp(e_0\phi(x)\beta), \tag{7.46}$$

therefore

$$\rho_{ions}(x) = e_0\, n_+(x)\; -\; e_0\, n_-(x) = -2\, e_0\, n_0 \sinh e_0\phi\beta, \tag{7.47}$$

where e_0 is the unit charge and n_0 bulk number density of coions and counterions. The volume charge density due to positive charges of the lipid headgroups we can write in the form:

$$\rho_{Zw}(x) = \frac{\alpha\, e_0\, \mathcal{P}(x)}{D\, a_0} \quad , \tag{7.48}$$

where a_0 is the area per lipid, $\mathcal{P}(x)$ is probability that the lipid headgroup dipole is oriented for the angle $\omega = \arccos(x/D)$, i.e. $\mathcal{P}(x)$ is the probability that the positive charge of the headgroup is located at the distance x from the negatively charged

surface of phosphate groups (see Fig. 7.10):

$$\mathcal{P}(x) = \Lambda \, \exp(-e_0\phi(x)/kT) \quad , \tag{7.49}$$

where $x \leq D$. The normalization condition

$$\frac{1}{D}\int_0^D \mathcal{P}(x)\,\mathrm{d}x = 1 \quad , \tag{7.50}$$

leads to :

$$\Lambda = \frac{D}{\int_0^D \exp(-e_0\phi(x)/kT)\,\mathrm{d}x} \quad . \tag{7.51}$$

Using Eqs. (7.47), (7.26), (7.27) and (7.29) it follows from Eq.(7.24):

$$\frac{\mathrm{d}}{\mathrm{d}x}\left[\varepsilon_0\,\varepsilon_r(x)\frac{\mathrm{d}\phi}{\mathrm{d}x}\right] = 2\,e_0\,n_0\sinh e_0\phi\beta - \frac{\alpha\,e_0\,\exp(-e_0\phi(x)/kT)}{a_0\int_0^D \exp(-e_0\phi(x)/kT)\,\mathrm{d}x} \quad . \tag{7.52}$$

The boundary conditions are (see for example [GongadzeRienen(2012)]) :

$$\left.\frac{\mathrm{d}\phi}{\mathrm{d}x}\right|_{(x=0)} = -\frac{\sigma}{\varepsilon_0\,\varepsilon_r(x=0)} \quad . \tag{7.53}$$

where the surface charge density $\sigma = -e_0/a_0$. Note that the area per lipid a_0 is different in gel and liquid phase. $E = |\frac{\mathrm{d}\phi}{\mathrm{d}x}| = \frac{\mathrm{d}\phi}{\mathrm{d}x}$ since $\sigma < 0$.

7.4.2 Results

In order to assess the validity of our approach we have computed the electric potential for lipid compositions of (case-A) 20% of zwitterionic lipids and (case-B) 80% of zwitterionic lipids. The following figure clearly illustrates the surface potential at $x = 0$ and the distribution in both the cases. We have also referred to different concentrations of the physiological medium and the surface potential is studied. The absolute value of surface potential is high for the case-A due to a high number of negatively charged lipids in the mixed-lipid layer when compared to case-B. The orientation angle of zwitterionic lipids seems to play a key role in case-B by the adsorption of ions within the screening length. It also implies that the double layer diffuses with decreasing concentration of salt solution. The potential at the membrane surface $x = 0$ is due to mixed lipids and their interaction with the water-dipoles. This potential increases with decreasing salt concentration of the medium. The relative permittivity distribution for both the cases is same for the entire calculation domain.

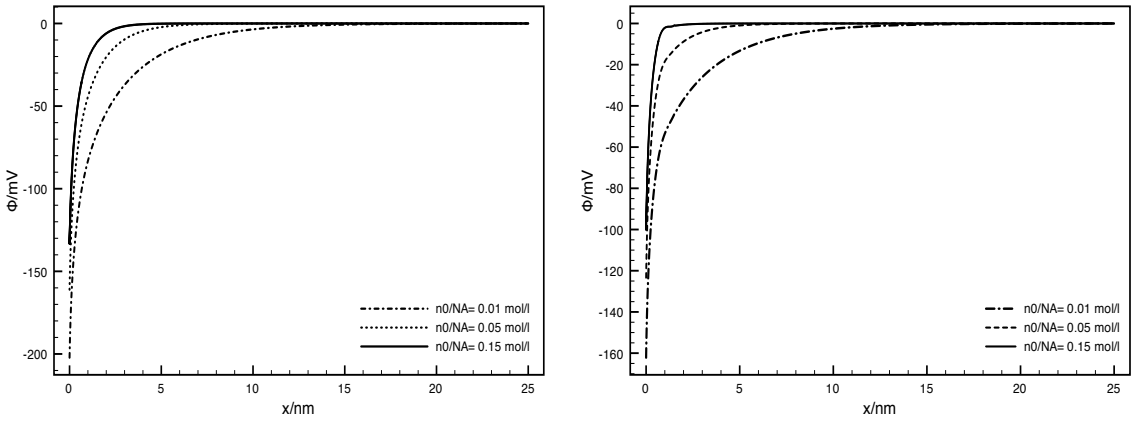

(A) (B)

Figure 7.11: Electric potential ϕ as a function of the distance from the charged planar surface x. Three values of bulk concentration of salt n_0/N_A : 0.15 mol/l (full line), 0.05 mol/l (dotted line) and 0.01 mol/l (dashed line) and two values of parameter α: 0.2 (panel A) and 0.8 (panel B) were considered. The values of model parameters are the same as in Fig.7.12.

However, a closer look into the Debye length regime of the relative permittivity reveals the smooth and sharper changes in case-A and case-B respectively which shows the dependency of number of zwitterionic lipids in the layer and thereby the effect of orientation angle of lipid dipoles. A special case with $\alpha = 1$ and with no salt ions in the medium yields us the model of pure zwitterionic lipid model in contact with water (see sect. 7.3) with LPB equation of permittivity. In the following section this special case is discussed and the results are compared with the results obtained in sect. 7.3.

7.4.3 Special Case: Pure Zwitterionic Lipid Layer in Contact with Water

In the above proposed MLPB model, if we consider the parameter $\alpha = 1$, then the lipid layer is said to be composed of zwitterionic lipids only. And if the medium is free of salt ions, then the model describes a special case of pure zwitterionic lipids in contact with water dipoles. When compared with Model-1, this special case of MLPB model does not include the spatial dependent number density of water ($n_w(x)$) and the permittivity expression is given by LPB while the latter has Booth expression for $\varepsilon_r(x)$. The Poisson equation for this special case and with planar geometry can be

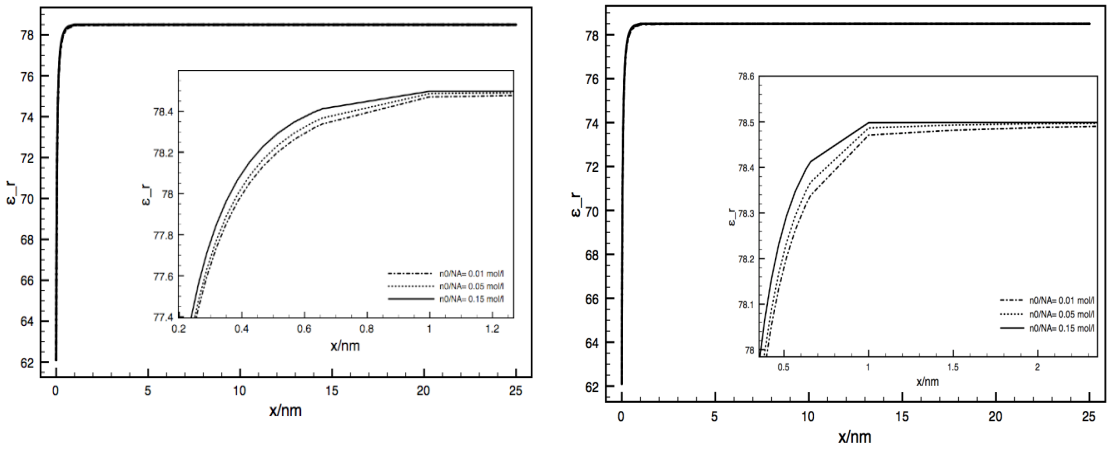

(A) (B)

Figure 7.12: Relative dielectric permittivity ε_r (Equation (7.42)) as a function of the distance from the charged planar surface x. Three values of bulk concentration of salt n_0/N_A: 0.15mol/l (full line), 0.05mol/l (dotted line) and 0.01mol/l (dashed line) and two values of parameter α: 0.2 (panel A) and 0.8 (panel B) were considered. The modified LPB equation (7.30) was solved numerically as described in the text. The dipole moment of water $p_0 = 3.1\,D$, $a_0 = 49.6\mathring{A}^2$, bulk concentration of salt $n_0/N_A = 0.15$mol/l, where N_A is the Avogadro number.

written as:

$$\frac{\mathrm{d}}{\mathrm{d}x}\left[\varepsilon_0\,\varepsilon_r(x)\frac{\mathrm{d}\phi}{\mathrm{d}x}\right] = -\rho_{Zw}(x) \quad , \tag{7.54}$$

where $\phi(x)$ is the electric potential, $\rho_{Zw}(x)$ is the macroscopic (net) volume charge density of positive charges of zwitterionic ions and $\varepsilon_r(x)$ is the relative permittivity determined by Eq. (7.42) i.e.

$$\varepsilon_r(x) = n^2 + \frac{3}{2}\left(\frac{2+n^2}{3}\right)^2 \frac{n_{0w}{p_0}^2\beta}{\varepsilon_0}\,\frac{\mathcal{L}\left(\gamma p_0 E(x)\beta\right)}{\gamma p_0 E(x)\beta} \quad . \tag{7.55}$$

The volume charge density due to positive charges of the lipid head groups is calculated using Eq. (7.26) for gel and liquid phase of lipids. The boundary conditions are

$$\left.\frac{\mathrm{d}\phi}{\mathrm{d}x}\right|_{(x=0)} = -\frac{\sigma}{\varepsilon_0\,\varepsilon_r(x=0)} \quad . \tag{7.56}$$

where the surface charge density $\sigma = -e_0/a_0$. The area per lipid a_0 is different in gel and liquid phase. $E = |\frac{d\phi}{dx}| = \frac{d\phi}{dx}$ since $\sigma < 0$. The solution of the above MLPB model for the case of zwitterionic lipid layer in contact with water for a planar geometry using FEM is explained below.

7.4.4 Results

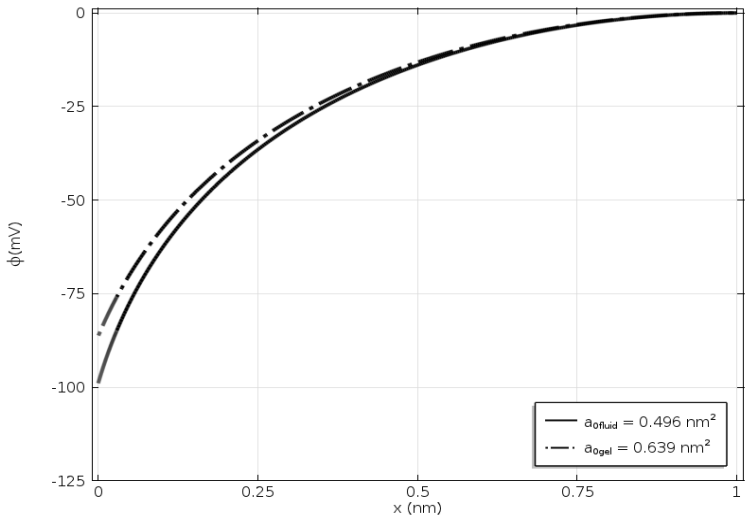

Figure 7.13: Calculated electric potential for the fluid and gel phase of zwitterionic lipid layer using Langevin-Boltzmann expression of permittivity. The dipole moment of the water Langevin dipoles $p_0 = 3.1$ Debye, bulk concentration of water dipoles is $n_{0w}/NA = 55\ mol/l$ and α_{0gel} is 0.025 as per Eq. (7.36).

The MLPB model for the special case is solved for both gel and liquid phase of zwitterionic lipids. The following results are obtained in FEM based Comsol Multiphysics 4.2a®. Figure 7.13 shows the electric potential distribution in the head group of fluid and gel phase of lipids. The difference between the values using Booth expression and Langevin-Boltzmann expression is about 50 mV.

7.5 Discussion

As described earlier, the contact between a mixed charged lipid layer and an electrolyte solution results in a rearrangement of the ion distribution and orientational ordering of water near the surface. We also took into account the cavity field in the saturation regime. Furthermore, the electronic polarization is also considered. Hence,

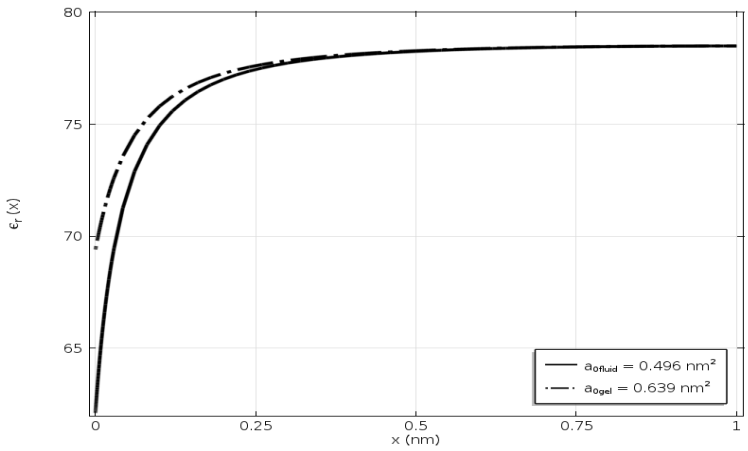

Figure 7.14: Spatially varying relative permittivity for the fluid and gel phase of zwitterionic lipid layer. The dipole moment of the water Langevin dipoles $p_0 = 3.1$ Debye, bulk concentration of water dipoles is $n_{0w}/NA = 55mol/l$ and α_{0gel} is 0.025 as per Eq. (7.36).

this leads to a modification of the electric potential close to the surface which may influence the protein adsorption, lateral pressure on the membrane and so on. Additionally, due to the accumulation of the counterions near the charged surface, it may be predicted that the relative permittivity near the negatively surface is significantly reduced. The percentage of zwitterionic lipids in the monolayers affect the distribution of ions in the medium and the surface charge, too. This infers that a change in the orientational angle of zwitterionic lipid layer can alter the phase of the membrane and thereby the permittivity profile within the diameter of the head-group. The model of zwitterionic lipid layer in contact with water establishes the significance of zwitterionic lipids for their contribution to the electrostatic potential in the screening length region. The model of mixed lipid layer in monovalent salt solution and water confirms the above within debye length and also shows its dependence on the salt concentration within and after debye length. In addition, these models overcome the limitations of GC model except that the finite size of ions is also neglected here to avoid the steric effects.

7.6 Digest

- In this chapter, we have proposed two electrostatic models: Model-1: Zwitterionic lipid layer in contact with water and Model-2: Mixed anionic-zwitterionic lipid layers in monovalent salt solution and water.

- Model-1 aims to calculate the contribution of zwitterionic lipids to the membrane potential.
- Lipid head groups has non-zero dipole moment.
- Water molecules as Langevin dipoles.
- Excluded volume effect and saturation effect.
- Booth expression for spatial variation of permittivity considering cavity effect.
- Model-2: Modified Langevin-Poisson-Boltzmann model for mixed anionic-zwitterionic lipid layers in monovalent electrolyte and water dipoles.
- Negatively charged ions embedded into the zwitterionic lipid layer.
- Water molecules as Langevin dipoles.
- Excluded volume effect and saturation effect.
- Modified Langevin-Poisson-Boltzmann model of permittivity considering cavity effect and electronic polarization.
- Finite volume of ions and water molecules is neglected in both models.

8
Conclusions and Outlook

The conclusions drawn from two parts of the work are presented in this chapter.

8.1 Conclusions

Several studies in the area of neuronal implants focus on the electrodes structures and their interaction with the neurons, assuming the complex phenomena of biological cells as simple as possible. However, the intention of this work is the other way round. The abstraction of complex phenomena of biological cell plays crucial role in improvising the function of implants. To that effect, we keep a magnifying glass on the neuronal pulse propagation called *action potential* to study its interaction with electrodes.

8.1.1 Part-I

This part of the thesis dealt with the classical electro-neurophysiology and mathematical modeling of neurons. The aim was to simulate the action potential propagation in a 3D axon and its coupling with electrodes of a neurochip. To this end, we have reviewed the neurophysiology and the classical electrical model of nerve signaling, the Hodgkin-Huxley model. The complexity of HH model to mimic the neuron was a huge barrier to achieve the goals. The excitable system of neuron was then treated as a dynamical system and the simplification of HH model was reviewed. We have discussed about the fast-slow variable models and FHN model as the pioneer of such

models. The FHN model treated as a *simple model of choice* and therefore implemented to realize the action potential in an axon. The parameters were fitted for the given size of axon according to the established relations between parameters. The effect of radial diffusion on the physical attributes of pulse like speed and width of wave front was studied. The action potential propagation properties such as branching and collision were studied and the results are found to be in good agreement with the literature. The branching structures of axon was used to abstract a network of neurons. The coupling of action potential in such network with the electrodes of MEA was implemented using the classical approach of frequency-domain EQS modeling. To have a good compromise between the accuracy of model and computational power,a medium branched structure of axon was simulated in a neurochip. The simulation results are qualitatively comparable with the neurochip recordings.

8.1.2 Outlook

- A dynamical system analysis of the 3D model can be performed.
- The present results can be made quantitatively reliable by performing dimensional analysis.
- The axon model can be extended to the whole neuron model by taking cell body, dendrites and synapses into account.
- Neurochip simulations for volume filled with networks can be extended through parallelization.
- Effect of double layer at the electrodes and neighboring axons on the action potential initiation and propagation is an interesting subject to take up.
- Apparently, these studies will help in optimization of electrodes for neurochip.

8.1.3 Part-II

The innumerable ways of parametric variations used to mimic the action potential as described by HH model is never-ending, as long as the ion-channels pertaining to a particular cell type is thought to be responsible for the *phenomena*. To that effect, we studied the membrane structure in detail and reviewed all the physical, thermodynamical properties along with electrical properties of its major constituents. The *lipids*, major constituents of membranes, exhibit melting transitions and the thermodynamic properties of these components influence the membrane on the whole. We have then reviewed the *soliton model*, which is based on the thermodynamic nerve pulse propagation i.e. the change in lateral area density of membrane in the transition

regime gives rise to a sound pulse which transmits the signal. As a part of stability analysis of the soliton model, we performed the collision of solitons and found that it follows the conservation laws and contradicts the concept of annihilation of pulses upon collision. Thus the model is said to be viable in a realistic physiological nerve environment and may provide an immediate and reliable explanation of mechanical and thermodynamic effects associated with it. To study the effect of soliton on the electrostatic potential of membrane and to realize the actual *action potential* in electrical terms we then moved to the electrostatics of lipid membranes. In which we modeled the contribution of zwitterionic lipids to the membrane potential in Poisson-Boltzmann framework. The water molecules are taken as Langevin dipoles and the spatial variation of permittivity is considered along with excluded volume effect and saturation effects. The model is then applied to a bilayer with asymmetric lipids on each side and a net electrostatic potential was found across the membrane in the absence of salt ions. From an idealized scenario to reality, the model was improvised to a mixed anionic-zwitterionic lipid layer in contact with physiological monovalent electrolyte. The spatial variation of permittivity also considers the cavity effect and electronic polarization. Both the models show the importance of lipid phase and lipid charge on the membrane potential.

8.1.4 Outlook

The future prospects for this part of the thesis are listed below.

- Effect of external electric field on the orientation angle of the zwitterionic lipids.
- Effect of density pulse on the field of the membrane (refer [Heimburg(2007)])

  The asymmetrically charged membranes gives rise to transmembrane voltage. At physiological conditions the potential is approximately proportional to the charge density [Heimburg(2007)].

$$\psi_0 = \frac{1}{\epsilon_0 \epsilon k}\sigma = \frac{1}{\epsilon_0 \epsilon k}.q_L.\rho^A \tag{8.1}$$

  where q_L is the mean number of charges per lipid. This couples the lateral density with the charge density. During the density pulse the charge density changes by about 20% and thus it can be expected that the density pulse is accompanied by a voltage change. This is called as electromechanical coupling. This effect has been well described in the literature. The membrane behaves like a piezoelectric crystal. Upon the exertion of force it changes the transmembrane voltage. The magnitude of this pulse will strongly depend on the value of the charge densities on the two sides of the membrane. We assume

that the capacitive energy of a membrane is a consequence of compression and accompanying voltage change.

- Coupling of electrode with the action potential due to soliton propagation

Bibliography

[Abbott et al.(1958)] B. C. Abbott, A. V. Hill, J. V. Howarth, The positive and negative heat production associated with a nerve impulse, Proc. R. Soc. London. B 148 (1958) 149–187.

[Andersen et al.(2009)] S. S. L. Andersen, A. D. Jackson, T. Heimburg, Towards a thermodynamic theory of nerve pulse propagation, Progr. Neurobiol. 88 (2009) 104–113.

[Antonov et al.(1980)] V. F. Antonov, V. V. Petrov, A. A. Molnar, D. A. Predvoditelev, A. S. Ivanov, The appearance of single-ion channels in unmodified lipid bilayer membranes at the phase transition temperature, Nature 283 (1980) 585–586.

[Appali et al.(2010)] R. Appali, S. Petersen, U. van Rienen, A comparision of Hodgkin-Huxley and soliton neural theories Adv. Radio Sci. 8 (2010) 75–79.

[Appali(2012)] R. Appali, U. van Rienen and T. Heimburg, A comparison of the Hodgkin-Huxley model and the soliton theory for the action potential in nerves, APLBL 16 (2012) 275-299.

[Argentina et al.(2000)] M. Argentina, P. Coullet, V. Krinsky, Head-on collisions of waves in an excitable FitzHugh-Nagumo system: a transition from wave annihilation to clssical wave behavior, J. Theor. Biol. 205 (2000) 47–52.

[Aslanidi and Mornev(1997)] O. V. Aslanidi, O. A. Mornev, Can colliding nerve pulses be reflected?, JETP Lett. 65 (1997) 579–585.

[Arms and Camp(1995)] K. Arms, P. Camp, Biology, Harcourt Brace College Publishers, New York, 4. edition, 1995.

[Baumann(2004)] W. H. Baumann et al., Cell monitoring system with multiparametric CMOS sensorchips, in Proceedings, $\mu-$ TAS II, Malmo (2004) 554–556.

[Bazant(2009)] M. Z. Bazant, et al., Towards an understanding of induced-charge electrokinetics at large applied voltages in concentrated solutions., Adv. Colloid Interface Sci. 152.1 (2009) 48–88.

[Bernstein(1902)] J. Bernstein, Untersuchungen zur Thermodynamik der bioelektrischen Ströme. 1 Theil, Pflügers Arch. 92 (1902) 521–562.

[Blicher et al.(2009)] A. Blicher, K. Wodzinska, M. Fidorra, M. Winterhalter, T. Heimburg, The temperature dependence of lipid membrane permeability, its quantized nature, and the influence of anesthetics, Biophys. J. 96 (2009) 4581–4591.

[Booth(1951)] F. Booth, The dielectric constant of water and the saturation effect, J. Chem. Phy. 19 (1951) 391–394.

[Boussinesq1872] J. V. Boussinesq,Thorie des ondes et remous qui se propagent le long d'un canal rectangulaire horizontal, en communiquant au liquide contenu dans ce canal des vitesses sensiblement pareilles de la surface au fond, J. Math. Pures. Appl.17, (1872). 55–108.

[Brockman1994] H. Brockman, Dipole potential of lipid membranes, Chemistry and Physics of Lipids73(194)57-79.

[Butt(2003)] H.J. Butt, K. Graf, M. Kappl, Physics and Chemistry of Interfaces, Wiley-VCH Verlag Wiley-VCH VerlagWeinheim (2003) .

[Cevc(1990)] G. Cevc, Membrane electrostatics, Biochim. Biophys. Acta 1031 (1990) 311.

[Cole and Curtis(1939)] K. S. Cole, H. J. Curtis, Electrical impedance of the squid giant axon during activity, J. Gen. Physiol. 220 (1939) 649–670.

[Ebel et al.(2001] H. Ebel, P. Grabitz, T. Heimburg, Enthalpy and volume changes in lipid membranes. i. the proportionality of heat and volume changes in the lipid melting transition and its implication for the elastic constants, J. Phys. Chem. B 105 (2001) 7353–7360.

[Feynman(1963)] R. Feynman, The Feynman Lectures on Physics, Vol. 2, (Addison-Wesley, Boston, (1963).

[FitzHugh(1961)] R. FitzHugh, Impulses and physiological states in theoretical models of nerve membrane, Biophys. J. 1 (1961) 445–466.

[FitzHugh(1962)] W. K. Chandler, R. FitzHugh and K. S. Cole, Theoretical stability properties of a space-clamped axon, Biophys. J. 2 (1962) 105–127.

[Flehr(2006)] J. Flehr, Simulation des extrazellulären elektrischen Feldes von Nervenzellen während eines Aktionspotentials, PhD thesis, University of Rostock (2006).

[Flewelling(1986)] R. F. Flewelling and W. L. Hubbell, Hydrophobic ion interactions with membranes. thermodynamic analysis of tetraphenylphosphonium binding to vesicles., Biophys. J 49 (1986) 531–540.

[Frohlich(1964)] H. Frhlich, Theory of dielectrics, Clarendon Press Oxford, UK (1964).

[Galvani(1791)] A. Galvani, Abhandlung über die Kräfte der Electricität bei der Muskelbewegung, volume 52 of *Ostwald's Klassiker der exakten Wissenschaften (1894)*, 1791.

[Gerstner(2002)] W. Gerstner and M. W. Kistler, Spiking neuron models. Single neurons, populations, plasticity, Cambridge Univ. Press, p. 34, (2002).

[Gongadze(2011)] E. Gongadze et al, Langevin Poisson-Boltzmann equation: point-like ions and water dipoles near a charged surface, Gen. Physiol. Biophys. 30 (2011) 130.

[GongadzeIglic(2012)] E. Gongadze and A. Iglič, Decrease of permittivity of an electrolyte solution near a charged surface due to saturation and excluded volume effects, Bioelectrochemistry 87 (2012) 199–203.

[GongadzeRienen(2012)] E. Gongadze et al, Spatial variation of permittivity of an electrolyte solution in contact with a charged surface: a mini review., Comput. Meth. Biomech. Biomed. Eng. 10.1080/10255842.2011.624769 (2012).

[Grabitz(2002)] P. Grabitz, V. P. Ivanova and T. Heimburg, Relaxation kinetics of lipid membranes and its relation to the heat capacity, Biophys. J. 82 (2002) 299–309.

[Gross(1977)] G. W. Gross et al.,, A new fixed-array multimicroelectrode system designed for long-term recording of extracellular single unit activity in vitro, Neuosci. Lett. 6 (1977) 101–105.

[Gurtovenko(2007)] A. A. Gurtovenko and I. Vattulainen, Lipid transmembrane asymmetry and intrinsic membrane potential: Two sides of the same coin, J. Am. Chem. Soc.129(2007)5358-5359.

[Halstenberg et al.(1998)] S. Halstenberg, T. Heimburg, T. Hianik, U. Kaatze, R. Krivanek, Cholesterol-induced variations in the volume and enthalpy fluctuations of lipid bilayers, Biophys. J. 75 (1998) 264–271.

[Haeusser(2000)] M. Haeusser, The hodgkin-huxley theory of the action potential, Nat. Neurosci. 3 (2000) 1165.

[Heimburg and Jackson(2005)] T. Heimburg, A. D. Jackson, On soliton propagation in biomembranes and nerves, Proc. Natl. Acad. Sci. USA 102 (2005) 9790–9795.

[Heimburg(2007)] T. Heimburg, Thermal biophysics of membranes, Wiley VCH, Berlin, Germany, 2007.

[Heimburg and Jackson(2007)] T. Heimburg, A. D. Jackson, On the action potential as a propagating density pulse and the role of anesthetics, Biophys. Rev. Lett. 2 (2007) 57–78.

[Heimburg and Jackson(2007)] T. Heimburg, A. D. Jackson, The thermodynamics of general anesthesia, Biophys. J. 92 (2007) 3159–3165.

[Heimburg and Jackson(2008)] T. Heimburg, A. D. Jackson, Thermodynamics of the nervous impulse., in: K. Nag (Ed.), Structure and Dynamics of Membranous Interfaces., Wiley, 2008, pp. 317–339.

[Heimburg(2009a)] T. Heimburg, Die Physik von Nerven, Physik Journal 8 (2009a) 33–39. English translation: "The physics of nerves". arXiv:1008.4279v1 [physics.bio-ph].

[Heimburg(2009b)] T. Heimburg, Physical properties of biological membranes, in: H. G. Bohr (Ed.), Encyclopedia of Applied Biophysics, Wiley VCH, Weinheim, 2009b, pp. 593–616.

[Heimburg(2010)] T. Heimburg, Lipid ion channels, Biophys. Chem. 150 (2010) 2–22.

[Helmholtz(1879)] H. A. Helmholtz, Studien über elektrische Grenzschichten, Ann. Phys. 7 (1879) 337–382.

[Hindmarsh and Rose(1984)] J. L. Hindmarsh, R. M. Rose, A model of neuronal bursting using three coupled first order differential equations, Proc. Roy. Soc. Lond. B 221 (1984) 87–102.

[Hodgkin and Katz(1949)] A. L. Hodgkin, B. Katz, The effect of sodium ions on the electrical activity of the giant axon of the squid, J. Physiol. London 108 (1949) 37–77.

[Hodgkin and Huxley(1952a)] A. L. Hodgkin, A. F. Huxley, Currents carried by sodium and potassium ions through the membrane of the giant axon of loligo., J. Physiol. London 116 (1952) 449–472.

[Hodgkin and Huxley(1952b)] A. L. Hodgkin, A. F. Huxley, A quantitative description of membrane current and its application to conduction and excitation in nerve, J. Physiol. London 117 (1952) 500–544.

[Hoppensteadt1997] Frank C. Hoppensteadt, An Introduction to the mathematics of neurons: Modeling in the frequency domainedition, 2 ofCambridge University Press, 1997.

[Howarth et al.(1968)] J. V. Howarth, R. Keynes, J. M. Ritchie, The origin of the initial heat associated with a single impulse in mammalian non-myelinated nerve fibres., J. Physiol. 194 (1968) 745–793.

[Howarth(1975)] J. Howarth, Heat production in non-myelinated nerves, Phil. Trans. Royal Soc. Lond. 270 (1975) 425–432.

[Iglic(2010)] A. Iglič, E. Gongadze and K. Bohinc , Excluded volume effect and orientational ordering near charged surface in solution of ions and Langevin dipoles, Bioelectrochemistry 79 (2010) 223.

[Iwasa and Tasaki(1980)] K. Iwasa, I. Tasaki, Mechanical changes in squid giant-axons associated with production of action potentials, Biochem. Biophys. Research Comm. 95 (1980) 1328–1331.

[Iwasa et al.(1980)] K. Iwasa, I. Tasaki, R. C. Gibbons, Swelling of nerve fibres associated with action potentials, Science 210 (1980) 338–339.

[Izhikevich(2004)] E. M Izhikevich, Which model to use for cortical spiking neurons?, IEEE Transactions on Neural Networks, 15, (2004)1063–1070.

[Izhikevich(2007)] E. M Izhikevich, Dynamical systems in neuroscience: The geometry of excitability and bursting, MIT Press, Boston, 2007.

[Johnson and Flagler(1950)] F. H. Johnson, E. A. Flagler, Hydrostatic pressure reversal of narcosis in tadpoles., Science 112 (1950) 91–92.

[Johnston and Wu(1995)] D. Johnston, S. M. S. Wu, Cellular Neurophysiology, MIT Press, Boston, 1995.

[Keener and Sneyd(1998)] J. Keener, J. Sneyd, Mathematical Physiology, Springer-Verlag , New York, 1998.

[Kharakoz(2001)] D. P. Kharakoz, Phase-transition-driven synaptic exocytosis: A hypothesis and its physiological and evolutionary implications, Biosci. Rep. 210 (2001) 801–830.

[Kobatake et al.(1971)] Y. Kobatake, I. Tasaki, A. Watanabe, Phase transition in membrane with reference to nerve excitation, Adv. Biophys. 208 (1971) 1–31.

[Koester(2010)] P. J. Koester et al, Modular glass chip system measuring the electrical activity and adhesion of neuronal cells-application and drug testing with sodium valproic acid., Lab on Chip 10 (2010) 1579.

[Kosek(1995)] J. Kosek and M. Marek,Collision-stable waves in excitable reaction-diffusion systems, Phys. Rev. Lett.74 (1995) 2134.

[KraljIglic(1996)] V. Kralj-Iglič and A. Iglič, A simple statistical mechanical approach to the free energy of the electric double layer including the excluded volume effect., J. Phys. II France 6.4 (1996) 477–491.

[Kroon(1989)] A. I. P. M. de Kroon, J. de Gier, and B. de Kruijf, Association of synthetic model peptides with phosphalipid vesicles induced by a membrane potential., Biochim. Biophys. Acta 981 (1989) 371–373.

[Landau and Lifshitz(1987)] L. D. Landau, E. M. Lifshitz, Fluid Mechanics, volume 6 of *Course of Theoretical Physics*, Pergamon Press, 1987.

[Laub et al.(2012)] K. R. Laub, K. Witschas, A. Blicher, S. B. Madsen, A. Lückhoff, T. Heimburg, Comparing ion conductance recordings of synthetic lipid bilayers with cell membranes containing trp channels, Biochim. Biophys. Acta 1818 (2012) 1–12.

[Lautrup et al.(2011)] B. Lautrup, R. Appali, A. D. Jackson, T. Heimburg, The stability of solitons in biomembranes and nerves, Eur. Phys. J. E 34 (6) (2011) 1–9.

[Maher(1999)] M. P. Maher et al.,, The neurochip: A new multielectrode device for stimulating and recording from cultured neurons, J. Neurosci. Meth. 87 (1999) 45–56.

[Manoranjan(1988)] V. S. Manoranjan, T. Ortega and J. M. Sanz-Serna, Soliton and antisoliton interactions in the good Boussinesq equation, J. Math. Phys. 29(9) (1988) 1964–1968.

[Mbamala(2006)] EC. Mbamala, A. Fahr and S. May, Electrostatic model for mixed cationic-zwitterionic lipid bilayers, Langmuir: the ACS journal of surfaces and colloids 22(11) (2006) 5129–5136.

[McLaughlin1989] S. McLaughlin, The electrostatic properties of membranes, Annu. Rev. Biophys. Chem., 18, 1, (1989), 113–136.

[Morris(1981)] C. Morris and H. Lecar, Voltage oscillations in the barnacle giant muscle fiber, Biophys. J. 35 (1981) 193–213.

[Mosgaard(2012)] L. D. Mosgaard, A. D. Jackson and T. Heimburg, Low frequency sound propagation in lipid membranes, Advances in Planar Lipid Bilayers and Liposomes 16 (2012) 51–74.

[Nagumo et al.(1962)] J. Nagumo, S. Arimoto, S. Yoshizawa, An active pulse transmission line simulating nerve axon, Proc. IRE 50 (1962) 2061 – 2070.

[Overton(1902)] E. Overton, Beiträge zur allgemeinen Muskel- und Nervenphysiologie: II. Mittheilung. Ueber die Unentbehrlichkeit von Natrium- (oder Lithium-)lonen für den Contractionsact des Muskels, Pflügers Arch. 92 (1902) 346–386.

[Outhwaite(1976)] CW. Outhwaite, Treatment of solvent effects in potneital theory of electrolyte-solutions, Mol. Phy. 31 (1976) 1345.

[Outhwaite(1983)] CW. Outhwaite, Towards a mean electrostatic potential treatment of an ion dipole misxture or a dipolar system next to a plane wall, Mol. Phy. 48 (1983) 599.

[Outhwaite(2002)] S. Lamperski and C. W. Outhwaite, Exclusion volume term in the inhomogeneous Poisson-Boltzmann theory for high surface charge., Langmuir 18.9 (2002) 3423–3424.

[Petrov(1994)] V. Petrov, S. K. Scott, K. Showalter, Excitability, wave reflection, and wave splitting in a cubic autocatalysis reaction-diffusion system, Philos. Trans. R. Soc. 443, (1994) 631–642.

[Phillipson(2005)] P. E. Phillipson and P. Schuster, A comparitive study of the Hodgkin-Huxley and FitzHugh-Nagumo models of neuron pulse propagation, Int. J. of Bifurcation and Chaos 15 (2005) 3851–3866.

[Pine(1980)] J. Pine, Recording action potentials from cultured neurons with extracellular microcircuit electrodes, J. Neurosci. Meth 2 (1980) 19–31.

[Press(1994)] W. H. Press, S. A. Teukolsky, W. T. Vetterling and B. P. Flannery, Numerical recipes in C (2nd. ed., Cambridge University Press (1994).

[Rajagopal(1983)] K. Rajagopal, A generalized-model for the nerve impulse propagation, Phys. Lett. A 99 (1983) 261–264.

[Ritchie and Keynes(1985)] J. M. Ritchie, R. D. Keynes, The production and absorption of heat associated with electrical activity in nerve and electric organ, Quart. Rev. Biophys. 392 (1985) 451–476.

[Sakmann(2009)] B. Sakmann and E. Neher, Single-channel Recording, Springer Science and Business Media, (2009).

[Schrader et al.(2002)] W. Schrader, H. Ebel, P. Grabitz, E. Hanke, T. Heimburg, M. Hoeckel, M. Kahle, F. Wente, U. Kaatze, Compressibility of lipid mixtures studied by calorimetry and ultrasonic velocity measurements, J. Phys. Chem. B 106 (2002) 6581–6586.

[Sommerfeld(1992)] A. Sommerfeld, Mechanik der deformierbaren Medien, volume 2 of *Vorlesungen über theoretische Physik*, Harri Deutsch, 1992.

[Tasaki(1949)] I. Tasaki, Collision of two nerve impulses in the nerve fiber, Biochem Biophys Acta 3 (1949) 494–497.

[Tasaki et al.(1968)] I. Tasaki, A. Watanabe, R. Sandlin, L. Carnay, Changes in fluorescence, turbidity and birefringence associated with nerve excitation., Proc. Natl. Acad. Sci. USA 61 (1968) 883–888.

[Tasaki et al.(1980)] I. Tasaki, K. Iwasa, R. C. Gibbons, Mechanical changes in crab nerve fibers during action potentials, Jap. J. Physiol. 30 (1980) 897–905.

[Tasaki and Iwasa(1982)] I. Tasaki, K. Iwasa, Further studies of rapid mechanical changes in squid giant axon associated with action potential production, Jap. J. Physiol. 32 (1982) 505–518.

[Tasaki(1982)] I. Tasaki, Physiology and electrochemistry of nerve fibers, Academic Press, New York, 1982.

[Tasaki et al.(1989)] I. Tasaki, K. Kusano, M. Byrne, Rapid mechanical and thermal changes in the garfish olfactory nerve associated with a propagated impulse, Biophys. J. 55 (1989) 1033–1040.

[Tasaki and Byrne(1990)] I. Tasaki, M. Byrne, Volume expansion of nonmyelinated nerve fibers during impulse conduction., Biophys. J. 57 (1990) 633–635.

[Tasaki and Byrne(1992)] I. Tasaki, P. M. Byrne, Heat production associated with a propagated impulse in bullfrog myelinated nerve fibers, Jpn. J. Physiol. 42 (1992) 805–813.

[Tasaki(1999)] I. Tasaki, Evidence for phase transition in nerve fibers, cells and synapses, Ferroelectrics 220 (1999) 305–316.

[Tuckwell(1988)] H. Tuckwell Introduction to Theoretical Neurobiology: Volume 1, Linear Cable Theory and Dendritic Structure, Cambridge Studies in Mathematical Biology, Cambridge University Press, 1988.

[vanRienen(2001)] U. van Rienen, Numerical Methods in Computational Electrodynamics - Linear Systems in Practical Applications, Springer, Lecture Notes in Computational Science and Engineering, 12, 2001.

[vanRienen(2003)] U. van Rienen, J. Flehr, U. Schreiber, V. Motrescu, Modeling and simulation of electro-quasistatic fields, International Series of Numerical Mathematics 146 (2003) 17–31.

[vanRienen(2005)] U. van Rienen, J. Flehr, U. Schreiber, S. Schulze, U. Gimsa, W. Baumann, D.G. Weiss, J. Gimsa, R. Benecke, H.-W. Pau, Electro-Quasistatic Simulations in Bio-Systems Engineering and Medical Engineering, Advances in Radio Science 3 (2005) 39–49.

[Velikonja(2013)] A. Velikonja, S. Perutkova, E. Gongadze, P. Kramar, A. Polak, A. Maek-Lebar and A. Igli, Monovalent ions and water dipoles in contact with dipolar zwitterionic lipid headroups - theory and MD simulations, Int. J. Mol. Sci., 14 (2013) 2846–2861.

[Villagran Vargas et al.(2011)] E. Villagran Vargas, A. Ludu, R. Hustert, P. Gumrich, A. D. Jackson, T. Heimburg, Periodic solutions and refractory periods in the soliton theory for nerves and the locust femoral nerve, Biophys. Chem. 153 (2011) 159–167.

[Volta(1800)] A. Volta, Untersuchungen über den Galvanismus, volume 118 of *Ostwald's Klassiker der exakten Wissenschaften (1900)*, 1796-1800.

[Weiland(1977)] T. Weiland, Eine Methode zur Lösung der Maxwellschen Gleischungen füer sechskomponentige Felder auf dikreter Basis, AEÜ 31 (1977) 116–120.

[Wilke and Atzler(1912)] E. Wilke, E. Atzler, Experimentelle Beiträge zum Problem der Reizleitung im Nerven, Pflügers Arch. 146 (1912) 430–446.

[Xylouris(2010)] K. Xylouris, G. Queisser, G. Wittum, A three-dimensional mathematical model of active signal processing in axons, Comput. Vis. Sci.13(2010)409–418.

[Zhao(2010)] Y.Zhao et al., Spatio-temporal modelling of wave formation in an excitable chemical medium based on a revised FitzHugh-Nagumo model, ACSE Research Report no. 1008 (2010) Automatic control systems and Engineering, Univeristy of Sheffield.

Appendix

$C++$ code to solve the soliton model, developed by B. Lautrup and R. Appali is appended here.

```
#include <stdio.h>
#include <math.h>
#include <stdlib.h>
#include <time.h>
#include "drand48.h"

typedef double real;                        // real values
inline real sqr(real x) { return x*x; }     // the square

// choice of run

#define COLLIDE

// single decaying soliton

#ifdef SINGLE

const char *outname = "single.data";    // output file name

int iters = 1000000;                    // iterations
int print = 10000;                      // print interval
int write = 10000;                      // write interval
int ask = 2000000;                      // query interval

const int N = 1000;                     // lattice size
real dx = 0.1;                          // cell size
real dt = 0.001;                        // time step

#endif

// decaying soliton

#ifdef DECAY

const char *outname = "decay.data"; // output file name

int iters = 1000000;                        // iterations
int print = 10000;                      // print interval
int write = 10000;                      // write interval
int ask = 2000000;                      // query interval

const int N = 1000;                     // lattice size
real dx = 0.1;                          // cell size
real dt = 0.001;                        // time step

real kappa = 0.05;                      // viscosity

#endif

// disturbed soliton

#ifdef NOISE

const char *outname = "noise.data";

int iters = 1000000;                    // iterations
int print = 10000;                      // print interval
int write = 10000;                      // write interval
int ask = 2000000;                      // query interval

const int N = 1000;                     // lattice size, must be even
real dx = 0.1;                          // cell size
real dt = 0.001;                        // time step

const int modes = 100;                  // number of white noise modes
real amplitude = 0.01;                  // amplitude (fraction of soliton top a)

#endif

// Gaussian wave form

#ifdef GAUSS

char *outname = "gauss.data";
```

```
int iters = 100000;                     // iterations
int print = 10000;                      // print interval
int write = 10000;                      // write interval
int ask = 1000000;                      // query interval

const int N = 2000;                     // lattice size, must be even
real dx = 0.1;                          // cell size
real dt = 0.001;                        // time step

#endif

// colliding soliton

#ifdef COLLIDE

char *outname = "collide.data";

int iters = 400000;                     // iterations
int print = 10000;                      // print interval
int write = 2000;                       // write interval
int ask = 1000000;                      // query interval

const int N = 2000;                     // lattice size, must be even
real dx = 0.1;                          // cell size
real dt = 0.001;                        // time step

#endif

// disturbed soliton

#ifdef DISTURB

char *outname = "disturb.data";

//int iters = 50000;                        // iterations
int iters = 100000;                 // iterations
int print = 5000;                       // print interval
int write = 1000;                       // write interval
int ask = 2000000;                      // query interval

const int N = 2000;                 // lattice size, must be even
real dx = 0.1;                      // cell size
real dt = 0.001;                    // time step

#endif


real A = N*dx;                      // x interval from 0 to A


// soliton parameters

const real B1 = -16.6;                  // constants
const real B2 = 79.5;
const real beta0 = sqrt(1-B1*B1/6/B2);
const real beta1 = 0.734761;

//real beta = beta0+1e-10;                  // choice of velocity
//real beta = 0.98;                 // choice of velocity
real beta = beta1;
real a = -B1/B2*(1-sqrt((beta*beta-beta0*beta0)/(1-beta0*beta0)));
real b = -B1/B2*(1+sqrt((beta*beta-beta0*beta0)/(1-beta0*beta0)));
real width = 1.l/sqrt(1-sqr(beta))*log((3.*b-a+2.*sqrt(b*(2.*b-a)))/(b-a));

real k = sqrt(B2/6);
real kin = 0.5*sqr(beta)/k*(-2*sqrt(a*b)+(a+b)*log((sqrt(b)+sqrt(a))/(sqrt(b)-sqrt(a))));
real disp = 0.5*k/24.*((6.*(sqr(a)+sqr(b))-4.*a*b)*sqrt(a*b)-3.*(a+b)*sqr(b-a)*log((sqrt(b)↙
    +sqrt(a))/(sqrt(b)-sqrt(a))));
real comp = kin+disp;
real energy = 2.*comp;

// allocate memory
```

```
typedef real realmatrix[N+1];       // matrix with one to spare

realmatrix U,V;             // variables at integer times

int iter;
real t;

FILE *out;

real pi = 2*asin(1.0);

real E,ET,EC,ED;                    // energies
real IU,IUU,IUV;
real XM;

time_t elapsed = 0;

//---------------------------------------------------------------------------

real Q(real u)
{
    return (u>=0)? u*(1+0.5*B1*u+1./3.*B2*u*u):u;
}

real AA(real u)
{
    return (u>=0)? u*u*(1+1./3.*B1*u+1./6.*B2*u*u):u*u;
}
//---------------------------------------------------------------------------

real Soliton(real x)
{
    return 2.*a*b/(a+b+(b-a)*cosh(x*sqrt(1-beta*beta)));
}



real Gauss(real x)
{
    real amplitude = 0.22;
    real width = 5;

    return amplitude*exp(-x*x/(width*width));
}

//---------------------------------------------------------------------------



void Initialize()
{
    int i;

#ifdef NOISE
    // initialize amplitudes and phases of noise

    int k;
    real amplitudes[modes+1];
    real phases[modes+1];

    srand48(1234567);
    for( i = 1; i <= modes; i++)
    {
        amplitudes[i] = amplitude*(2*drand48()-1);
        phases[i] = 2*pi*drand48();
    }
#endif

    // initialize arrays

    for(i = 0; i <= N; i++)
    {
        real x = -0.5*A+i*dx;
        real u,v;
```

```
#if defined(SINGLE)
        u = Soliton(x);
        v = -beta*u;

#elif defined(DECAY)
        u = Soliton(x);
        v = -beta*u;

#elif defined(NOISE)
        u = Soliton(x);
        v = -beta*u;
        for( k = 1; k <= modes; k++ )
        {
            u += a*amplitudes[k]*sin(2*pi*k*x/A + phases[k]);
        }

#elif defined(GAUSS)
        u = Gauss(x);
        v = -beta*u;

#elif defined(COLLIDE)
        real k =0.2;
        u = Soliton(x-k*A)+Soliton(x+k*A);
        v = beta*Soliton(x-k*A)-beta*Soliton(x+k*A);

#elif defined(DISTURB)
        real p = 0.5;
        u = Soliton(x);
        v = -p*beta*u;
#endif

        U[i] = u;
        V[i] = v;

        XM = 0;

    }
}

//---------------------------------------------------------------------------

void DoCycle()
{
    int i;
    realmatrix U1,V1;               // basic variables at half integer times (temporary)
    realmatrix W,F;                 // helping variables (temporary)

    // W at t

    for( i = 0; i < N; i++ )
    {
        W[i] = (U[i+1]-U[i])/dx;
#if defined(DECAY)
        W[i] += -kappa*0.5*(V[i+1]+V[i]);
#endif
    }
    W[N] = W[0];

    // F at t

    for( i = 1 ; i <= N; i++ )
        F[i] = Q(U[i])-(W[i]-W[i-1])/dx;
    F[0] = F[N];

    // U and V at t+dt/2

    for( i = 0; i < N; i++ )
    {
        U1[i] = 1./2*(U[i+1]+U[i])+1./2*dt*(V[i+1]-V[i])/dx;
        V1[i] = 1./2*(V[i+1]+V[i])+1./2*dt*(F[i+1]-F[i])/dx;
    }
    U1[N] = U1[0];
    V1[N] = V1[0];
```

```
    // W at t+dt/2

    for( i = 1; i <= N; i++ )
    {
        W[i] = (U1[i]-U1[i-1])/dx;
#if defined(DECAY)
        W[i] += -kappa*0.5*(V1[i]+V1[i-1]);
#endif
    }
    W[0] = W[N];

    // F at t+dt/2

    for( i = 0 ; i < N; i++ )
        F[i] = Q(U1[i])-(W[i+1]-W[i])/dx;
    F[N] = F[0];

    // U and V at t+dt calculated from the slopes at t+dt/2

    for( i = 1; i <= N; i++ )
    {
        U[i] += dt*(V1[i]-V1[i-1])/dx;
        V[i] += dt*(F[i]-F[i-1])/dx;
    }
    U[0] = U[N];
    V[0] = V[N];

    // find non-wrapping x-value of absolute maximum

    int j = 0;                      // position of max
    for( i = 1; i < N; i++ )
        if( U[i] > U[j] ) j = i;
    real x = j*dx;
    real r = XM+0.5*A-A*(int)(XM/A+0.5);
    real d = x-r;
    if( -d > A-15*dx ) d += A;
    else
    if( d > A-15*dx ) d -= A;
    XM += d;
}

//---------------------------------------------------------------------------

void DoIntegrals()
{
    int i;
    realmatrix W;

    // calculate W (the U-derivative) from the central difference

    for( i = 1; i < N; i++ ) W[i] = 0.5*(U[i+1]-U[i-1])/dx;
    W[0] = W[N] = 0.5*(U[1]-U[N-1])/dx;

    // calculate integrals

    ET = EC = ED = 0;
    IU = IUU = IUV = 0;
    for( i = 0; i < N; i++ )
    {
        ET += 0.5*sqr(V[i]);
        ED += 0.5*sqr(W[i]);
        EC += 0.5*AA(U[i]);

        IU += U[i];
        IUU += sqr(U[i]);
        IUV += U[i]*V[i];
    }
    ET *= dx;
    ED *= dx;
    EC *= dx;
    E = ET+EC+ED;

    IU *= dx;
```

```
    IUU *= dx;
    IUV *= dx;
}

//--------------------------------------------------------------------------------

void WriteRealMatrix(realmatrix &m)
{
    int i;

    fprintf(out,"{");
    for( i = 0; i <= N; i++ )
    {
        if( i > 0 ) fprintf(out,",");
        fprintf(out,"%.10f",m[i]);
    }
    fprintf(out,"}");
}

//--------------------------------------------------------------------------------

#define realOUTPUT(x) fprintf(out," "#x" = %.8f;\n",x);
#define intOUTPUT(x) fprintf(out," "#x" = %d;\n",x);

void WriteInit()
{
    int i;
    fopen_s(&out,outname,"w");

    // input parameters

    fprintf(out,"{\n");                 // start of complete Mathematica expression

    realOUTPUT(A);
    realOUTPUT(dx);
    realOUTPUT(dt);

#if defined(DECAY)
    realOUTPUT(kappa);
#endif

    realOUTPUT(B1);
    realOUTPUT(B2);
    realOUTPUT(beta0);
    realOUTPUT(beta);
    realOUTPUT(a);
    realOUTPUT(b);
    realOUTPUT(width);
    realOUTPUT(energy);

#ifdef NOISE
    realOUTPUT(amplitude);
    intOUTPUT(modes);
#endif

    intOUTPUT(iters);
    intOUTPUT(write);


    // X matrix

    realmatrix X;
    for( i = 0; i <= N; i++ ) X[i] = -0.5*A+i*dx;
    fprintf(out," X = ");
    WriteRealMatrix(X);
    fprintf(out,";");

    // begin iteration data

    fprintf(out,"\n data={");
    fclose(out);
}

void WriteData()
```

```
{
    DoIntegrals();
    fopen_s(&out, outname,"a+");

    if( iter > 0 ) fprintf(out,",");
    fprintf(out,"\n{");
    fprintf(out,"%.8f,\n",t);
    WriteRealMatrix(U);
    fprintf(out,",\n%.10f,%.4f,%.10f,%.10f,%.10f",E,XM,IU,IUU,IUV);
    fprintf(out,",");
    WriteRealMatrix(V);
    fprintf(out,"\n}");
    fclose(out);
}
void WriteFinal()
{
    fopen_s(&out,outname,"a+");
    fprintf(out,"};");              // terminate iteration data

    // write other termination data here

    intOUTPUT(elapsed);

    // end of complete Mathematica expression

    fprintf(out,"\n}\n");
    fclose(out);
}

//--------------------------------------------------------------------------------

int main()
{
    printf("data file name = %s",outname);
    printf("\nsoliton energy =      %8.6g %8.6g %8.6g %8.6g\n",energy,kin,disp,comp);
    Initialize();
    WriteInit();
    printf("\nseconds  cycle       t   energy       x-max  u-int      u2-int     uv-int");
    time_t start=time(NULL);
    for( iter = 0; iter <= iters; iter++, t += dt )
    {
        if( iter%print == 0 )
        {
            DoIntegrals();
            printf("\n%4l %7d %9.3f %8.8f %9.3f %8.8f %8.8f %8.8f", elapsed,iter,t,E,XM,IU,↙
    IUU,IUV);
        }
        if( iter%ask == 0 ) { time_t wait = time(NULL); getc(stdin); start += time(NULL)-   ↙
    wait; }
        if( iter%write == 0) WriteData();

        DoCycle();
        elapsed = time(NULL)-start;
    }
    WriteFinal();
    printf("\n");
    return 0;
}
```

Declaration of Originality

I, Revathi Appali, hereby certify that this material, which I now submit for assessment leading to the award of Doktor-Ingenieur (Dr.-Ing.) is my own work and to the best of my knowledge, it contains no material previously submitted for the award of any other degree at any institution, except where due acknowledgment is made in the text.

.....

Rostock, March 5, 2013 Revathi Appali

List of Publications

Journal Articles

1. R. Appali, S. Petersen, U. van Rienen. A comparison of Hodgkin-Huxley and Soliton Neural Theories. Adv. Radio Sci., 8, 15, 2010 (doi:10.5194/ars-8-75-2010).

2. B. Lautrup, R. Appali, A. D. Jackson and T. Heimburg. 2011. The stability of solitons in biomembranes and nerves. Eur.Phys. J. E. 34: 57.

Book Chapters

3. R. Appali, B. Lautrup, T. Heimburg, and U. van Rienen. 2012. Soliton collision in biomembranes and nerves - A stability study. B. Michielsen and J.-R. Poirier (eds.), in: Scientific Computing in Electrical Engineering SCEE 2010, Mathematics in Industry 16, Springer, pp. 205-212.

4. R. Appali, U. van Rienen and T. Heimburg. 2012. A comparison of the Hodgkin-Huxley model and the soliton theory for the action potential in nerves. Advances in Planar Lipid Bilayers and Liposomes 16: 275-299.

Conference Articles

5. R. Appali, S. Petersen, J. Gimsa, U. van Rienen: 3D-Simulation of Action Potential Propagation in a Squid Giant Axon, Comsol Conference 2009, Banglore, Nov. 13-14, 2009.

6. R. Appali, S. Petersen, J. Gimsa, U. Van Rienen. Thermodynamic Theory of Nerve Signal Propagation and First Simulation of Soliton Model, Biomedical Engineering. Volume 55, Issue s1, Pages 186189, 2010 (ISSN (Online) 1862-278X, ISSN (Print) 0013-5585, DOI: 10.1515/BMT.2010.712)

7. U. van Rienen, R. Appali et al. Analysis and Simulation of Electrical Interactions of Implants with Biosystems, Biomedical Engineering. Volume 55, Issue s1, Pages 167170, 2010 (ISSN (Online) 1862-278X, ISSN (Print) 0013-5585, DOI: 10.1515/BMT.2010.712)

REVATHI APPALI

Personal Data

Contact Address	Ziolkowski Str.10 18059-Rostock	*Email Address*	revathi.appali@uni-rostock.de
Date of Birth	16 May 1985	*Telephone No.*	+49-(0)176-66695639
Place of Birth	Hanamkonda, India	*Nationality*	Indian

Education

2009-present

PhD in Electrical Engineering (Dr.Ing)
Scholarship student in the DFG-Research Training Group "welisa"
Thesis on "Modelling the coupling of action potential and electrode"
Institute of General Electrical Engineering
Faculty of Computer Science and Electrical Engineering
University of Rostock, Germany
Supervised by Prof. Dr. Ursula van Rienen, IAE, University of Rostock

2006-2008

Master of Science in Computational Engineering (M.Sc.)
Faculty of Computer Science and Electrical Engineering
University of Rostock, Germany
Modules covered included numerical mathematics, partial differential equations, finite element methods, control theory, Systems Biology, FEM, Micro technology etc.,.
Master thesis on *"Development of Simulation Environment for a Four-Wheel Parallel Hybrid"*
IAV Automotives, Gifhorn, Germany
Supervised by Prof. Bernhard Lampe, University of Rostock and Dr. Thomas Boehme, IAV. Thematic focus:

- Analysis of new hybrid components
- Simulation of hybrid components
- Matlab Simulink

2002-2006

Bachelor of Technology in Mechanical Engineering (B.Tech.)
First class with Distinction (74.8%)
Balaji Institute of Technology and Sciences
Affiliated to JNTU-Hyderabad, India
The final year project *"Inventory management system"* developed software for inventory maintenance and control in the production company generating automatic alerts to place the orders.

2000-2002

Intermediate Public Examination
First class with Distinction (91.1%)
S.V.S Junior College, Hanamkonda, India
Studied Mathematics, Physics and Chemistry

1997-2000 **Secondary School Certificate (S.S.C)**
First class with Distinction (85.5%)
Presidency High School, Bhongir, India

Research Experience

03.2010 &11.2010 **Visiting PhD student at Membrane Biophysics Group, Niels Bohr Institute, Copenhagen, Denmark**

04.2007-03.2008 **Research Assistant, Systems Biology and Bioinformatics group**
University of Rostock (www.sbi.uni-rostock.de), Germany
Development of an automatic MS- Excel workflow for the pre-processing of experimental data from western blots in preparation for mathematical modelling. This involved data normalization and merging data from several experiments. The work was conducted in collaboration with the wet-lab of Prof. Robert Jaster at the Medical Faculty in the University of Rostock.

Publications

Journal articles

1. R. Appali, S. Petersen, U. van Rienen.A comparison of Hodgkin-Huxley and Soliton Neural Theories. Adv. Radio Sci., 8, 1–5, 2010 (doi:10.5194/ars-8-75-2010).
2. B. Lautrup, R. Appali, A. D. Jackson and T. Heimburg. 2011. The stability of solitons in biomembranes and nerves. Eur.Phys. J. E. 34: 57.

Book Chapters

1. R. Appali, B. Lautrup, T. Heimburg, and U. van Rienen. 2012. Soliton collision in biomembranes and nerves - A stability study. B. Michielsen and J.-R. Poirier (eds.), in: Scientific Computing in Electrical Engineering SCEE 2010, Mathematics in Industry 16, Springer, pp. 205-212.
2. R. Appali, U. van Rienen and T. Heimburg. 2012. A comparison of the Hodgkin-Huxley model and the soliton theory for the action potential in nerves. Advances in Planar Lipid Bilayers and Liposomes 16: 275-299.